MEMOIRS

OF THE

COLLEGE OF SCIENCE

UNIVERSITY OF KYOTO

SERIES A

THE
PHYSICAL
SOCIETY

VOL. XXVI, Nos. 1 & 2

October 1950

KYOTO

11277

B. Arakatsu

Commemoration Number

dedicated to

PROFESSOR BUNSAKU ARAKATSU

By

His Friends and Pupils

on his sixtieth birthday,

March 25th, 1950.

Professor Bunsaku Arakatsu

Professor Bunsaku Arakatsu, the sixtieth anniversary of whose birth we celebrate, was born on March 25th, 1890, in Hyogo Prefecture, Japan. He studied physics at the College of Science of the Kyoto Imperial University from 1915 to 1918. On graduation he was immediately appointed a Lecturer of Physics, and three years later, he was appointed an Assistant Professor of Physics.

In 1926 he was sent to Europe and the United States of America to study physics. He first visited Professor P. Scherrer's laboratory at the Eidgenössische Technische Hochschule, Zürich, Switzerland, where he worked on electron distribution in the lithium atom. It was one of the most important problems in those days, since it had an intimate bearing on wave mechanics which had been initiated by Professor Schrödinger some time ago. He then visited Cambridge, England, and stayed for some months in the late Lord Rutherford's laboratory at the Cavendish Laboratory. There he was greatly impressed by the atmosphere of the laboratory and its attitude towards scientific researches.

When he returned home in 1928, he took the degree of *Rigakuhakushi* (D. Sc.) at the Kyoto Imperial University and was appointed a Professor of Physics in the Taihoku Imperial University, Formosa, which had been newly established there. He set up a physical laboratory and worked on various important problems in atomic physics as well as in nuclear physics.

In 1936 he was appointed a Professor of Physics in his Alma Mater, the Kyoto Imperial University, in succession to the late Professor M. Ishino who had then retired from his post. In 1938 he was elected a member of the Institute of Chemical Research attached to the Kyoto Imperial University, and established a physical laboratory there.

Professor Arakatsu was of good service to his University as a member of the University Senate and Dean of the Faculty of Science. Also, he has made great contributions to the academic world as the editor of the Japanese Journal of Physics and as a member of the Japan Society for the Promotion of Scientific Research. In 1948 he was elected a member of the Research Conference of National Arts and Sciences of the New System.

His keen interest being invariably fixed upon the investigation of atomic and nuclear physics, Professor Arakatsu has been, and still is, with ever increasing ardour, engaged in both theoretical and experimental researches in those fields. As will be seen from a list of his published papers, his earlier work was concerned with positive ray analysis, which was carried out with the late Professor Ishino and by which the existence of chlorine isotope was clearly indicated. During the next ten years he published some papers on atomic spectra as well as on general relativity.

In 1932 he built up a high voltage generator of the Cockcroft-Walton type in the Taihoku Imperial University and investigated Li+p, B+p and D+D reactions under various unfavourable conditions in Formosa. The heavy hydrogen used in his experiments was prepared by electrolysis in his laboratory itself.

A 600 Kv generator was established in 1937 in the Institute of Physics of the Kyoto Imperial University through the financial support of his intimate friend, the late H. Kuroda, a Managing Director of the Ensuiko Sugar Company. With this apparatus he and his pupils observed the photo-fission of uranium and thorium, the photo-disintegration of various elements and the Compton scattering as well as pair creation phenomena by using 17 and 6.1 Mev γ-rays. Recently he certified α-ray-emission in the case of beryllium by the bombardment of 17 and 6.1 Mev γ-rays.

Professor Arakatsu has long been interested in the application of

nuclear physics to other branches of science for the sake of human welfare, and several important topics of research using radio-isotopes have been, and are being, pursued with his advice. He has also been interested in producing high speed rotation by magnetic suspension, the rotating speed recently obtained being 3×10^6 revolutions per minute.

The key-note of his character is his extraordinary love of Science. His unusual energy both in pursuing his own researches and in keeping himself informed of every item concerning the latest developments in physical science, seems to have its source in this love, and does not fail to impart inspiration to those who come within the sphere of his personal influence. Being a good teacher and excellent director, more than thirty pupils are now working in various departments of both pure and applied physics under his kind direction. The works carried out by his pupils in his laboratory are also given in the appended list of papers by his pupils.

Having just reached the age of sixty, Professor Arakatsu has retired from his post, but his ideas and the activity of his laboratory will be carried forwards by his successors.

In celebration of the sixtieth anniversary of his birth, his friends and pupils present this commemoration number. They take this opportunity of expressing their sincere and heartfelt appreciation for his warm friendship and kind guidance for many years, and of acknowledging his valuable contributions to scientific progress. They also wish him good health and happiness for the future.

S. Tomotika and K. Kimura.

List of Professor B. Arakatsu's Papers on Scientific Subjects.

1. On the limiting size of colloidal particles in a Brownian motion: Results for gold and copper particles. (with M. Fukuda) Mem. Coll. Sci., Kyoto Imp. Univ., A, **4** (1920), 179.
2. On the negatively charged particles in the positive ray tube. (with M. Ishino) Mem. Coll. Sci., Kyoto Imp. Univ., A, **4** (1921), 355.
3. The theory of general relativity in a physically flat space. Mem. Coll. Sci., Kyoto Imp. Univ., A, **8** (1925), 263.
4. Self reversal lines of lead in explosion spectrum and the series relations in them. Mem. Coll. Sci., Kyoto Imp. Univ., A, **9** (1926), 451.
5. Self-reversal of lines in the explosion spectrum of tin. Mem. Coll. Sci., Kyoto Imp. Univ., A, **10** (1926), 31.
6. The reversal of lines in the explosion spectrum of lead. Mem. Coll. Sci., Kyoto Imp. Univ., A, **10** (1927), 171.
7. Röntgenographische Bestimmung der frei Elektronen in Lithium-metall. (with P. Scherrer) Helv. Phys. Acta, **2** (1929), 153.
8. Bestimmung der Elektrizitätsverteilung in Lithium-Atom. (with P. Scherrer) Helv. Phys. Acta, **3** (1930), 428.
9. On the scattering power of X-rays of various materials. (*in Japanese*) Ōyō-Butsuri, **1** (1932), 150, 172, 240.
10. The continuous spectrum of hydrogen associated with each of the lines in the Balmer series. (with Y. Ōta and K. Kimura) Mem. Fac. Sci. & Agr., Taihoku Imp. Univ., **5** (1932), 1.
11. On some peculiar phenomena of the electrodeless ring discharge through hydrogen in a long tube. (with K. Kimura) Mem. Fac. Sci. & Agr., Taihoku Imp. Univ., **5** (1932), 15.
12. The principle of the conservation of angular momentum or the principle of the conservation of the symmetry or antisymmetry of the total wave function (Bose or Fermi statistics) in molecules? (with Y. Ōta) Mem. Fac. Sci. & Agr., Taihoku Imp. Univ. **5** (1932), 25.
13. The activation of air by the electrodeless ring discharge. (with K. Kimura) Mem. Fac. Sci. & Agr., Taihoku Imp. Univ., **5** (1932), 143.

14. The electrodeless ring discharge through potassium vapour. (with Y. Uemura) Mem. Fac. Sci. & Agr., Taihoku Imp. Univ., **5** (1932), 159.

15. On the anomalous absorption of gamma-rays. (The possibility of the quantum jump of the rest-mass of an electron) Mem. Fac. Sci. & Agr., Taihoku Imp. Univ., **5** (1932), 163.

16. Notes on spin angular momentum in the process of the artificial disintegration of lithium atoms. Mem. Fac. Sci. & Agr., Taihoku Imp. Univ., **10** (1934), 81.

17. The construction of a small high voltage source suitable for the production of high speed ions. (with K. Kimura and Y. Uemura) (*in Japanese*) Ōyō-Butsuri, **4** (1935), 222.

18. Artificial transmutation of deuteron. (with K. Kimura and Y. Uemura) (*in Japanese*) Kagaku, **5** (1935), 144.

19. Experimental transmutation of certain light elements bombarded by ions of hydrogen and heavy hydrogen. I. (with K. Kimura and Y. Uemura) Mem. Fac. Sci. & Agr., Taihoku Imp. Univ., **18** (1936), 75.

20. Expulsion of neutrons from lead by cosmic rays. (with K. Kimura and Y. Uemura) Nature, **140** (1937), 277.

21. Photo-fission of uranium and thorium produced by the gamma-rays of lithium and fluorine bombarded with high speed protons. (with Y. Uemura, M. Sonoda. S. Shimizu, K. Kimura and K. Muraoka) Proc. Phys.-Math. Soc., Japan, **23** (1941), 440.

22. The range of the photo-fission-fragments of uranium produced by the gamma-rays of lithium bombarded with protons. (with M. Sonoda, Y. Uemura and S. Shimizu) Proc. Phys.-Math. Soc., Japan, **23** (1941), 633.

23. A type of nuclear photo-disintegration: The expulsion of alpha-particles from various substances irradiated by the gamma-rays of lithium and fluorine bombarded with high speed protons. (with M. Sonoda, Y. Uemura, S. Shimizu and K. Kimura) Proc. Phys.-Math. Soc., Japan, **25** (1943), 173.

24. Measurement of capture cross section of uranium nuclei for thermal neutron. (with T. Hanatani and K. Kimura) (*in Japanese*) Unpublished (June, 1945).

25. Fission cross section and absorption cross section of uranium nuclei for thermal neutron. (with T. Hanatani) (*in Japanese*) Unpublished (June, 1945).

26. Cloud chamber observation of photo-alpha particles produced by 17 Mev gamma-rays. (with S. Shimizu, T. Hanatani and J. Muto) Journ. Phys. Soc., Japan, **1** (1946), 24.

27. On the magnetic suspension mechanism for research of high speed rotation. (with A. Katase, J. Kokame and S. Yano) (*in Japanese*) Rep. Inst. Chem. Res., Kyoto Univ., **17** (1949), 87.

28. High speed rotation with the rotor suspended by "magnetic bearing" (with A. Katase, J. Kokame and S. Yano) (*in Japanese*) Ōyō-Butsuri, **18** (1949), 35.

29. Study on high speed rotation, II. (with A. Katase, J. Kokame and S. Yano) (*in Japanese*) Rep. Inst. Chem. Res., Kyoto Univ., **18** (1949), 92.

30. Studies on clay. I. (with T. Shidei) (*in Japanese*) Rep. Inst. Chem. Res., Kyoto Univ., **19** (1949), 28.

31. Study on high speed rotation, III. (with A. Katase, J. Kokame and S. Yano) (*in Japanese*) Rep. Inst. Chem. Res., Kyoto Univ. **19** (1949), 31.

32. Study on high speed rotation, IV. (with A. Katase, J. Kokame and S. Yano) (*in Japanese*) Bull. Inst. Chem. Res., Kyoto Univ., **21** (1950), 60.

33. On the photo-disintegration of beryllium by the high energy rays. (with M. Sonoda, Y. Uemura, S. Yasumi and Y. Saji) Mem. Coll. Sci., Univ. of Kyoto, A **26** (1950), 97.

34. Study on high speed rotation, V. (with A. Katase, J. Kokame and Y. Saji) Bull. Inst. Chem. Res., Kyoto Univ., **22** (1950), 67.

35. Photo-disintegration of beryllium by the high energy gamma-rays. (with M. Sonoda, Y. Uemura, S. Yasumi and Y. Saji) Bull. Inst. Chem. Res., Kyoto Univ., **22** (1950), 71.

36. Study on the ion source. (with Y. Uemura, S. Yasumi, M. Sakisaka and S. Miyashiro) Bull. Inst. Chem. Res., Kyoto Univ., **23** (1950), (in press).

List of Papers by Professor Arakatsu's Pupils.

1. Y. Ōta,
   Studies on concentrating the hydrogen isotope H^2 by the electrolysis of water. Part I. Mem. Fac. Sci. & Agr., Taihoku Imp. Univ., **19** (1934), 71.

2. Y. Ōta,
   Studies on concentrating the hydrogen isotope H^2 by the electrolysis of water. Part II. 'The production of heavy water and its apparatus' Mem. Fac. Sci. & Agr., Taihoku Imp. Univ., **15** (1935), 165.

3. K. Kimura,
   Determination of the energy of photo-neutrons liberated from deutron by radium C gamma-rays. Mem. Coll. Sci., Kyoto Imp. Univ., A, **22** (1939), 237.

4. K. Kimura and Y. Uemura,
   A counting instrument with linear amplifier. Mem. Coll. Sci., Kyoto Imp. Univ., A, **23** (1940), 1.

5. K. Kimura,
   Study on radioactivity of hokutolite in Taiwan by means of a counter with linear amplifier. Mem. Coll. Sci., Kyoto Imp. Univ., A, **23** (1940), 7.

6. T. Hagiwara,
   Liberation of fast neutrons in the nuclear explosion of uranium irradiated by thermal neutrons. Mem. Coll. Sci., Kyoto Imp. Univ., A, **23** (1940), 19.

7. Y. Uemura,
   Measurement of coefficient of friction by photo-elastic method. (*in Japanese*) Rep. Inst. Chem. Res., Kyoto Univ., **16** (1947), 53.

8. S. Shimizu,
   Vital phenomena treated as physical problems. (*in Japanese*) Saishin-Igaku, **2** (1947), 309.

9. S. Shimizu and J. Muto,
   A note on the angular distribution of pair-electrons of 17 Mev gamma-rays. Mem. Coll. Sci., Univ. of Kyoto, A, **25** (1949), 61.

10. K. Kimura, R. Ishiwari, T. Hayashi and K. Nishikawa,

Measurement of radioactivity of sedimentation products of Ikeda mineral spring. (*in Japanese*) Rep. Inst. Chem. Res., Kyoto Univ., **17** (1949), 89.

11. K. Fujii and S. Terai,
On an electric loss of the low fired (below 1000° C) clays under high frequency. (*in Japanese*) Rep. Inst. Chem. Res., Kyoto Univ., **17** (1947), 91.

12. Y. Uemura,
Preparation of test-piece of gelatin-jelly for photo-elasticity. (*in Japanese*) Rep. Inst. Chem. Res., Kyoto Univ., **17** (1947), 93.

13. K. Kimura, Y. Uemura and T. Yanabu,
Study on the extrusion press using clay. (*in Japanese*) Rep. Inst. Chem. Res., Kyoto Univ., **18** (1949), 81.

14. Y. Uemura and T. Yanabu,
On the relation between the coefficient of friction and "writing ease" of the pencil. (*in Japanese*) Rep. Inst. Chem. Res., Kyoto Univ., **18** (1949), 84.

15. K. Kimura, T. Hayashi, K. Nishikawa and K. Ishizaki,
On the eliminating method of natural counts of G-M counter. (*in Japanese*) Rep. Inst. Chem. Res., Kyoto Univ., **18** (1949), 86.

16. Y. Uemura,
Study on the plastic deformation from the drawing mechanism by means of photo-elasticity. (*in Japanese*) Rep. Inst. Chem. Res., Kyoto Univ., **18** (1949), 88.

17. R. Ishiwari and K. Yuasa,
A new decade scaler. (*in Japanese*) Rep. Inst. Chem. Res., Kyoto Univ., **18** (1949), 90.

18. Y. Uemura and T. Yanabu,
On the extrusion press. (*in Japanese*)
On the physical properties of pencil. (*in Japanese*)
On the clay suitable for making pencil. (*in Japanese*)
First Report of the Committee for Pencil, Osaka Pref., Aug., (1949), 3—44.

19. R. Ishiwari and K. Yuasa,
On the disintegration of ${}_{7}N^{14}$ by slow neutrons: Accurate determination of the energy of reaction. (*in Japanese*) Rep. Inst. Chem. Res., Kyoto Univ., **19** (1949), 19.

20. Y. Uemura, S. Shimizu, S. Yasumi and Y. Saji,
The absorption of gamma-radiation of 17 Mev and 6.1 Mev in several elements. (*in Japanese*) Rep. Inst. Chem. Res., Kyoto Univ., **19** (1949), 21.

21. S. Shimizu, Y. Uemura, R. Ishiwari, Y. Saji and J. Muto,
Nuclear reaction $Cu^{63}(\gamma, n)\,Cu^{62}$ produced by 17.6 Mev gamma-rays. (*in Japanese*) Rep. Inst. Chem. Res., Kyoto Univ., **19** (1949), 23.

22. T. Yanabu, T. Yoshida and Y. Uemura,
Studies on clay, II. (*in Japanese*) Rep. Inst. Chem. Res., Kyoto Univ., **19** (1949), 29.

23. K. Kimura, Y. Uemura and S. Yamashita,
Automatic diameter selection of pins (part of roller chains). Rep. Inst. Chem. Res., Kyoto Univ., **19** (1949), 32.

24. R. Ishiwari and K. Yuasa,
A decade scaling circuit. Mem. Coll. Sci., Univ. of Kyoto, A, **25** (1949), 155.

25. M. Sonoda,
A type of Geiger-Müller counter suitable for the measurement of high energy gamma-rays. Mem. Coll. Sci., Univ. of Kyoto, A, **25** (1949), 175.

26. M. Sonoda,
On the proportional counter. Mem. Coll. Sci., Univ. of Kyoto, A, **25** (1949), 185.

27. S. Shimizu,
Photo-induced reaction $Cu^{63}(\gamma, n)\,Cu^{62}$ produced by the gamma-rays of lithium bombarded with high speed protons. Mem. Coll. Sci., Univ. of Kyoto, A, **25** (1949), 193.

28. Y. Uemura,
The deep-drawing process. (*in Japanese*)
The general view on the technique of iron and steel of Japan, 1950 (with S. Koyabu, S. Ono and S. Kawamoto).

29. K. Kimura and K. Ohira,
Electron bombardment conductivity of BaO + SrO. Bull. Inst. Chem, Res., Kyoto Univ., **20** (1950), 41.

30. S. Shimizu, Y. Ōno and T. Naiki,

On some properties of Dewar vessels. Bull. Inst. Chem. Res., Kyoto Univ., **20** (1950), 42.

31. S. Shimizu and O. Horibe,
Portable radiation detector instrument. Bull. Inst. Chem. Res., Kyoto Univ., **20** (1950), 43.

32. T. Yoshida, T. Yanabu, Y. Uemura and K. Kimura,
On the stability of the tube potentiometer. Bull. Inst. Chem. Res., Kyoto Univ., **21** (1950), 54.

33. K. Kimura, T. Hayashi, Y. Ishizaki and K. Nishikawa,
An attempt to eliminate the natural counts of the G-M counter. Bull. Inst. Chem. Res., Kyoto Univ., **21** (1950), 54.

34. K. Kimura, T. Hayashi, Y. Ishizaki and K. Nishikawa,
On the gamma-rays of K^{40}. Bull. Inst. Chem. Res., Kyoto Univ., **21** (1950), 55.

35. Y. Uemura, S. Shimizu and Y. Saji,
On the properties of 2π-type beta-ray G-M counter. Bull. Inst. Chem. Res., Kyoto Univ., **21** (1950), 56.

36. S. Shimizu, Y. Uemura and Y. Saji,
On a stable 2π-type beta-ray counter. Bull. Inst. Chem. Res., Kyoto Univ., **21** (1950), 57.

37. M. Sonoda, J. Muto and S. Yasumi,
Observation of the B (n, α) Li reactions by the Wilson cloud chamber. Bull. Inst. Chem. Res., Kyoto Univ., **21** (1950), 57.

38. M. Sonoda,
On the property of the proportional counter. Bull. Inst. Chem. Res., Kyoto Univ., **21** (1950), 58.

39. M. Sonoda,
The efficiency of the G-M counter for high energy gamma-quanta. Bull. Inst. Chem. Res., Kyoto Univ., **21** (1950), 58.

40. K. Kimura, S. Tokunaga, K. Yuasa and R. Ishiwari,
Observation of cosmic-rays with photographic emulsions (1). Bull. Inst. Chem. Res., Kyoto Univ., **21** (1950), 59.

41. Y. Uemura, R. Ishiwari and K. Yuasa,
Study on pulse shapes of alpha-ray counter with ionization chamber and linear amplifier. Bull. Inst. Chem. Res., Kyoto Univ., **21** (1950), 60.

42. K. Yuasa and R. Ishiwari,
A method of measuring ion mobility using an alpha-ray counter. Bull. Inst. Chem. Res., Kyoto Univ., **21** (1950), 61.

43. Y. Saji,
Absolute measurement of beta-rays by 2π-type counter. (*in Japanese*) Saishin-Igaku, **5** (1950), 744.

44. M. Sonoda,
Flow-type beta-ray proportional counter. (*in Japanese*) Saishin-Igaku, **5** (1950), 748.

45. R. Ishiwari,
Statistical treatment of counting data. (*in Japanese*) Saishin-Igaku, **5** (1950), 751.

46. S. Tokunaga,
Measurement of the branching ratio of thorium C by a photographic method. Mem. Coll. Sci., Univ. of Kyoto, A, **26** (1950), 109.

47. R. Ishiwari and K. Yuasa,
The energy released in the disintegration of nitrogen by thermal neutrons. Mem. Coll. Sci., Univ. of Kyoto, A, **26** 151.

48. S. Shimizu, S. Yasumi, Y. Saji and J. Muto,
The (γ, n) reaction of molybdenum produced by the Li (p, γ)-γ-rays. Mem. Coll. Sci., Univ. of Kyoto, A, **26** (1950), 85.

49. K. Kimura, S. Tokunaga, R. Ishiwari and K. Yuasa,
Observation of cosmic rays with nuclear emulsions. Mem. Coll. Sci., Univ. of Kyoto, A, **26** (1950), 167.

50. M. Sakisaka, S. Miyashiro, Y. Uemura and S. Yasumi,
Studies on the ion source placed in a magnetic field. Mem. Coll. Sci., Univ. of Kyoto, A, **26** (1950), 143.

51. K. Ohira,
Researches on the activation energy of (Ba, Sr) O by electron bombardment. Mem. Coll. Sci., Univ. of Kyoto, A, **26** (1950), 131.

52. K. Kimura,
Application of radioisotopes. Bull. Inst. Chem. Res., Kyoto Univ., A, **22** (1950), 1.

53. Y. Uemura,
Measurement of absorption coefficients of 17 Mev and 6.1 Mev gamma-

rays in several elements. Bull. Inst. Chem. Res., Kyoto Univ., 22 (1950), 18.

54. J. Kokame, A. Katase and S. Yano,
On the whirling of rotating shaft at high rotational speed. Bull. Inst. Chem. Res., Kyoto Univ., 22 (1950), 68.

55. S. Yano, A. Katase and J. Kokame,
On the torque acting on the rotor rotating in the rotating magnetic field. Bull. Inst. Chem. Res., Kyoto Univ., 22 (1950), 69.

56. K. Kimura, K. Yuasa, R. Ishiwari and S. Tokunaga,
Observation of cosmic rays with photographic emulsion. II. Bull. Inst. Chem. Res., Kyoto Univ., 22 (1950), 70.

57. M. Sonoda,
The efficiency of the Geiger-Müller counter for the high energy gamma-rays. Bull. Inst. Chem. Res., Kyoto Univ., 22 (1950), 70.

58. S. Shimizu, Y. Uemura, R. Ishiwari, O. Horibe and S. Okamoto,
Some experiments on P^{32}. Bull. Inst. Chem. Res., Kyoto Univ., 22 (1950), 72.

59. Y. Uemura, M. Sakisaka and S. Miyashiro,
On some device of the gas leak apparatus for measuring the pumping speed. Bull. Inst. Chem. Res., Kyoto Univ., 23 (1950), (in press).

60. K. Kimura, K. Yuasa, S. Yamashita and R. Ishiwari,
On the characteristics of ionization chamber with screen-grid. Bull. Inst. Chem. Res., Kyoto Univ., 23 (1950), (in press).

61. K. Kimura and K. Ōhira,
Electron bombardment conductivity of (Ba, Sr) O II. Bull. Inst. Chem. Res., Kyoto Univ., 23 (1950), (in press).

62. Y. Uemura, Y. Saji and S. Shimizu,
On some properties of 2π-type counter (II). Bull. Inst. Chem. Res., Kyoto Univ., 23 (1950), (in press).

63. K. Kimura, I. Kumabe, I. Nakatao, H. Ueyanagi and A. Kusumegi,
Trial manufacture of electron accelerator using cavity resonator. Bull. Inst. Chem. Res., Kyoto Univ., 23 (1950), (in press).

64. K. Kimura, I. Kumabe, I. Nakatao, H. Ueyanagi and A. Kusumegi,
E_p-I_p characteristic curves of magnetron. Bull. Inst. Chem. Res.,

Kyoto Univ., **23** (1950), (in press).

65. S. Shimizu, H. Takegoshi, H. Nishimura and N. Ogura,
Operation of an electron-multiplier. Bull. Inst. Chem. Res., Kyoto Univ., **23** (1950), (in press).

66. Y. Uemura, M. Takai and K. Takemura,
Measurement of the coefficient of friction. Bull. Inst. Chem. Res., Kyoto Univ., **23** (1950), (in press).

67. K. Kimura, Y. Uemura, T. Yanabu and T. Yoshida,
Dielectric properties of mud pastes under alternating field of low frequency. Bull. Inst. Chem. Res., Kyoto Univ., **23** (1950), (in press).

68. K. Kimura, T. Hayashi, Y. Ishizaki and K. Nishikawa,
On the delayed coincidence circuits (I). Bull. Inst. Chem. Res., Kyoto Univ., **23** (1950), (in press).

69. K. Kimura and S. Tokunaga,
Observation of cosmic-rays with photographic emulsions. (*in Japanese*)
Nippon-Butsuri-Gakkaishi **5** (1950), 147.

Memoirs of the College of Science, University of Kyoto, Series A,
Vol. XXVI, Nos. 1 & 2, Article 1, 1950.

On the Bending of a Rectangular Plate with Four Clamped Edges

By

K. Munakata

(Received March 29, 1950)

1. Introduction

As is well known, the problem of the bending of a rectangular plate under the action of surface pressure on one of its faces is one of the most important problems in the theory of elasticity. The problem was already investigated mathematically by Ritz (**1**), Hencky (**2**), Love (**3**), Timoshenko (**4**) and others, using various methods of solution. Love's analysis is very complicated, but his method of simplifying the boundary conditions by means of a conformal transformation seems to be effective for the treatment of the case of a plate with four clamped edges. In the present paper the writer gives an alternative analysis which is developed along a similar line to Love's, but is more concise.

Now, the interior of a rectangle in the z-plane can be mapped into the interior of a circle in the ζ-plane by the relation:

$$z = A\int_0^{\zeta} \frac{d\zeta}{\sqrt{1 - 2\gamma\zeta^2 + \zeta^4}}, \tag{1}$$

where

$$A = \frac{2a}{(1+k)K}, \tag{2}$$

$$\gamma = \cos 2\alpha = 1 - 2\left(\frac{1-k}{1+k}\right)^2, \tag{3}$$

and K is the complete elliptic integral of the first kind with modulus k. The correspondence of various points is shown in the annexed figure, and the ratio of the two sides of the rectangle is given by

$$b/a = K'/2K. \tag{4}$$

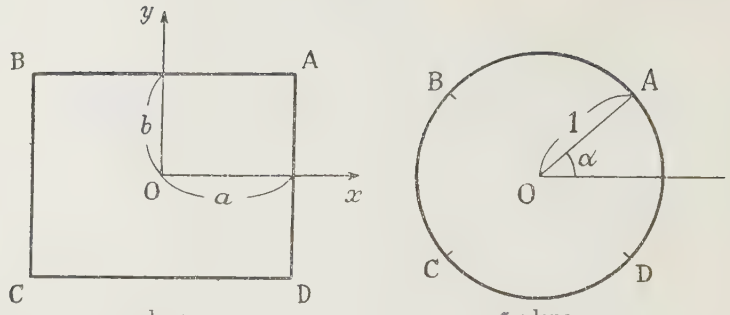

z-plane. ζ-plane.

2. General solution

We consider a small deflection of a homogeneous isotropic rectangular plate with uniform thickness $2h$ which is subject to a surface pressure P on one of its faces. If w be the lateral displacement of a point in the middle plane, the equation of equilibrium takes the form:

$$\frac{\partial^4 w}{\partial x^4} + 2\frac{\partial^4 w}{\partial x^2 \partial y^2} + \frac{\partial^4 w}{\partial y^4} = \frac{P}{D}, \tag{5}$$

where $D = \frac{2}{3}\frac{Eh^3}{1-\sigma^2}$ is the flexural rigidity, E Young's modulus and σ Poisson's ratio.

Let a particular solution of (5) be denoted by $w = w_1$. Then, the general solution takes the form:

$$w = w_1 + x\Phi_1 + y\Phi_2 + \Psi, \tag{6}$$

where Φ_1, Φ_2 and Ψ are any harmonic functions, and $x\Phi_1 + y\Phi_2 + \Psi$ is called a biharmonic function.

When the four edges of the plate are clamped, the boundary conditions are expressed by

$$\left.\begin{aligned} w = 0, \quad \frac{\partial w}{\partial x} = 0 \quad \text{at} \quad x = \pm a; \\ w = 0, \quad \frac{\partial w}{\partial y} = 0 \quad \text{at} \quad y = \pm b. \end{aligned}\right\} \tag{7}$$

If we introduce the complex conjugate variables $z = x + iy$ and $\bar{z} = x - iy$, equation (5) is transformed to

$$\frac{\partial^4 w}{\partial z^2 \partial \bar{z}^2} = \frac{P}{16D}, \tag{8}$$

and when the pressure distribution is uniform, this equation can be

integrated immediately and we have

$$w = \frac{P}{64D}\left\{z^2\bar{z}^2 + \bar{z}F_1(z) + z\overline{F_1}(\bar{z}) + F_2(z) + \overline{F_2}(\bar{z})\right\}, \qquad (9)$$

where $F_1(z)$ and $F_2(z)$ are arbitrary analytic functions of z.

3. A transformed problem

Henceforth we consider the matter in the ζ-plane. Since z is an analytic function of ζ, the functions $F_1\{z(\zeta)\}$ and $F_2\{z(\zeta)\}$ are also analytic with respect to ζ. Let these be denoted by $f_1(\zeta)$ and $f_2(\zeta)$ respectively. Then, the solution (9) becomes

$$w = \frac{P}{64D}\left\{z^2\bar{z}^2 + \bar{z}f_1(\zeta) + z\bar{f}_1(\bar{\zeta}) + f_2(\zeta) + \bar{f}_2(\bar{\zeta})\right\}. \qquad (10)$$

Taking account of the conformal character of the transformation it can readily be seen that the boundary conditions in the ζ-plane become (with $\zeta = re^{i\theta}$)

$$w = 0, \quad \frac{\partial w}{\partial r} = 0 \quad \text{at} \quad r = 1, \qquad (11)$$

or in complex forms

$$w = 0, \quad \zeta\frac{\partial w}{\partial \zeta} + \bar{\zeta}\frac{\partial w}{\partial \bar{\zeta}} = 0 \quad \text{at} \quad \zeta\bar{\zeta} = 1. \qquad (12)$$

Substituting the expression for w as given by (10) in the right-hand sides of these equations, we have

$$[z^2\bar{z}^2 + \bar{z}f_1 + zf_1 + f_2 + \bar{f}_2]_{\zeta\bar{\zeta}=1} = 0; \qquad (13)$$

$$\left[2z\bar{z}\left(\bar{z}\zeta\frac{dz}{d\zeta} + z\bar{\zeta}\frac{d\bar{z}}{d\zeta}\right) + \bar{z}\zeta\frac{df_1}{d\zeta} + z\bar{\zeta}\frac{d\bar{f}_1}{d\zeta}\right.$$

$$\left. + \frac{dz}{d\zeta}\zeta\bar{f}_1 + \frac{d\bar{z}}{d\bar{\zeta}}\bar{\zeta}f_1 + \zeta\frac{df_2}{d\zeta} + \bar{\zeta}\frac{d\bar{f}_2}{d\bar{\zeta}}\right]_{\zeta\bar{\zeta}=1} = 0. \qquad (14)$$

Now, if use is made of Legendre's polynominal $P_n(\gamma)$, the transformation equation (1) can also be expressed in the form of a series as:

$$z = A\sum_{n=0}^{\infty}\frac{P_n(\gamma)}{2n+1}\zeta^{2n+1}. \qquad (15)$$

Let the Taylor series of $f_1(\zeta)$ and $f_2(\zeta)$ be respectively

$$f_1(\zeta) = \sum_{n=0}^{\infty} a_n \zeta^n ,$$

$$f_2(\zeta) = \sum_{n=0}^{\infty} b_n \zeta^n .$$

Since, in the present problem, the deflection of the plate is necessarily symmetrical with respect to both the x- and y-axes, it can easily be seen that all of the a_{2n}'s and b_{2n+1}'s vanish and the remaining coefficients are all real. Thus, we have

$$\left.\begin{aligned} f_1(\zeta) &= \sum_{n=0}^{\infty} a_{2n+1} \zeta^{2n+1} , \\ f_2(\zeta) &= \sum_{n=0}^{\infty} b_{2n} \zeta^{2n} . \end{aligned}\right\} \tag{16}$$

4. Fulfilment of the boundary conditions

Multiplying (15) and the corresponding conjugate complex expression side by side and putting $\zeta\bar{\zeta} = 1$, we obtain

$$\begin{aligned} \left[\frac{z\bar{z}}{A^2}\right]_{\zeta\bar{\zeta}=1} &= \left[\left(P_0\zeta + \frac{1}{3}P_1\zeta^3 + \frac{1}{5}P_2\zeta^5 + \cdots\cdots\right)\right. \\ &\qquad \left.\times\left(P_0\bar{\zeta} + \frac{1}{3}P_1\bar{\zeta}^3 + \frac{1}{5}P_2\bar{\zeta}^5 + \cdots\cdots\right)\right]_{\zeta\bar{\zeta}=1} \\ &= P_0^2 + \frac{1}{3\cdot 3}P_1^2 + \frac{1}{5\cdot 5}P_2^2 + \cdots\cdots \\ &\qquad + \left(\frac{1}{3}P_0P_1 + \frac{1}{3\cdot 5}P_1P_2 + \frac{1}{5\cdot 7}P_2P_3 + \cdots\right)(\zeta^2 + \bar{\zeta}^2) \\ &\qquad + \left(\frac{1}{5}P_0P_2 + \frac{1}{3\cdot 7}P_1P_3 + \frac{1}{5\cdot 9}P_2P_4 + \cdots\right)(\zeta^4 + \bar{\zeta}^4) \\ &\qquad + \cdots\cdots\cdots\cdots\cdots , \end{aligned}$$

which may be written in the form:

$$\left[\frac{z\bar{z}}{A^2}\right]_{\zeta\bar{\zeta}=1} = Q_0 + Q_1(\zeta^2 + \bar{\zeta}^2) + Q_2(\zeta^4 + \bar{\zeta}^4) + \cdots\cdots , \tag{17}$$

where

$$\left.\begin{aligned} Q_0 &= P_0^2 + \frac{1}{3\cdot 3}P_1^2 + \frac{1}{5\cdot 5}P_2^2 + \cdots\cdots, \\ Q_1 &= \frac{1}{3}P_0P_1 + \frac{1}{3\cdot 5}P_1P_2 + \frac{1}{5\cdot 7}P_2P_3 + \cdots\cdots, \\ Q_2 &= \frac{1}{5}P_0P_2 + \frac{1}{3\cdot 7}P_1P_3 + \frac{1}{5\cdot 9}P_2P_4 + \cdots\cdots, \\ &\cdots\cdots\cdots\cdots\cdots\cdots\cdots\cdots. \end{aligned}\right\} \tag{18}$$

By squaring both sides of (17) we get

$$\left[\frac{z^2\bar{z}^2}{A^4}\right]_{\zeta\bar{\zeta}=1} = R_0 + R_1(\zeta^2 + \bar{\zeta}^2) + R_2(\zeta^4 + \bar{\zeta}^4) + \cdots, \tag{19}$$

where

$$\left.\begin{aligned} R_0 &= Q_0^2 + 2Q_1^2 + 2Q_2^2 + \cdots\cdots, \\ R_1 &= 2Q_0Q_1 + 2Q_1Q_2 + 2Q_2Q_3 + \cdots\cdots, \\ R_2 &= Q_1^2 + 2Q_0Q_2 + 2Q_1Q_3 + \cdots\cdots, \\ &\cdots\cdots\cdots\cdots\cdots\cdots\cdots\cdots. \end{aligned}\right\} \tag{20}$$

Finally, by combining equations (15) and the first of (16) we have

$$\begin{aligned} &\left[\frac{1}{A}(zf_1 + \bar{z}f_1)\right]_{\zeta\bar{\zeta}=1} \\ &= 2\left(P_0a_1 + \frac{1}{3}P_1a_3 + \frac{1}{5}P_2a_5 + \cdots\cdots\right) \\ &\quad + \left(\frac{1}{3}P_1a_1 + \frac{1}{5}P_2a_3 + \frac{1}{7}P_3a_5 + \cdots\cdots\right. \\ &\qquad\qquad \left. + P_0a_3 + \frac{1}{3}P_1a_5 + \cdots\cdots\right)(\zeta^2 + \bar{\zeta}^2) \\ &\quad + \left(\frac{1}{5}P_2a_1 + \frac{1}{7}P_3a_3 + \frac{1}{9}P_4a_5 + \cdots\cdots\right. \\ &\qquad\qquad \left. + P_0a_5 + \cdots\cdots\right)(\zeta^4 + \bar{\zeta}^4) \\ &\quad + \cdots\cdots\cdots\cdots\cdots\cdots\cdots\cdots. \end{aligned} \tag{21}$$

Substituting (16), (19) and (21) into the first boundary condition (13) and equating all the terms with equal powers of ζ to zero, we obtain the following set of equations:

$$\left.\begin{aligned}
&2A\left(P_0a_1+\frac{1}{3}P_1a_3+\frac{1}{5}P_2a_5+\cdots\cdots\right)+2b_0+A^4R_0=0\,,\\
&A\left(\frac{1}{3}P_1a_1+\frac{1}{5}P_2a_3+\frac{1}{7}P_3a_5+\cdots\cdots\right.\\
&\qquad\left.+P_0a_3+\frac{1}{3}P_1a_5+\cdots\cdots\right)+b_2+A^4R_1=0\,,\\
&A\left(\frac{1}{5}P_2a_1+\frac{1}{7}P_3a_3+\frac{1}{9}P_4a_5+\cdots\cdots\right.\\
&\qquad\left.+P_0a_5+\cdots\cdots\right)+b_4+A^4R_2=0\,,\\
&\cdots\cdots\cdots

with

$$\left.\begin{aligned} S_0 &= 2\left(P_0^2 + \frac{1}{3}P_1^2 + \frac{1}{5}P_2^2 + \cdots\cdots\right), \\ S_1 &= \left(1 + \frac{1}{3}\right)P_0P_1 + \left(\frac{1}{3} + \frac{1}{5}\right)P_1P_2 + \left(\frac{1}{5} + \frac{1}{7}\right)P_2P_3 + \cdots, \\ S_2 &= \left(1 + \frac{1}{5}\right)P_0P_2 + \left(\frac{1}{3} + \frac{1}{7}\right)P_1P_3 + \left(\frac{1}{5} + \frac{1}{9}\right)P_2P_4 + \cdots, \\ &\cdots\cdots\cdots\cdots\cdots\cdots\cdots\cdots\cdots\cdots. \end{aligned}\right\} \quad (25)$$

5. Results of numerical computations

Elimination of b_{2n}'s from (22) and (23) gives equations for determining a_{2n+1}'s which can be written in the form:

$$\begin{bmatrix} 2P_0, & 2P_1, & 2P_2, & \cdot & \cdot \\ \frac{1}{3}P_1, & P_0 + \frac{3}{5}P_2, & P_1 + \frac{5}{7}P_3, & \cdot & \cdot \\ \frac{1}{5}P_2, & \frac{3}{7}P_3, & P_0 + \frac{5}{9}P_4, & \cdot & \cdot \\ \cdot & \cdot & \cdot & \cdot & \cdot \\ \cdot & \cdot & \cdot & \cdot & \cdot \end{bmatrix} \begin{bmatrix} a_1 \\ a_3 \\ a_5 \\ \cdot \\ \cdot \end{bmatrix} = A^3 \begin{bmatrix} -T_0 \\ R_1 - T_1 \\ 2R_2 - T_2 \\ \cdot \\ \cdot \end{bmatrix}. \quad (26)$$

The deflection of the centre of the plate is given by

$$\begin{aligned} w_{\max} &= \frac{P}{64D} \cdot 2b_0 \\ &= -\frac{P}{64D}\left\{2A\left(P_0a_1 + \frac{1}{3}P_1a_3 + \frac{1}{5}P_2a_5 + \cdots\cdots\right) + A^4R_0\right\}. \quad (27) \end{aligned}$$

With the purpose of examining the convergence of the present procedure, numerical calculations have been carried out for the case of a square plate, by taking two, three and four terms of a_{2n+1}'s into account respectively. The results obtained are

$$w_{\max}/(Pa^4/8D) = 0.1736,\ 0.1658 \text{ and } 0.1638.$$

These results may be compared with Love's approximate value 0.16597 and also with more accurate values 0.1622 and 0.1617 which were obtained by Hencky and Timoshenko respectively.

In conclusion, the writer wishes to express his hearty thanks to Professor S. Tomotika for his continual guidance throughout this work.

REFERENCES

1. W. Ritz, Über eine neue Methode zur Lösung gewisser Variationsprobleme der mathematischen Physik. J. f. Math. (Crelle), **135** (1909), 1.
2. H. Hencky, *Der Spannungszustand in rechteckigen Platten* (1913).
3. A. E. H. Love, Biharmonic analysis, especially in a rectangle and its application to the theory of elasticity. Proc. London Math. Soc., **29** (1929), 189.
4. S. Timoshenko, *Theory of Plates and Shells* (1940), 222.

Physical Institute,
Faculty of Science,
University of Kyoto.

Memoirs of the College of Science, University of Kyoto, Series A,
Vol. XXVI, Nos. 1 & 2, Article 2, 1950.

The Pressure Distributions on the Surface of an Obstacle in a Running Viscous Fluid at Small Reynolds Numbers

By

S. Tomotika and **T. Aoi**

(Received May 10, 1950)

1. Introduction

It is well known that the steady flow of an incompressible viscous fluid past a solid obstacle can be successfully dealt with on the basis of Oseen's linearized equations of motion. A number of investigations have been carried out so far by several writers, but they were mainly concerned with the discussion on the drag experienced by an obstacle.

It seems worth while, however, to discuss whether or not the actual flow pattern around a body as observed in experiments can be obtained theoretically from the solution of Oseen's linearized equations of motion. In a previous paper (1), we have therefore carried out detailed investigations on the steady flows of an incompressible viscous fluid past a sphere as well as past a circular cylinder, by making use of the exact analytical solutions of Oseen's equations. The flow patterns around these obstacles have been computed in detail, and the drags experienced by these bodies have also been discussed, making special reference to the pressure drag and the frictional drag separately. Thus, we have arrived at several interesting and important results which are in good agreement with the results of observation.

In this supplementary short note we intend to discuss the pressure distributions on the surface of a sphere and of a circular cylinder, each placed in the steady flow of a viscous fluid at small Reynolds numbers.

Part I. Case of a Sphere

2. Pressure distributions on the surface of a sphere

In the first place, the essential parts of Goldstein's general solution (2) of Oseen's equations in the case of a sphere, which are

necessary for our investigation, will be briefly reproduced for reference.

We assume that at a great distance from an obstacle the fluid flows with constant velocity U in the positive direction of the x-axis. If we denote by u, v and w the rectangular components of the velocity of perturbation due to the presence of the obstacle, Oseen's linearized equations of motion are given in the forms:

$$U\frac{\partial}{\partial x}(u, v, w) = -\frac{1}{\rho}\left(\frac{\partial}{\partial x}, \frac{\partial}{\partial y}, \frac{\partial}{\partial z}\right)p + \nu\nabla^2(u, v, w), \qquad (1)$$

where p is the pressure, ρ the density of the fluid, ν its kinematic coefficient of viscosity and ∇^2 stands for $\partial^2/\partial x^2 + \partial^2/\partial y^2 + \partial^2/\partial z^2$. The fluid being assumed to be incompressible, the equation of continuity is given by

$$\frac{\partial u}{\partial x} + \frac{\partial v}{\partial y} + \frac{\partial w}{\partial z} = 0. \qquad (2)$$

The components of velocity of the perturbation which satisfy these equations are given by

$$\left.\begin{aligned} u &= -\frac{\partial\phi}{\partial x} + \frac{1}{2k}\frac{\partial\chi}{\partial x} - \chi, \\ v &= -\frac{\partial\phi}{\partial y} + \frac{1}{2k}\frac{\partial\chi}{\partial y}, \\ w &= -\frac{\partial\phi}{\partial z} + \frac{1}{2k}\frac{\partial\chi}{\partial z}; \end{aligned}\right\} \qquad (3)$$

while the pressure relative to that at infinity is given by

$$p = \rho U\frac{\partial\phi}{\partial x}, \qquad (4)$$

provided that

$$\nabla^2\phi = 0, \qquad (5)$$

and

$$\nabla^2\chi - 2k\frac{\partial\chi}{\partial x} = 0, \qquad (6)$$

where we have put $k = U/2\nu$.

Introducing spherical polar coordinates (r, θ, ω), the appropriate general solution of equation (5) is expressed in the form:

$$\phi = U\sum_{n=0}^{\infty} A_n \frac{P_n(\mu)}{r^{n+1}}, \tag{7}$$

where $P_n(\mu)$ denotes the Legendre function and A_n's are constants of integration.

On the other hand, the appropriate solution of equation (6) is given by

$$\chi = Ue^{\mu\xi}\sum_{m=0}^{\infty} B_m \chi_m(\xi) P_m(\mu), \tag{8}$$

where we have put $\xi = kr$, $\mu = \cos\theta$, and B_m's are constants of integration. The function $\chi_m(\xi)$ is expressed in terms of the modified Bessel function as:

$$\chi_m(\xi) = (2m + 1)\sqrt{\frac{\pi}{2\xi}} K_{m+\frac{1}{2}}(\xi). \tag{9}$$

We shall denote the components of the velocity of perturbation along r increasing, θ increasing and ω increasing by v_r, v_θ and v_ω respectively. Then, it is evident that $v_\omega = 0$, and after some reductions, we have

$$\begin{aligned} v_r = {} & U\sum_{n=0}^{\infty} \frac{(n+1)A_n}{r^{n+2}} P_n(\mu) \\ & - \frac{U}{2} e^{\mu\xi}\sum_{m=0}^{\infty} B_m \left\{ \frac{m}{2m-1}\chi_{m-1}(\xi) P_m(\mu) + \mu\chi_m(\xi) P_m(\mu) \right. \\ & \qquad \left. + \frac{m+1}{2m+3}\chi_{m+1}(\xi) P_m(\mu) \right\}, \end{aligned} \tag{10}$$

$$\begin{aligned} v_\theta = {} & U\sin\theta \sum_{n=1}^{\infty} \frac{A_n}{r^{n+2}} P_n'(\mu) \\ & + \frac{U}{2}\sin\theta\, e^{\mu\xi}\sum_{m=0}^{\infty} B_m \left\{ \frac{1}{2m-1}\chi_{m-1}(\xi) P_m'(\mu) + \chi_m(\xi) P_m(\mu) \right. \\ & \qquad \left. - \frac{1}{2m+3}\chi_{m+1}(\xi) P_m'(\mu) \right\}, \end{aligned}$$

where accents denote differentiation with respect to μ.

If the radius of the sphere be denoted by a, the boundary conditions at the surface of the sphere are given by

$$v_r = -U\cos\theta\,, \quad v_\theta = U\sin\theta \tag{11}$$

at $r = a$, and these conditions yield the relations between the constants of integration A_n and B_m. Further, after some calculations, it is found that the constants B_m can be determined by solving the following simultaneous equations:

$$\sum_{m=0}^{\infty} B_m \lambda_{m,n}(\xi_0) = \begin{cases} -6 & (n=1)\,, \\ 0 & (n=2,3,\cdots)\,, \end{cases} \tag{12}$$

where ξ_0 stands for ka. For the expressions of the functions $\lambda_{m,n}$, reference should be made to our previous paper (**1**) or to Goldstein's paper (**2**).*

We shall next proceed to the computation of the pressure distributions along a meridian line on the surface of the sphere. Now, the pressure p at any point in the fluid is given by (4), together with the expression for ϕ as given by (7). Since, however, $\partial\phi/\partial x \to 0$ as $r \to \infty$, this p represents, as mentioned already, the pressure relative to that at infinity.

Thus, if we denote the absolute pressure at any point in the fluid by p anew and the corresponding pressure at infinity by p_∞, we have

$$p - p_\infty = \rho U \frac{\partial\phi}{\partial x}\,. \tag{13}$$

In particular, if we denote the pressure on the surface of the sphere by p_s, we have

$$\frac{p_s - p_\infty}{\frac{1}{2}\rho U^2} = \frac{2}{U}\left(\frac{\partial\phi}{\partial x}\right)_{r=a}. \tag{14}$$

Equation (7) gives us immediately the following result:

$$\left(\frac{\partial\phi}{\partial x}\right)_{r=a} = -U\sum_{n=0}^{\infty}\frac{(n+1)A_n}{a^{n+2}}\mu P_n(\mu) + U\sum_{n=1}^{\infty}\frac{A_n}{a^{n+2}}(1-\mu^2)P_n'(\mu)\,.$$

But, this can be transformed into a more elegant form, if we make

* It is to be remarked here that the expressions for our functions $\lambda_{m,n}$ can be obtained from the corresponding Goldstein's by interchanging the suffixes m and n.

use of some recurrence formulae for the Legendre function as well as of the following relations:

$$\left.\begin{aligned}
&\sum_{n=0}^{\infty} \frac{(n+1)A_n}{a^{n+2}} P_n(\mu) \\
&= -\mu + \frac{1}{2} e^{\mu\xi_0} \sum_{m=0}^{\infty} B_m \left\{ \frac{m}{2m-1} \chi_{m-1}(\xi_0) P_m(\mu) \right. \\
&\qquad \left. + \mu \chi_m(\xi_0) P_m(\mu) + \frac{m+1}{2m+3} \chi_{m+1}(\xi_0) P_m(\mu) \right\}, \\
&\sum_{n=1}^{\infty} \frac{A_n}{a^{n+2}} P_n'(\mu) \\
&= 1 - \frac{1}{2} e^{\mu\xi_0} \sum_{m=0}^{\infty} B_m \left\{ \frac{1}{2m-1} \chi_{m-1}(\xi_0) P_m'(\mu) \right. \\
&\qquad \left. + \chi_m(\xi_0) P_m(\mu) - \frac{1}{2m+3} \chi_{m+1}(\xi_0) P_m'(\mu) \right\},
\end{aligned}\right\} \quad (15)$$

which follow immediately from the boundary conditions (11) together with (10).

We thus have

$$\left(\frac{\partial \phi}{\partial x}\right)_{r=a} = U - \frac{U}{2} e^{\mu\xi_0} \sum_{m=0}^{\infty} B_m \left\{ \frac{m}{2m-1} \chi_{m-1}(\xi_0) P_{m-1}(\mu) \right.$$
$$\left. + \chi_m(\xi_0) P_m(\mu) + \frac{m+1}{2m+3} \chi_{m+1}(\xi_0) P_{m+1}(\mu) \right\}. \quad (16)$$

Hence, bearing in mind that the function $\chi_m(\xi)$ is given by (9), we have ultimately

$$\frac{p_s - p_\infty}{\frac{1}{2}\rho U^2} = 2 - e^{\mu\xi_0} \sqrt{\frac{\pi}{2\xi_0}} \sum_{m=0}^{\infty} B_m \left\{ m K_{m-\frac{1}{2}}(\xi_0) P_{m-1}(\mu) \right.$$
$$+ (2m+1) K_{m+\frac{1}{2}}(\xi_0) P_m(\mu)$$
$$\left. + (m+1) K_{m+\frac{3}{2}}(\xi_0) P_{m+1}(\mu) \right\}, \quad (17)$$

and this gives the exact general expression for the pressure coefficient on the surface of the sphere.

Making use of this exact expression, detailed numerical calculations of the values of the pressure coefficient on the surface of the sphere have been carried out in two cases in which the Reynolds number of the flow $R = Ud/\nu$, where d is the diameter of the sphere, is equal to 1 and 2 respectively. The results are shown in Table I and Fig. 1. It is found that there is a good qualitative agreement with experiment.

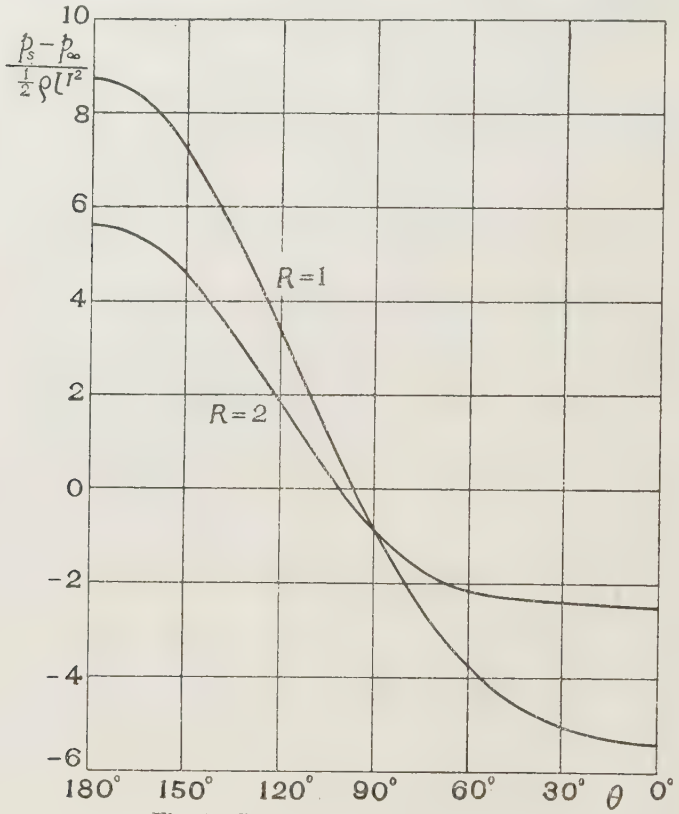

Fig. 1. Pressure distributions on a sphere.

TABLE I.

θ	$R=1$	$R=2$
0°	−5.419	−2.505
30°	−5.070	−2.432
60°	−3.738	−2.160
90°	−0.863	−0.876
120°	3.325	1.800
150°	7.192	4.521
180°	8.770	5.642

Part II. Case of a circular cylinder

3. Pressure distributions on the surface of a circular cylinder

In the previous paper (1) we have obtained the exact analytical solution of Oseen's equations in two dimensions in the case of steady flow of an incompressible viscous fluid past a circular cylinder, by developing similar analysis to Goldstein's in the case of a sphere. Only the essentials necessary for our present discussion will be given here briefly for reference.

We assume that the fluid at infinity flows with constant velocity U in the positive direction of the x-axis, and let u and v be the rectangular components of the velocity of perturbation caused by the presence of the body, which become vanishingly small at a great distance from the body. Then, Oseen's linearized equations of motion are given by

$$U\frac{\partial}{\partial x}(u, v) = -\frac{1}{\rho}\left(\frac{\partial}{\partial x}, \frac{\partial}{\partial y}\right)p + \nu\nabla^2(u, v), \tag{18}$$

where p, ρ and ν have the same meanings as before, and ∇^2 stands for the operator $\partial^2/\partial x^2 + \partial^2/\partial y^2$.

The fluid being assumed to be incompressible, the equation of continuity becomes

$$\frac{\partial u}{\partial x} + \frac{\partial v}{\partial y} = 0. \tag{19}$$

A general solution of these equations can be expressed in the form:

$$\left.\begin{aligned} u &= -\frac{\partial\phi}{\partial x} + \frac{1}{2k}\frac{\partial\chi}{\partial x} - \chi, \\ v &= -\frac{\partial\phi}{\partial y} + \frac{1}{2k}\frac{\partial\chi}{\partial y}; \end{aligned}\right\} \tag{20}$$

and

$$p = \rho U\frac{\partial\phi}{\partial x}, \tag{21}$$

provided

$$\nabla^2\phi = 0, \tag{22}$$

and

$$\nabla^2\chi - 2k\frac{\partial\chi}{\partial x} = 0, \tag{23}$$

where, as before, we have put $k = U/2\nu$.

Introducing polar coodinates (r, θ), the appropriate general solution of equation (22) is given by

$$\phi = UA_0 \log r - U\sum_{n=1}^{\infty} \frac{A_n}{n} \frac{\cos n\theta}{r^n}, \tag{24}$$

where A_n's are constants of integration.

Also, it is found that a general solution of equation (23) which is appropriate to our problem is given by

$$\chi = Ue^{kr\cos\theta} \sum_{m=0}^{\infty} B_m K_m(kr) \cos m\theta, \tag{25}$$

where K_m is the modified Bessel function and B_m's are constants of integration.

Instead of using the rectangular components of velocity u, v, the radial and circumferential components may conveniently be used. If we denote them by v_r and v_θ, we have, after some calculations,

$$\left.\begin{aligned} v_r &= -U\sum_{n=0}^{\infty} A_n \frac{\cos n\theta}{r^{n+1}} - \frac{U}{4} e^{kr\cos\theta} \sum_{m=0}^{\infty} B_m \Big\{ K_{m-1}(kr)\cos m\theta \\ &\qquad + 2K_m(kr)\cos\theta\cos m\theta + K_{m+1}(kr)\cos m\theta \Big\}, \\ v_\theta &= -U\sum_{n=1}^{\infty} A_n \frac{\sin n\theta}{r^{n+1}} + \frac{U}{4} e^{kr\cos\theta} \sum_{m=0}^{\infty} B_m \Big\{ K_{m-1}(kr)\sin m\theta \\ &\qquad + 2K_m(kr)\sin\theta\cos m\theta - K_{m+1}(kr)\sin m\theta \Big\}. \end{aligned}\right\} \tag{26}$$

Denoting the radius of the circular cylinder by a, the boundary conditions to be satisfied at its surface are

$$v_r = -U\cos\theta, \quad v_\theta = U\sin\theta \tag{27}$$

at $r = a$, and these conditions give us immediately the relations between the constants A_n and B_m. Further, it is found that B_m's can be determined by the following simultaneous equations:

$$\sum_{m=0}^{\infty} B_m \lambda_{m,n}(\xi_0) = \begin{cases} 4 & (n=1), \\ 0 & (n=2,3,\cdots), \end{cases} \tag{28}$$

where $\xi_0 = ka$ and the functions $\lambda_{m,n}$ are expressed in terms of the modified Bessel functions I_n and K_n as follows:

$$\lambda_{m,n}(\xi_0) = I_{m-n}(\xi_0)\,K_{m-1}(\xi_0) + I_{m+n}(\xi_0)\,K_{m+1}(\xi_0) + I_{m-n+1}(\xi_0)\,K_m(\xi_0) + I_{m+n-1}(\xi_0)\,K_m(\xi_0)\,. \qquad (29)$$

Now, by (21) and (24), the pressure at any point in the fluid is given by

$$p = \rho U^2 \sum_{n=0}^{\infty} A_n \frac{\cos(n+1)\theta}{r^{n+1}}\,.$$

Obviously this represents the pressure relative to that at infinity, since $p \to 0$ as $r \to \infty$. If, therefore, we use p anew to denote the absolute pressure and also if we denote the corresponding pressure at infinity by p_∞, we have

$$\frac{p - p_\infty}{\frac{1}{2}\rho U^2} = 2\sum_{n=0}^{\infty} A_n \frac{\cos(n+1)\theta}{r^{n+1}}\,. \qquad (30)$$

If, in particular, p_s denotes the pressure on the surface of the cylinder, we have

$$\frac{p_s - p_\infty}{\frac{1}{2}\rho U^2} = 2\sum_{n=0}^{\infty} A_n \frac{\cos(n+1)\theta}{a^{n+1}}\,. \qquad (31)$$

Putting the expressions for v_r and v_θ as given by (26) into the boundary conditions (27), we readily have

$$\sum_{n=0}^{\infty} A_n \frac{\cos n\theta}{a^{n+1}} = \cos\theta - \frac{1}{4} e^{ka\cos\theta} \sum_{m=0}^{\infty} B_m \Big\{ K_{m-1}(ka)\cos m\theta + 2K_m(ka)\cos\theta\cos m\theta + K_{m+1}(ka)\cos m\theta \Big\}\,,$$

$$\sum_{n=1}^{\infty} A_n \frac{\sin n\theta}{a^{n+1}} = -\sin\theta + \frac{1}{4} e^{ka\cos\theta} \sum_{m=0}^{\infty} B_m \Big\{ K_{m-1}(ka)\sin m\theta + 2K_m(ka)\sin\theta\cos m\theta - K_{m+1}(ka)\sin m\theta \Big\}\,,$$

and consequently

$$\sum_{n=0}^{\infty} A_n \frac{\cos(n+1)\theta}{a^{n+1}} = 1 - \frac{1}{4} e^{ka\cos\theta} \sum_{m=0}^{\infty} B_m \Big\{ K_{m-1}(ka)\cos(m-1)\theta + 2K_m(ka)\cos m\theta + K_{m+1}(ka)\cos(m+1)\theta \Big\}\,.$$

Thus, the pressure coefficient on the surface of the cylinder becomes finally

$$\frac{p_s - p_\infty}{\frac{1}{2}\rho U^2} = 2 - \frac{1}{2} e^{ka\cos\theta} \sum_{m=0}^{\infty} B_m \left\{ K_{m-1}(ka) \cos(m-1)\theta \right.$$

$$\left. + 2K_m(ka) \cos m\theta + K_{m+1}(ka) \cos(m+1)\theta \right\}, \quad (32)$$

and this exact formula can conveniently be used to compute the pressure distributions on the surface of the circular cylinder.

Numerical calculations have been carried out in two cases in which the Reynolds number of the flow $R = Ud/\nu$, where d is the diameter of the cylinder, is equal to 0.8 and 4 respectively. The results are shown in Table II and Fig. 2. In this figure, Thom's experimental results (3) for $R = 3.5$ are also shown by small black circles.*

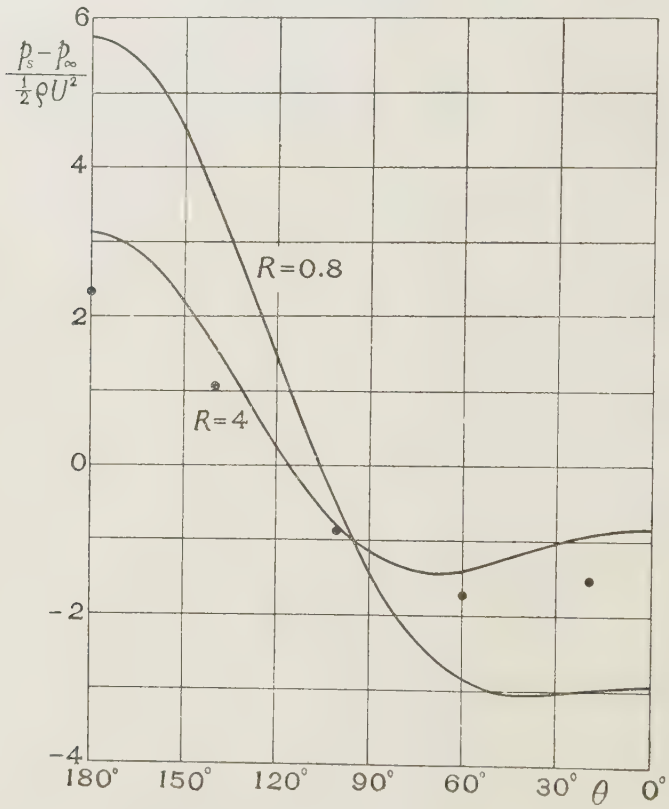

Fig. 2. Pressure distributions on a circular cylinder.

* Thom's experiments were conducted in an oil whose kinematic coefficient of viscosity was $\nu = 0.4$ cm²/sec. The diameter d of the cylinder used by him was 0.318 cm and the undisturbed velocity U of the stream was 4.4 cm/sec.

TABLE II.

θ	$R = 0.8$	$R = 4$
0°	− 2.924	− 0.834
30°	− 3.028	− 1.021
60°	− 2.824	− 1.401
90°	− 1.416	− 1.158
120°	1.430	0.245
150°	4.448	2.194
180°	5.758	3.111

4. Summary and conclusion

In this paper, the computations of the pressure distributions on the surface of a sphere as well as on the surface of a circular cylinder have been made, by making use of the exact analytical solutions of Oseen's linearized equations of motion for the steady flows of an incompressible viscous fluid past these obstacles.

For this purpose, we have first obtained the exact formula for the pressure coefficient in each case, and then detailed numerical computations have been made. Thus, it has been found that the calculated pressure distributions are in good agreement with observation.

Comparing the results of the present paper with those in our previous paper (1), it may be concluded that, as we have expected, Oseen's linearized equations of motion are capable of representing satisfactorily the steady flow of an incompressible viscous fluid past an obstacle, provided that the Reynolds number of the flow is fairly small.

REFERENCES

1. S. Tomotika and T. Aoi, The steady flow of viscous fluid past sphere and circular cylinder at small Reynolds numbers. Quart. Journ. Mech. and Applied Math., Oxford, **3** (1950), 140–161.
2. S. Goldstein, The steady flow of viscous fluid past a fixed obstacle at small Reynolds numbers. Proc. Roy. Soc. London, A, **123** (1929), 225–235.
3. A. Thom, The flow past circular cylinders at low speeds. Proc. Roy. Soc. London, A, **141** (1933), 651–669.

Physical Institute,
Faculty of Science,
University of Kyoto.

Memoirs of the College of Science, University of Kyoto, Series A,
Vol. XXVI, Nos. 1 & 2, Article 3, 1950.

On the Hodograph Method and Analytic Continuation of Solution in the Theory of Compressible Fluid Flow*

By

K. Tamada

(Received July 3, 1950)

1. Introduction

The hodograph method is very useful for the exact treatment of the two-dimensional stationary flow of a compressible fluid. Difficulties occur however when we deal by this method with flows of practical interest, such as the continuous flow past an obstacle and the flow through a nozzle. This is mainly due to the fact that in such cases of flows the series solution constructed in the hodograph plane converges only in a certain restricted region of the field of flow, and therefore the process of analytic continuation of the solution to the remaining region is necessary in order to cover the whole field of flow. This problem of analytic continuation is in general very difficult and seems to have been left unsolved.

In the present paper the writer gives a method for obtaining such an analytic continuation for the fundamental solution which has a branch-point of the prescribed order in the hodograph plane. As an illustrative example, the flow past a circular cylinder is treated in detail by this method.

The writer wishes to express his cordial thanks to Prof. S. Tomotika and Mr. K. Munakata for their continued interest and valuable advices throughout the present work.

* This work has been done in 1947 and a preliminary report in Japanese has been published in stenciled form (1). Publication in English has been unwillingly delayed however for various reasons. Recently the writer has become aware of the interesting papers by S. Bergman (2), M. J. Lighthill (3), T. M. Cherry (4), and S. Goldstein, M. J. Lighthill, and J. W. Craggs (5), where the same problem of analytic continuation has been treated. Their methods are quite different from that used in the present paper. It is found however that for the special case of flow past a circular cylinder, the result of the present paper is in exact agreement with those obtained in (4) and (5).

2. Fundamental equation

As is well known, the two-dimensional steady irrotational flow of a non-viscous compressible fluid, whose pressure is a function of the density alone, is governed in the hodograph plane by the equation:

$$q^2c^2\psi_{qq} + q(c^2 + q^2)\psi_q + (c^2 - q^2)\psi_{\theta\theta} = 0\,, \tag{1}$$

where ψ is the stream function, q, θ the magnitude and the angle of inclination of the velocity vector respectively, and c is the speed of sound at any point. If we assume, as usual, the adiabatic law for the pressure-density relation, c is given as a function of q in the form:

$$\left(\frac{c}{c_\infty}\right)^2 = 1 - \frac{\gamma - 1}{2} M^2 \left\{\left(\frac{q}{q_\infty}\right)^2 - 1\right\}, \tag{2}$$

where q_∞, c_∞ are respectively the velocity magnitude and the speed of sound at a certain standard point suitably chosen in the field of flow, M the Mach number at the standard point, and γ the ratio of the two specific heats of the fluid. For the case of flow past an obstacle, the point in the undisturbed stream at infinity may be conveniently chosen as the standard point. Further, in our future work, we take for convenience the velocity magnitude q_∞ at the standard point as the unit of velocity, so that $q = 1$ there. Inserting (2) in (1), the fundamental equation for the case of adiabatic flow becomes

$$q^2(1 - N^2q^2)\psi_{qq} + q\left(1 + \frac{3 - \gamma}{\gamma - 1} N^2q^2\right)\psi_q + \left(1 - \frac{\gamma + 1}{\gamma - 1} N^2q^2\right)\psi_{\theta\theta} = 0, \tag{3}$$

with

$$N^2 = M^2\left(\frac{2}{\gamma - 1} + M^2\right)^{-1} = q^{-2}{}_{\max}\,,$$

where $q_{\max}$ is the maximum velocity attainable in the field of flow.

As is well known, the equation (3) has a system of particular solutions of the form:

$$\psi = A_\mu w^\mu F^{(\mu)}(N^2q^2)\,, \qquad w = qe^{i\theta}\,, \tag{4}$$

where μ and A_μ are arbitrary constants, and $F^{(\mu)}(N^2q^2)$ is a hypergeometric function defined as

$$F^{(\mu)}(N^2q^2) = \sum_{n=0}^{\infty} k_n^{(\mu)}(N^2q^2)^n ,$$

with

$$k_n^{(\mu)} = \frac{\Gamma(\mu+1)\,\Gamma(a_\mu+n)\,\Gamma(b_\mu+n)}{\Gamma(n+1)\,\Gamma(\mu+n+1)\,\Gamma(a_\mu)\,\Gamma(b_\mu)}, \qquad (5)$$

$$a_\mu + b_\mu = \mu - \frac{1}{\gamma-1}, \qquad a_\mu b_\mu = -\frac{\mu(\mu+1)}{2(\gamma-1)}.$$

It is evident that the hypergeometric series (5) is convergent for $N^2q^2 < 1$, i. e., for $q < q_{\max}$.

3. Fundamental solutions

The limiting case $M \to 0$ (i. e., $N \to 0$) is evidently the case of an incompressible fluid, and in this case the fundamental equation (3) degenerates into the Laplace equation. Then, as can easily be seen, the solution:

$$\psi_0 = \Im\left\{(1-w)^{-\frac{1}{2}} + (1-w)^{\frac{1}{2}}\right\}$$

(where $\Im$ means imaginary part) represents the flow of incompressible fluid past a circular cylinder without circulation. Whilst the solution:

$$\psi_0 = \Im(1-w)^{\frac{1}{2}}$$

expresses the flow of an incompressible fluid through a converging and diverging nozzle. Thus, it will be of fundamental importance to generalize the solution of the type:

$$\psi_0 = (1-w)^{\lambda} \qquad (\lambda: \text{a real constant}) \qquad (6)$$

so as to allow for compressibility.

To this end, we first expand (6) for $|w| = q < 1$ into the series:

$$\psi_0(w) = \sum_{m=0}^{\infty} \binom{\lambda}{m} (-w)^m , \qquad (7)$$

where

$$\binom{\lambda}{m} = \frac{\Gamma(\lambda+1)}{\Gamma(m+1)\,\Gamma(\lambda-m+1)}. \qquad (7a)$$

Then, following usual procedure, we replace each w^m in this series by the corresponding solution (4) for a compressible fluid. It is clear that the resulting series:

$$\psi_\lambda(q,\ \theta) = \sum_{m=0}^{\infty} A_m \binom{\lambda}{m} (-w)^m F^{(m)}(N^2q^2) \tag{8}$$

is also a solution of the fundamental equation (3) so far as it is convergent. The constants A_m's are now to be determined so that the solution (8) should possess a singularity of similar character to that of the starting function (6) at the same point $w = 1$ ($q = 1,\ \theta = 0$) in the hodograph plane. It is evident here that the character of the said singularity depends upon the remainder after the first m terms of the series (8) for large m. Now, the asymptotic behaviour for large m of the hypergeometric function occurring in (8) has recently been investigated by Z. Hasimoto in his doctoral thesis (**6**). According to him, it is valid for large m and $N^2q^2 < \alpha^{-2}$ (subsonic) that

$$F^{(m)}(N^2q^2) \sim \eta^{-\frac{1}{2}}(1 - N^2q^2)^{\frac{1}{2(\gamma-1)}} \omega^m\,, \tag{9}$$

where

$$\eta = \left(\frac{1 - \alpha^2N^2q^2}{1 - N^2q^2}\right)^{\frac{1}{2}},\quad \omega = \frac{2}{1+\eta}\left(\frac{\eta+\alpha}{1+\alpha}\right)^{\alpha}(1 - N^2q^2)^{\frac{\alpha-1}{2}},\quad \alpha = \sqrt{\frac{\gamma+1}{\gamma-1}}. \tag{9a}$$

Therefore, replacing each $F^{(m)}(N^2q^2)$ in (8) by its asymptotic form, we obtain an asymptotic expression of the solution $\psi_\lambda(q, \theta)$ in the vicinity of the singular point in the form:

$$\psi_\lambda(q, \theta) \sim \eta^{-\frac{1}{2}}(1 - N^2q^2)^{\frac{1}{2(\gamma-1)}} \sum_{m=0}^{\infty} A_m \binom{\lambda}{m} (-\omega w)^m + (\text{regular term})\,.$$

This form suggests that the appropriate values of the constants in (8) would be

$$A_m = \omega_1^{-m}, \qquad \omega_1 = [\omega]_{q=1}\,. \tag{10}$$

Then,

$$\psi_\lambda(q, \theta) \sim \eta^{-\frac{1}{2}}(1 - N^2q^2)^{\frac{1}{2(\gamma-1)}}\left(1 - \frac{\omega}{\omega_1}w\right)^{\lambda} + (\text{regular term})\,. \tag{11}$$*

This $\psi_\lambda(q, \theta)$ has apparently the singularity of the required order at the prescribed point $w = 1$, and it degenerates into (6) when N tends

* It may be interesting to note that the asymptotic form (11) is identical with the approximate solution given recently by I. Imai (**7**).

to zero. ($A_m \to 1$, $F^{(m)}(N^2q^2) \to 1$, when $N \to 0$.) Thus, we have shown that the series (8) with the constants A_m's given by (10) may be taken as the fundamental solution for compressible fluid flow, namely:

$$\psi_\lambda(q, \theta) = \sum_{m=0}^{\infty} \binom{\lambda}{m} (-\zeta)^m F^{(m)}(N^2q^2), \quad \zeta = \frac{w}{\omega_1} = \frac{q}{\omega_1} e^{i\theta}, \tag{12}$$

with

$$F^{(m)}(N^2q^2) = \sum_{n=0}^{\infty} k_n^{(m)} (N^2q^2)^n. \tag{12a}$$

It will be seen that (12) is convergent for $q < 1$.

4. A new form for the fundamental solution

Now, the physical field of flow extends usually beyond the range of convergence of the series solution given above, and consequently it is necessary to find the analytic continuation of the said series in order to cover the whole field of flow. It is this problem that we are concerned with in the following.

We first change the order of summation in the double series (12), and rewrite it in the form:

$$\psi_\lambda(q, \theta) = \sum_{n=0}^{\infty} (N^2q^2)^n f_n(\zeta), \tag{13}$$

with

$$f_n(\zeta) = \sum_{m=0}^{\infty} \binom{\lambda}{m} k_n^{(m)} (-\zeta)^m, \qquad \zeta = \frac{q}{\omega_1} e^{i\theta}. \tag{13a}$$

In the next place, we proceed to sum up the series (13a) for $f_n(\zeta)$. Taking into account that $f_n(\zeta)$ is an analytic function of $\zeta = (q/\omega_1)e^{i\theta}$, we introduce the expression (13) for $\psi_\lambda(q, \theta)$ into the fundamental equation (3), and equating the coefficient of each power of N^2 to zero, we obtain the following recurrence equation for $f_n(\zeta)$:

$$f_n(\zeta) = \frac{1}{2n(\gamma - 1)} \Big\{ -\zeta \frac{d}{d\zeta} f_{n-1}(\zeta) + (2\gamma - 1)(n - 1) f_{n-1}(\zeta) - (2\gamma + n)(n - 1)\zeta^{-n} \int \zeta^{n-1} f_{n-1}(\zeta) d\zeta \Big\}. \tag{14}$$

Now, we have obviously

$$f_0(\zeta) = (1 - \zeta)^\lambda, \tag{15}$$

and we can prove by means of the recurrence equation (14) that $f_n(\zeta)$ should have the form :

$$f_n(\zeta) = \zeta^{-n} \sum_{j=-n}^{n} a_j^{(n)} (1-\zeta)^{\lambda+j} + \sum_{m=2}^{n} c_m^{(\lambda)} k_{n-m}^{(m)} \zeta^{-m}, \tag{16}$$

where $a_j^{(n)}$'s are definite constants satisfying the following recurrence formula :

$$\begin{aligned} a_j^{(n)} = \frac{1}{2(\gamma-1)} \frac{1}{n(\lambda+j)} \Big\{ & (\lambda-n+j)(\lambda-n+j+1) \\ & - 2(\gamma-1)(\lambda+j-1)(n-1) + 2(n-1) \Big\} a_{j-1}^{(n-1)} \\ & + \frac{1}{n(\gamma-1)} \Big\{ \gamma(n-1) - (\lambda+j) \Big\} a_j^{(n-1)} + \frac{\lambda+j+1}{2n(\gamma-1)} a_{j+1}^{(n-1)}, \end{aligned} \tag{17}$$

with

$$a_0^{(0)} = 1, \quad a_j^{(0)} = 0 \quad (j = \pm 1;\ \pm 2, \cdots\cdots),$$

and $k_{n-m}^{(m)}$'s are the coefficients defined by (5). While, $c_m^{(\lambda)}$'s are constants of integration to be determined by the condition that (16) should coincide with (13a). Namely, expanding $f_n(\zeta)$ given by (16) in ascending power series of ζ and comparing the result with (13a), we get

$$c_m^{(\lambda)} = (-1)^{n-m+1} (k_{n-m}^{(m)})^{-1} \sum_{j=-n}^{n} \binom{\lambda+j}{n-m} a_j^{(n)}. \tag{18}$$

$$(m = 2,\ 3, \cdots\cdots,\ n)$$

This relation holds for $n \geqq m$, but it does not involve any singularity for $0 < n < m$. Hence, remembering that $c_m^{(\lambda)}$ is independent of n, we can infer the value of $c_m^{(\lambda)}$ by putting formally $n = 0$ in (18), namely

$$c_m^{(\lambda)} = (-1)^{m+1} \frac{\Gamma(\lambda+1)\,\Gamma(a_m)\,\Gamma(b_m)}{\Gamma(m+1)\,\Gamma(\lambda+m+1)\,\Gamma(a_m-m)\,\Gamma(b_m-m)}. \tag{19}$$

That this is true can be shown by mathematical induction, with the aid of the recurrence formula (17), though the details of the analysis are omitted here.

Inserting in (13) the expression (16) for $f_n(\zeta)$, and bearing in mind the relation :

$$(N^2q^2)^n\zeta^{-m} = (N^2\omega_1{}^2\bar{\zeta})^m(N^2q^2)^{n-m}$$

(where $\bar{\zeta}$ means conjugate complex of ζ), we obtain a new expression for $\psi_\lambda(q,\theta)$ in the form:

$$\psi_\lambda(q,\theta) = \psi_\lambda^*(q,\theta) + \chi_\lambda(q,\theta), \tag{20}$$

where

$$\psi_\lambda^*(q,\theta) = \sum_{n=0}^{\infty}(N^2\omega_1{}^2\bar{\zeta})^n \sum_{j=-n}^{n} a_j^{(n)}(1-\zeta)^{\lambda+j}, \tag{20a}$$

$$\chi_\lambda(q,\theta) = \sum_{m=0}^{\infty} c_m^{(\lambda)}(N^2\omega_1{}^2\bar{\zeta})^m F^m(N^2q^2), \tag{20b}$$

with the constants a_j^n and $c_m^{(\lambda)}$ given by (17) and (19) respectively. It should be noticed here that $\chi_\lambda(q,\theta)$ is independently a solution of the fundamental equation and is regular at the point $q=1$, $\theta=0$, as can be shown without difficulty. Consequently, $\psi_\lambda^*(q,\theta)$ given by (20a) must also be a solution which behaves like $\psi_\lambda(q,\theta)$ in the neighbourhood of the singular point $q=1$, $\theta=0$, and degenerates as well into (6) when $N\to 0$, i. e., $\psi_\lambda^*(q,\theta)$ may also be taken as a fundamental solution required.

5. Formulae for the analytic continuation

Now, the new series for $\psi_\lambda(q,\theta)$ obtained above proves to be still convergent outside the circle $q=1$ of convergence of the original series (12).* Hence, we can extend the solution $\psi_\lambda(q,\theta)$ originally defined by the series (12) in the domain $q<1$ over to the region $q>1$ by the expression (20).

Further, we can obtain from (20) the analytic continuation of (12) in a form of hypergeometric-trigonometric series similar to (12) in the following way. First, we expand $\psi_\lambda^*(q,\theta)$ as given by (19a) in descending power series of ζ:

$$\psi_\lambda^*(q,\theta) = \sum_{n=0}^{\infty}(N^2q^2)^n f_n^*(\zeta),$$

where

* This form (20a) of the fundamental solution is especially fitted for the purpose of practical calculation. In fact, by carrying out numerical calculations in the case of flow past a cylindrical body the writer has found that a single series of this type can describe the whole field of flow near the surface of the cylinder, and there is no need of analytic continuation even when the flow becomes partly ultrasonic.

$$f_n^*(\zeta) = \sum_{m=0}^{\infty} \binom{\lambda}{m} k_n^{(\lambda-m)} (-\zeta)^{\lambda-m}.$$

Then, interchanging the order of summation, we are led to the result:

$$\psi_\lambda^*(q, \theta) = \sum_{m=0}^{\infty} \binom{\lambda}{m} (-\zeta)^{\lambda-m} F^{(\lambda-m)}(N^2 q^2). \tag{21}$$

It can be shown that this series is convergent in the domain $1 < q < q_{\max}$. Eqs. (12), (20) and (20b), together with (21) just obtained, give finally the required formulae for the analytic continuation in the form:

$$\psi_\lambda(q, \theta) = \begin{cases} \sum_{m=0}^{\infty} \binom{\lambda}{m} (-\zeta)^m F^{(m)}(N^2 q^2), & (0 < q < 1) \\ \sum_{m=0}^{\infty} \binom{\lambda}{m} (-\zeta)^{\lambda-m} F^{(\lambda-m)}(N^2 q^2) + \chi_\lambda(q, \theta), & (1 < q < q_{\max}) \end{cases} \tag{22}$$

$$\psi_\lambda^*(q, \theta) = \begin{cases} \sum_{m=0}^{\infty} \binom{\lambda}{m} (-\zeta)^m F^{(m)}(N^2 q^2) - \chi_\lambda(q, \theta), & (0 < q < 1) \\ \sum_{m=0}^{\infty} \binom{\lambda}{m} (-\zeta)^{\lambda-m} F^{(\lambda-m)}(N^2 q^2), & (1 < q < q_{\max}) \end{cases} \tag{23}$$

where

$$\chi_\lambda(q, \theta) = \sum_{m=2}^{\infty} c_m^{(\lambda)} (N^2 \omega_1^2 \bar{\zeta})^m F^{(m)}(N^2 q^2). \tag{24}$$

$\psi_\lambda(q, \theta)$ and $\psi_\lambda^*(q, \theta)$ are connected by the relation:

$$\psi_\lambda(q, \theta) = \psi_\lambda^*(q, \theta) + \chi_\lambda(q, \theta). \tag{25}$$

It may be added here that $\chi_\lambda(q, \theta)$ can be shown to be convergent in the whole domain $0 < q < q_{\max}$ provided that $M < 1$.

6. Flow past a circular cylinder

As an illustrative example, we now apply the results obtained above to the case of flow past a circular cylinder without circulation. In this case, the solution for incompressible flow is, as mentioned previously, given by

$$\psi_0 = \Im\left\{(1-w)^{-\frac{1}{2}} + (1-w)^{\frac{1}{2}}\right\}. \tag{26}$$

The corresponding solution for compressible flow may be put in the form:

$$\psi^* = \Im\left\{\psi^*_{-\frac{1}{2}} + A_1\psi^*_{\frac{1}{2}} + A_3\psi^*_{\frac{3}{2}} + \cdots\cdots\right\}, \tag{27}$$

where $\psi^*_{-\frac{1}{2}}$ etc. are given by (23) and $A_1, A_3, \cdots\cdots$ are constants to be determined by the boundary condition. The fundamental solutions $\psi^*_{-\frac{1}{2}}$ etc. are used here instead of $\psi_{-\frac{1}{2}}$ etc., because of the symmetry of flow about the axis $\theta = 0$. In the following, we take only the first two terms in (27). Then the constant A_1 is determined to be equal to 1 by the condition that the cylinder should be blunt-nosed at the stagnation points. Hence,

$$\psi^* = \Im\left\{\psi^*_{-\frac{1}{2}} + \psi^*_{\frac{1}{2}}\right\}. \tag{28}$$

After some calculations, we obtain finally the result that

$$\psi^* = \begin{cases} -\sum_{m=2}^{\infty}\left\{\dfrac{(2m-2)!}{2^{2m-2}m!\,(m-2)!}\left(\dfrac{q}{\omega_1}\right)^m + 2(m+1)c_m^{(\frac{1}{2})}N^{2m}(\omega_1 q)^m\right\} \\ \qquad\qquad \times F^{(m)}(N^2q^2)\,\sin m\theta\,, \qquad (q<1) \\ \left(\dfrac{q}{\omega_1}\right)^{\frac{1}{2}}F^{(\frac{1}{2})}(N^2q^2)\cos\dfrac{\theta}{2} - \sum_{m=0}^{\infty}\dfrac{(2m+3)(2m)!}{2^{2m+1}m!\,(m+1)!}\left(\dfrac{q}{\omega_1}\right)^{-\frac{1}{2}-m} \\ \qquad\qquad \times F^{(-\frac{1}{2}-m)}(N^2q^2)\cos\dfrac{2m+1}{2}\theta\,, \quad (q>1) \end{cases} \tag{29}$$

where we have used an obvious relation:

$$c_m^{(\lambda-1)} = \left(\frac{m}{\lambda}+1\right)c_m^{(\lambda)}. \tag{30}$$

It will be seen that this result is in exact agreement with those obtained by T. M. Cherry (4) and S. Goldstein, M. J. Lighthill, and J. W. Craggs (5). Cherry has carried out numerical computation of the flow-field corresponding to (29). According to him, the solution (29) represents in the physical plane the flow past a nearly circular cylinder which has two axes of symmetry, one parallel and the other

perpendicular to the direction of the undisturbed stream. The shape of the cylinder gradually deforms as the Mach number of the stream is increased, and the deformation becomes so conspicuous at high Mach numbers that no definite conclusion can be obtained as to the state of flow past a cylinder of exactly circular shape.

If, however, we take at least the first three or four terms in (27), we can get certainly a closer approximation to the shape of the boundary, and it may become possible to discuss more completely the state of affairs in the field of flow at high Mach numbers. The results of calculations developed in this direction will be published in the near future.

REFERENCES

1. K. Tamada, On the hodograph method and analytic continuation of solution in the theory of compressible fluid flow. Preliminary Report, Tomotika Research Laboratory, Faculty of Science, University of Kyoto, No. **20** (1948) (in Japanese, and in stenciled form).
2. S. Bergman, On two-dimensional flows of compressible fluids. N. A. C. A. Tech. Note, No. **972** (1945).
3. M. J. Lighthill, The hodograph transformation in trans-sonic flow. III. Flow round a body. Proc. Roy. Soc. A, **191** (1947), 352—369.
4. T. M. Cherry, Flow of a compressible fluid about a cylinder. Proc. Roy. Soc. A, **192** (1947), 45—79.
5. S. Goldstein, M. J. Lighthill, and J. W. Craggs, On the hodograph transformation for high-speed flow. I. A flow without circulation. Quart. Journ. Mech. and Applied Math., **1** (1948), 344—357.
6. Z. Hasimoto, On the solution of some boundary value problems in compressible fluid flow. Dissertation, University of Kyoto, (1948).
7. I. Imai, Application of the W. K. B. method to the flow of a compressible fluid, I. Journ. Math. and Phys., **28** (1949), 173—182.

Memoirs of the College of Science, University of Kyoto, Series A,
Vol. XXVI, Nos. 1 & 2, Article 4, 1950.

A Study of Ultrasonics by Magnetostriction Vibrators

By

Yoshihito Takesada

(Received January 12, 1950)

1. Introduction and summary

The present paper describes the results of some experimental and theoretical studies on underwater ultrasonics. In experimental work here described, use has been made of some appropriate magnetostriction vibrators for the radiation and reception of underwater ultrasonics (up to about 60 Kc) (**1**).

It is shown, in the first place, that in case when an exciting current of equal strength is applied, the efficiency of a vibrator made of particular Al-Fe alloy containing about 13 % Al (which has been termed "Alfer" by Dr. H. Masumoto) is of the same order of magnitude as the efficiency of an Ni vibrator, but when an appropriate exciting current is applied, the Alfer vibrator is more sensitive than the Ni vibrator (**2**, **3**).

Next, it is shown that the efficiency of a modified vibrator made of ferro-magnetic substance with inserted thin plates of non-magnetic substance is far greater than that of a vibrator made of ferro-magnetic substance only. Thus, for example, the Ni vibrator with inserted Al thin plates is far more effective than the unmodified simple Ni vibrator.

In case when the sound waves of high power are radiated by a magnetostriction vibrator to the surrounding water, the medium becomes in a metastable state and consequently an abnormal absorption of sound waves occurs. Thus, the intensity of sound waves radiated from a vibrator is diminished abruptly in the very neighbourhood of the vibrator and then the damped sound waves propagate in the medium with the attenuation factor appropriate to the condition of the medium.

As is well known, the absorption coefficient of weak sound waves can be calculated by the aid of Stokes's formula, but the absorption coefficient of intense sound waves (ultrasonics) cannot be obtained by

the same formula. Thus, bearing in mind the fact that air-bubbles are liable to be generated in the water in the vicinity of a vibrator, theoretical discussions are made on the absorption of intense sound waves due to air-bubbles in the water, in two cases when the air-bubbles are pulsating and when they are not pulsating (4). It is thus shown that the abnormal absorption of ultrasonics in the water is mainly due to the pulsating air-bubbles.

2. A magnetostriction vibrator made of Al-Fe alloy

The magnetic properties of Al-Fe system alloys were studied in detail by Dr. H. Masumoto. He found that in the external magnetic field of 1200 Oe, the rate of elongation of the length $\delta l/l$ amounts to 50×10^{-6} in the case of 12.68 % Al-Fe alloy, which Dr. Masumoto has termed " Alfer." The present writer has measured the electro-acoustical transformation efficiency of a vibrator made of " Alfer " and found that the transformation efficiency of such a vibrator is of the same order of magnitude as in the case of an Ni vibrator (2).

By carrying out measurements on three Alfer vibrators which are made up of plates of 0.05 cm, 0.04 cm and 0.03 cm thickness respectively, we have investigated the effect of the thickness of thin plates in Alfer vibrators, and it has been found that the efficiency of an Alfer vibrator becomes larger as the thickness of thin plates forming the vibrator becomes smaller.

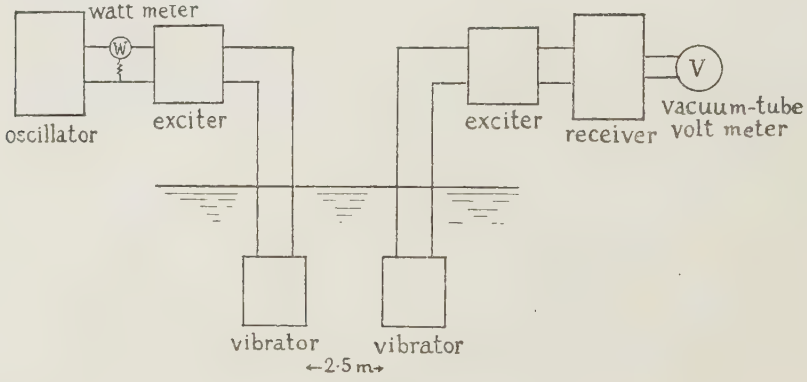

Fig. 1.

In order to compare the electro-acoustical transformation efficiency of the Alfer vibrator with that of the Ni vibrator, we have performed experiments by the device as illustrated in Fig. 1. The depth of the vibrators was 3 m and the exciting current was 15 ampere. The areas

of radiating surfaces of both the vibrators were the same and were 188 cm^2.

The results obtained are shown in Fig. 2, where the input power in watts is taken as the abscissa, while the received voltage in receiver in μV is taken as the ordinate. From this figure, it is found that the Alfer vibrator is more effective than the Ni vibrator.

By placing the Alfer vibrator in the water at various depths ranging from 1 m to 5 m, we have also investigated the effect of the hydrostatic pressure upon the efficiency of the Alfer vibrator. The results thus obtained are shown in Fig. 3 (a), which shows clearly that when the large static pressure is applied to the surface of the vibrator, the sound intensity radiated from the vibrator to the surrounding medium becomes large.

The lowest curve in Fig. 2 gives the sound intensity radiated from the Alfer vibrator placed at a depth of 3 m in the water with disturbed surface. It is seen that there occurs an appreciable attenuation of sound intensity when there are disturbances in the medium which cause the decrease in the hydrostatic pressure.

The relationship between

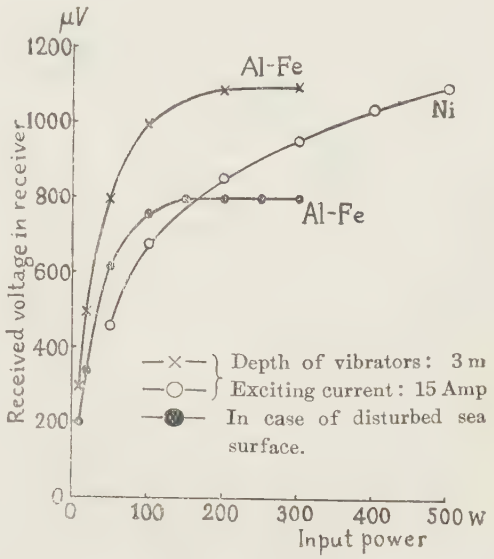

Fig. 2. Resonance frequency: 23.6 Kc
Density of water: 1.02
Temperature of water: 27° C

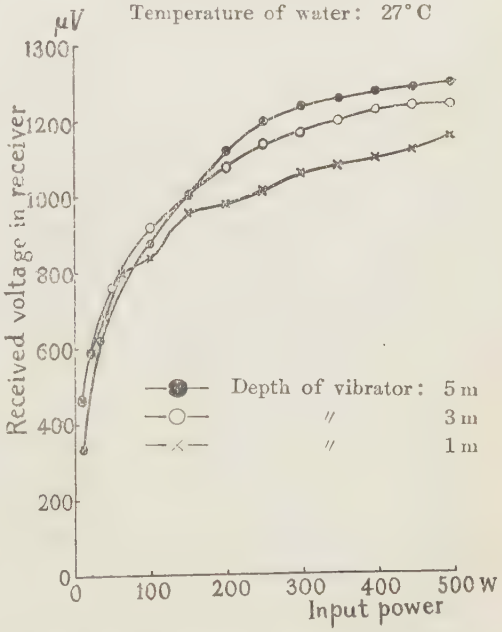

Fig. 3 (a). Resonance frequency: 19.2 Kc
Temperature of water: 26°.6 C
(at depth of 3 m)
Density of water: 1.02

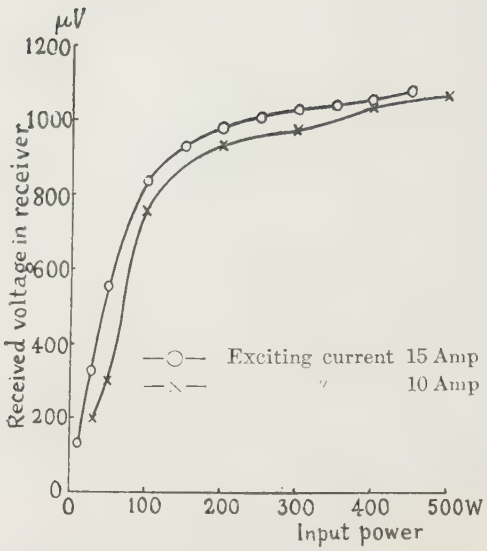

Fig. 3 (b). Resonance frequency: 23.6 Kc
Temperature of water: 25.6° C
Density of water: 1.0185
Depth of vibrator: 3 m

the efficiency of the vibrator and the exciting currents for the case of Alfer vibrator is shown in Figs. 3 (b) and 4. In the measurement for obtaining the results in Fig. 4, the radiating surface of the vibrator was of dimensions 5.0 cm × 2.65 cm and the number of turns of the coil was 18, while the resonance frequency was 22.9 Kc and the temperature of the water was 23.°8 C. From these figures we can find out the appropriate exciting current for obtaining the effective radiation of the Alfer vibrator.

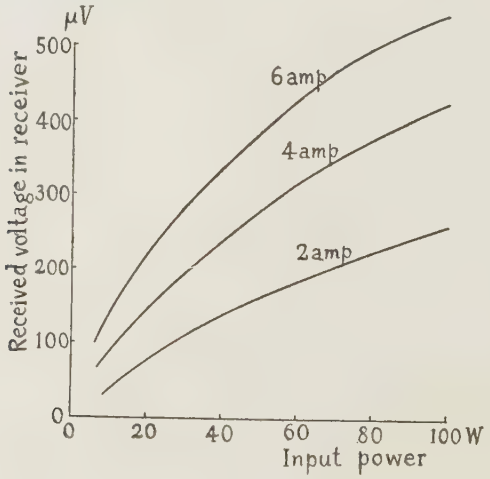

Fig. 4.

3. A magnetostriction vibrator with inserted non-magnetic substances

In order to obtain the effective sound radiation, it is necessary to give high hydrostatic pressure to the medium around a vibrator and consequently a modification of the vibrator becomes necessary. For the

purpose of avoiding the interaction of eddy currents between thin plates forming the vibrator, we have inserted thin non-magnetic plates between thin Ni plates alternately.

When the vibrator is doing the magnetostriction and radiating the sound waves to the surrounding medium, the discontinuous damping appears, as mentioned already, in the surrounding medium. We shall now consider the damping effect in various substances which are commonly used as the material of a vibrator. For reference, the sound velocities in Ni, Alfer, Al and glass, together with the densities of these materials, are first shown in Table I.

TABLE I.

Material	Ni	Alfer	Al	Glass
Sound velocity, c (cm/sec)	4760	4720	5250	4500～5600
Density, ρ (g/cm^3)	8.75	6.55	2.65	2.5～5.9

When the sound waves are transmitted from the vibrator to the surrounding medium, the percentage transmission power varies according as the acoustic resistance ρc of the material of the vibrator varies, and it is found that the percentage transmission powers of mechanical vibration from solids to the surrounding water are respectively 14.1 %, 17.6 % and 35.2 % for Ni, Alfer and Al vibrators. These values have been obtained by applying the laws of reflection and refraction of sound waves to the solid and water.

Thus, if the arithmetic mean of the percentage transmission powers of the constituents be taken as the percentage transmission power of the combined vibrator, the Ni vibrator with inserted thin Al plates becomes 24.65 %. In like manner, the percentage transmission power of the Alfer vibrator with inserted thin Al plates is 26.40 %. It is found therefore that the percentage of the transmitted sound power for the Ni vibrator is smaller than that for the Ni vibrator with inserted thin Al plates, the ratio of the transmission power of the latter to that of the former being $24.65/14.10 = 1.748$. Thus, we see that the percentage of effective transformation in the water of the Ni vibrator with inserted thin Al plates is 1.748 times greater than the simple vibrator made of Ni only. This shows clearly that when thin plates of non-magnetic materials are inserted alternately between thin plates of magnetic substances, there occurs an effective radiation from the surfaces of the plates of non-magnetic substances to the surrounding medium.

Next, we shall consider the damping coefficients of the thin plates forming the vibrator. In case when the thin plates of ferro-magnetic substance are subjected to the driving periodic force $F_1 e^{i\omega t}$, the equations of motion of the thin plates of ferro-magnetic substance and of the thin plates of non-magnetic substance are respectively

$$\left.\begin{aligned} m_{11}\ddot{x}_1 + r_{11}\dot{x}_1 + s_{11}x_1 + m_{12}\ddot{x}_2 + r_{12}\dot{x}_2 + s_{12}x_2 &= F_1 e^{i\omega t}, \\ m_{22}\ddot{x}_2 + r_{22}\dot{x}_2 + s_{22}x_2 + m_{21}\ddot{x}_1 + r_{21}\dot{x}_1 + s_{21}x_1 &= 0, \end{aligned}\right\} \tag{3.1}$$

where

m_{11} : mass of the plates of ferro-magnetic substance,

m_{22} : mass of the plates of non-magnetic substance,

m_{12} : apparent mass of the plates of ferro-magnetic substance, generated from the plates of non-magnetic substance in steady-state motion,

m_{21} : apparent mass of the plates of non-magnetic substance, generated from the plates of ferro-magnetic substance in steady-state motion,

r_{12} : damping coefficient of ferro-magnetic substance as affected by the non-magnetic substance in steady-state motion,

r_{21} : damping coefficient of non-magnetic substance as affected by the ferro-magnetic substance in steady-state motion,

r_{11} : damping coefficient of ferro-magnetic substance only,

r_{22} : damping coefficient of non-magnetic substance only,

$s_{11}x_1$: force required to produce a small displacement from the equilibrium position in the vibrating plate of ferro-magnetic substance,

$s_{22}x_2$: force required to produce a small displacement from the equilibrium position in the vibrating plate of non-magnetic substance,

$s_{12}x_2$: force acting on ferro-magnetic substance by non-magnetic substance,

$s_{21}x_1$: force acting on non-magnetic substance by ferro-magnetic substance.

Neglecting the transient-state motion, we shall consider only the steady-state motion. Then, particular solutions of the above two equations of motion are given by

$$x_1 = Ae^{i\omega t}, \qquad x_2 = Be^{i\omega t}. \tag{3.2}$$

Putting these expressions in the equations of motion we have

$$\left.\begin{aligned} A &= \frac{F_1 Z_{22}}{i\omega(Z_{22}Z_{11} - Z_{12}Z_{21})}, \\ B &= \frac{-F_1 Z_{21}}{i\omega(Z_{22}Z_{11} - Z_{12}Z_{21})}, \end{aligned}\right\} \tag{3.3}$$

where

$$\left.\begin{aligned} Z_{11} &= r_{11} + i(m_{11}\omega - s_{11}/\omega), \quad Z_{12} = r_{12} + i(m_{12}\omega - s_{12}/\omega), \\ Z_{22} &= r_{22} + i(m_{22}\omega - s_{22}/\omega), \quad Z_{21} = r_{21} + i(m_{21}\omega - s_{21}/\omega). \end{aligned}\right\} \tag{3.4}$$

Thus, we have

$$x_1 + x_2 = \frac{Z_{22} - Z_{21}}{i\omega(Z_{22}Z_{11} - Z_{12}Z_{21})} F_1 e^{i\omega t}. \tag{3.5}$$

On the other hand, the displacement of a magnetostriction vibrator made of ferro-magnetic substance only is given by

$$\xi = \frac{F_1}{i\omega Z_{11}} e^{i\omega t}. \tag{3.6}$$

Therefore, in order that the vibration of the Ni vibrator with inserted non-magnetic thin plates should have larger effective efficiency than that of the vibrator made of Ni plates only, it must be that

$$\left.\begin{aligned} \frac{x_1}{\xi} &= \frac{Z_{22}Z_{11}}{Z_{22}Z_{11} - Z_{12}Z_{21}} \geqq 1, \\ \frac{x_2}{\xi} &= \frac{-Z_{21}Z_{11}}{Z_{22}Z_{11} - Z_{12}Z_{21}} \geqq 1, \\ \frac{x_1 + x_2}{2\xi} &= \frac{(Z_{22} - Z_{21})Z_{11}}{2(Z_{22}Z_{11} - Z_{12}Z_{21})} \geqq 1. \end{aligned}\right\} \tag{3.7}$$

From these relations, we have

$$-Z_{21} \geqq Z_{22}, \qquad Z_{12} \leqq 0. \tag{3.8}$$

In the state of resonance, it follows therefore that $-r_{21} \geqq r_{22}$ and $r_{12} \leqq 0$. On the other hand, $-r_{21}$ must be equal to r_{12} in the state of resonance. Thus, we see that r_{22} is of the negative value, and this means that the resistance term in the equation of motion of the plate

of non-magnetic substance must take a negative value. Since, however, this is impossible in the practical case, r_{22} should take a small positive value.

When the efficiency of the vibrator with inserted non-magnetic substance is equal to the efficiency of the vibrator made of ferro-magnetic substance only, we have $x_1/\xi = x_2/\xi = 1$, from which it follows that $Z_{22} = -Z_{21}$ and $Z_{12} = 0$.

Consequently, it is seen that in order to obtain the most effective vibration in the Ni vibrator with inserted plates of non-magnetic substance, we must use such a non-magnetic substance of which r_{22}, r_{21} and r_{11} have the smallest positive values. Such a new vibrator is analogous to a vibrator whose non-magnetic material is loaded on the surface of ferro-magnetic vibrator. The mechanical Q of this new magnetostrictive transducer has a large value in comparison with the usual magnetostriction vibrator.

4. On large absorption of sound waves in the water

The abnormal absorption of the underwater sound waves seems to be due to the presence of air-bubbles in the water. We shall now discuss the effect of such air-bubbles in two cases when the air-bubbles are pulsating and when they are not pulsating.

In the first place, we shall calculate the absorption coefficient of sound waves due to the pulsation of air-bubbles, by assuming that they are of spherical form. The energy loss at the surface of a spherical air-bubble of radius r is given by the product of three quantities: the oscillating pressure of simple harmonic type, the area of the surface of the pulsating bubble and the radial velocity. Since the mean value of the sine term is $1/2$, the mean loss of sound energy per unit time becomes

$$W_1 = \frac{\rho\omega^2 A^2}{8\pi V}, \tag{4.1}$$

where ρ is the density of the water, ω the angular frequency of pulsation and V the velocity of propagation of sound waves, while A is the maximum rate of volume change of the air-bubble so that $A = 4\pi r^2\omega\xi_0$, where ξ_0 is the maximum displacement of a point on the surface of the bubble. Thus, we have

$$W_1 = \frac{2\pi\rho r^4\omega^4\xi_0^2}{V}. \tag{4.2}$$

Now, the volume dilatation of the air-bubble is given by

$$\Delta_1 = \frac{3}{r}\delta r_1 . \tag{4.3}$$

The variation of pressure due to sound waves is given by

$$\delta P = \rho V \dot{\xi} = \frac{\kappa \omega \xi}{V} , \tag{4.4}$$

where κ is the volume modulus of elasticity of the water.

If we denote the volume modulus of elasticity of the air by κ_1, the volume dilatation Δ_1 and the pressure variation δP are connected to each other by the relation $-\Delta_1 = \delta P/\kappa_1$, and therefore we have

$$-\Delta_1 = \frac{\kappa}{\kappa_1}\frac{\omega \xi}{V} . \tag{4.5}$$

Thus, by (4.3) and (4.5) we get

$$-\delta r_1 = \frac{r}{3}\frac{\kappa}{\kappa_1}\frac{\omega \xi}{V} . \tag{4.6}$$

On the other hand, if the sphere of radius r were filled with water instead of the air, we may have $\Delta_2 = \frac{3}{r}\delta r_2$ and $-\Delta_2 = \frac{\kappa}{\kappa}\frac{\omega \xi}{V} = \frac{\omega \xi}{V}$. Therefore, we have

$$-\delta r_2 = \frac{r}{3}\frac{\omega \xi}{V} . \tag{4.7}$$

In order to apply the above results to the practical case of air-bubbles in the sound field, we write $\xi_0 = \xi_{10} - \xi_{20} = \delta r_1 - \delta r_2$, where ξ_{10} is the displacement of a point on the surface of the air-bubble and ξ_{20} is the displacement of a point on the surface of a sphere with the same radius as the air-bubble, which is filled with water. Then, making use of the above expressions for δr_1 and δr_2 given by (4.6) and (4.7) respectively, we have

$$\xi_0 = \frac{r}{3}\left(1 - \frac{\kappa}{\kappa_1}\right)\frac{\omega \xi}{V} . \tag{4.8}$$

Substituting this into the right-hand side of (4. 2) and taking $\kappa_1 = 1.2 \times 10^6$, $\kappa = 2.25 \times 10^{10}$, $V = 1.5 \times 10^5$ and $\rho = 1.0$ in C. G. S. units, we have

$$W_1 = 0.746 \times 10^{-7} r^6 \omega^6 \xi^2 .$$

Thus, the energy loss per unit volume of the underwater sound waves is given by

$$W = nW_1 = 0.746 \times 10^{-7} r^6 \omega^6 \xi^2 n \,, \tag{4.9}$$

where n is the number of air-bubbles contained in unit volume of the water.

On the other hand, if we denote the sound intensity at any point $x = x$ by I and the corresponding quantity at the origin $x = 0$ by I_0, we have

$$I = I_0 e^{-2\alpha x} \,, \tag{4.10}$$

where α is the coefficient of absorption.

Hence, we have

$$W = -\frac{\partial I}{\partial x} = 2\alpha I = \rho V \omega^2 \xi^2 \alpha \,, \tag{4.11}$$

from which we get

$$\alpha = \frac{W}{\rho V \omega^2 \xi^2} \,. \tag{4.12}$$

By the aid of (4.9) and (4.12) the values of the absorption coefficient α have been calculated, assuming various values for the radius r of air-bubbles as well as for the number n of air-bubbles contained in unit volume of the water. The results are shown in Table II.

TABLE II.

Radius, r, of air-bubbles (cm)	Number, n, of air-bubbles in unit volume	Absorption coefficient			Strength at a distance of 1 cm from source with unit intensity		
		10 Kc	20 Kc	30 Kc	10 Kc	20 Kc	30 Kc
10^{-3}	1	7.74×10^{-12}	1.24×10^{-10}	6.27×10^{-10}	1	1	1
10^{-3}	2.39×10^{8}	1.85×10^{-3}	2.96×10^{-2}	1.50×10^{-1}	0.996	0.943	0.741
10^{-2}	1	7.74×10^{-6}	1.24×10^{-4}	6.27×10^{-4}	1	1	0.999
10^{-2}	10^{3}	7.74×10^{-3}	1.24×10^{-1}	6.27×10^{-1}	0.985	0.780	0.285
10^{-2}	2.39×10^{5}	1.85	2.96×10	1.50×10^{2}	0.025	0	0
3×10^{-2}	1	5.64×10^{-3}	9.02×10^{-2}	4.57×10^{-1}	0.989	0.835	0.401
5×10^{-2}	1	1.21×10^{-1}	1.94	9.80	0.785	0.021	0
10^{-1}	1	7.74	1.24×10^{2}	6.27×10^{2}	3×10^{-7}	0	0
10^{-1}	2.39×10^{2}	1.85×10^{3}	2.96×10^{4}	1.50×10^{5}	0	0	0
3×10^{-1}	1	5.64×10^{3}	9.02×10^{4}	4.57×10^{5}	0	0	0
5×10^{-1}	1	1.21×10^{5}	1.94×10^{6}	9.80×10^{6}	0	0	0

Next, we shall discuss the absorption coefficient of the sound waves in case when the air-bubbles are not pulsating. The acoustic resistance of the mixture of water and air-bubbles is given by

$$R = \sqrt{\frac{EE_0\{v\rho_0 + (1-v)\rho\}}{vE + (1-v)E_0}}, \tag{4.13}$$

where ρ_0 and E_0 are the density and the elasticity of the air respectively, while ρ and E are the corresponding quantities of the clear water respectively. v is the total volume of non-resonant air-bubbles in unit volume of the medium.

If we assume that there exist surfaces of discontinuity in the medium, the reflection of sound waves may occur at these surfaces. Let R and R' be the acoustic resistances of the media on two sides of one of such surfaces of discontinuity. Then, the loss of sound power due to the reflection of sound waves at this surface is given by

$$-W\left(\frac{R-R'}{R+R'}\right)^2.$$

If we assume that the sound waves are reflected at the non-pulsating air-bubbles, the loss of sound power in passing through a distance dx is therefore given by

$$dW = -W\left(\frac{R-R'}{R+R'}\right)^2 dx. \tag{4.14}$$

If we put $R' = (\rho + \delta\rho)(V + \delta V)$, this equation becomes

$$dW = -W\left(\frac{\delta R}{2R}\right)^2 dx. \tag{4.15}$$

On the other hand, if the absorption coefficient of sound waves in the medium be denoted by α, the loss of sound power in a thickness dx is given by

$$dW = -\alpha W dx. \tag{4.16}$$

Thus, comparing the above two expressions we have

$$\alpha = \left(\frac{\delta R}{2R}\right)^2. \tag{4.17}$$

Taking $\rho_0 = 0.0012$, $\rho = 1.0$, $E_0 = 1.2 \times 10^6$ and $E = 2.25 \times 10^{10}$ in C. G. S. units, we have, from (4.13),

$$R/R_0 = (1 + 18750\,v)^{-\frac{1}{2}}, \tag{4.18}$$

where R_0 is the acoustic resistance of the clear water.

This equation gives immediately

$$\delta R = -\,9375\,\frac{R^3}{R_0^2}\,\delta v\,, \tag{4.19}$$

and if use is made of this, the expression for α becomes

$$\alpha = \left(\frac{\delta v}{2.133 \times 10^{-4} + 4v}\right)^2.$$

Denoting the radius of non-resonant air-bubbles by r and the number of bubbles in unit volume of the medium by n, we put $\delta v = v - v' = \frac{4}{3}\pi r^3$ and $v = \frac{4}{3}\pi r^3 n$. Then, we have

$$\alpha = \left(\frac{1}{5.094 \times 10^{-5} r^{-3} + 4n}\right)^2. \tag{4.20}$$

The values of the absorption coefficient α have been calculated by this formula, obtaining the results as shown in Table III.

TABLE III.

Radius, r, of air-bubbles (cm)	Number, n, of air-bubbles in unit volume	Absorption coefficient, α
10^{-3}	1	3.84×10^{-10}
10^{-2}	1	3.31×10^{-4}
10^{-2}	10^3	6.10×10^{-8}
10^{-2}	10^5	6.25×10^{-12}
3×10^{-2}	1	1.91×10^{-3}
5×10^{-2}	1	5.15×10^{-2}
10^{-1}	1	6.10×10^{-2}

From this table it will readily be seen that the value of the absorption coefficient increases as the number of air-bubbles decreases. It follows therefore that larger absorption of sound occurs in the region near the boundary surface between the bubbly water and the clear water, where there are only a few air-bubbles in unit volume of the medium, than in intermediate regions where there are many air-bubbles.

Comparing Tables II and III it is readily seen however that large attenuation of the sound waves is mainly due to the presence of pulsating air-bubbles.

Further, by making use of the results given in Tables II and III we have obtained Fig. 5 which shows the relationship between the sound intensity at a distance of 1 cm from the vibrator and the radius of air-bubbles.

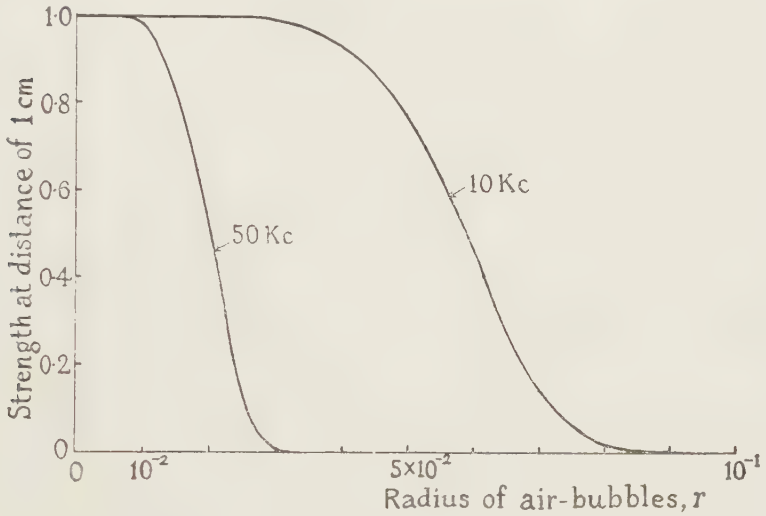

Fig. 5.

In conclusion, the writer wishes to express his cordial thanks to Professor M. Hasegawa and Assistant Professor Y. Tamura for their kind advices. Many thanks are also due to Professor S. Tomotika for his kind encouragement and valuable remarks.

REFERENCES

1. Y. Takesada, Kagaku, **19** (1949), 418.
2. Y. Takesada, Journ. Applied Phys. Japan, **18** (1949), 144.
3. Y. Takesada, Journ. Acous. Soc. America, **22** (1950), 290.
4. Y. Takesada, Journ. Phys. Soc. Japan, **4** (1949), 356.

Memoirs of the College of Science, University of Kyoto, Series A,
Vol. XXVI, Nos. 1 & 2, Article 5, 1950.

On the Activation of Thoria Emitter by Zirconium

By

Shukichi Fukagawa

(Received March 14, 1950)

1. Introduction

Since the invention of the thoriated tungsten filament by Langmuir, it has been in general use as an electron emitter. In this type emitter, the original value 4.55 ev of the work function of tungsten can be reduced to 2.63 ev because of the monoatomic layer of thorium coated on the surface of the filament.

This monoatomic layer, however, is not only easily disintegrated by the impact of ions or electrons, but its working temperature is limited within a very narrow range in the vicinity of 1800° K. To avoid these two disadvantages, an emitter whose tungsten filament is directly coated with thoria powder has been devised. Although such an emitter has been the subject of research by some persons, its range of operating temperature is narrow, and its action as an emitter is unstable. The author got the idea of placing the thin layer of zirconium between thoria and tungsten to utilize its strong absorption of oxygen.

In this paper, the thoria coated emitter produced by pasting the thoria powder directly on the tungsten filament will be denoted by "ThO_2—W" emitter, and the one firstly coated with zirconium powder and then with thoria will be denoted by "ThO_2—Zr—W" emitter.

In the first place, emissions from both type emitters were measured and reasonable values of the work function derived. It is noticeable that "ThO_2—Zr—W" emitter can give sufficient emission at relatively low temperatures.

Then the evaporation heat of zirconium atom on the emitter surface was measured. The value obtained by the author is reasonable as compared with others' data about other emitters.

The mechanism of electron emission from thoria semiconductor can be explained such that (1) the necessary excess thorium atoms can be produced only on the base metal (tungsten or zirconium), (2) the dissociation

$ThO_2 \rightarrow Th + 2O$ requires considerable energy and it can more easily occur by the presence of zirconium, and (3) excess thorium atoms diffuse through thoria layer towards the emitter surface and compensate the evaporation of thorium atoms there.

The author has verified this view, by ascertaining experimentally that in case of "ThO_2—Zr—W" emitter, the emission is limited only by thorium atom diffusion and in case of "ThO_2—W" emitter at low temperatures, the emission is limited by the dissociation of thoria on tungsten, but at higher temperatures, the situation is the same as in the former.

The heat of diffusion and the activation energy for reduction were also measured.

2. The work function of thoria emitter with zirconium layer

(1) *Experimental method*

A tube used in the experiments is illustrated in Fig. 1 (a). In the figure, ① is either the "ThO_2—W" emitter or the "ThO_2—Zr—W" emitter, ② represents anode to measure emission and ③ are guard rings to prevent the error caused by the lower temperature at the both ends of the filament.

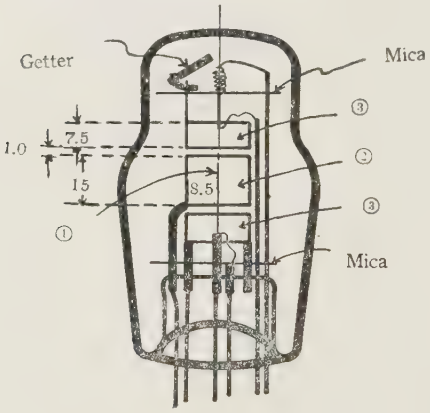

Fig. 1 (a). Diagram of emission measuring tube.
① Emitter
② Anode
③ Guard rings

The temperature measurement was made by an optical pyrometer, and color temperature was calibrated to the true temperature, taking the radiation constant 0.35 at $\lambda = 0.65\ \mu$.

The experimental relations between the heater current of the emitter and the temperature are shown in Fig. 2.

The emission currents into the anode ② were measured by the circuit as shown in Fig. 1 (b), which admits measuring in short times ranging from 10^{-3} sec. to 10^{-1} sec. and the initial values were taken. Because of the roughness at the surface of these emitters, the Schottky effect occurs, and the emission current will be given by the equation:

$$I_a = A\rho DT^2 \exp\left(-\frac{e\phi - \sqrt{eV_a}}{kT}\right), \qquad (1)$$

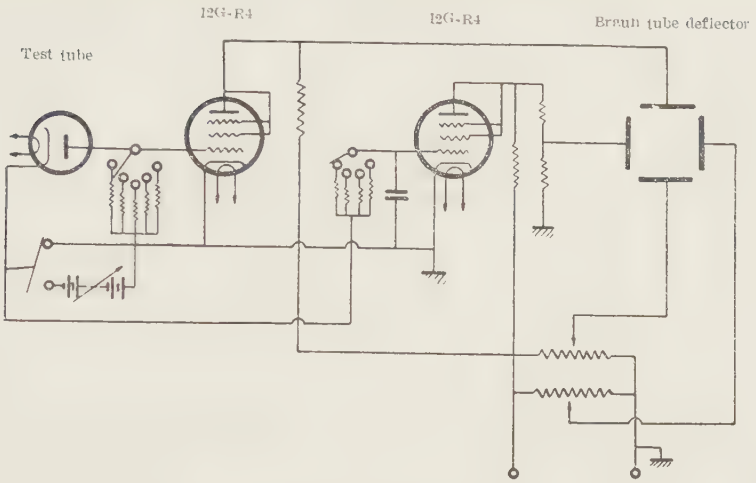

Fig. 1 (b). Diagram of emission measuring circuit.

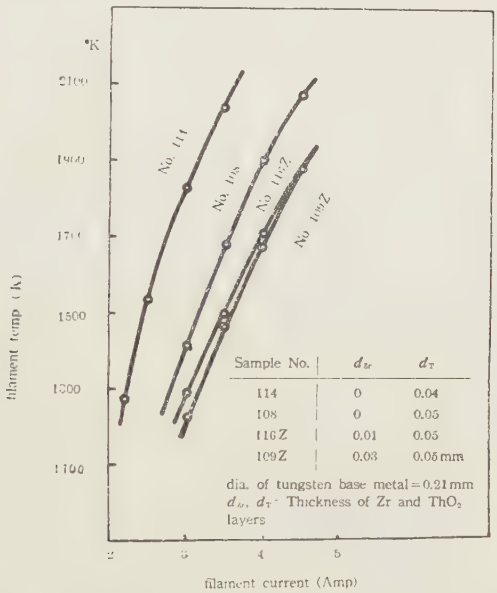

Fig. 2. Relations between filament heating current and their temperature for several samples.

where V_a is anode voltage and ρ is roughness factor of the surface of the emitter, instead of Dushman's equation:

$$I = DAT^2 \exp\left(-\frac{e\phi}{kT}\right). \qquad (2)$$

The measured values of I_a are plotted in Figs. 3 and 4, forming the Schottky lines. These give zero field emission i_s which corresponds to the value at $V_a \rightarrow 0$.

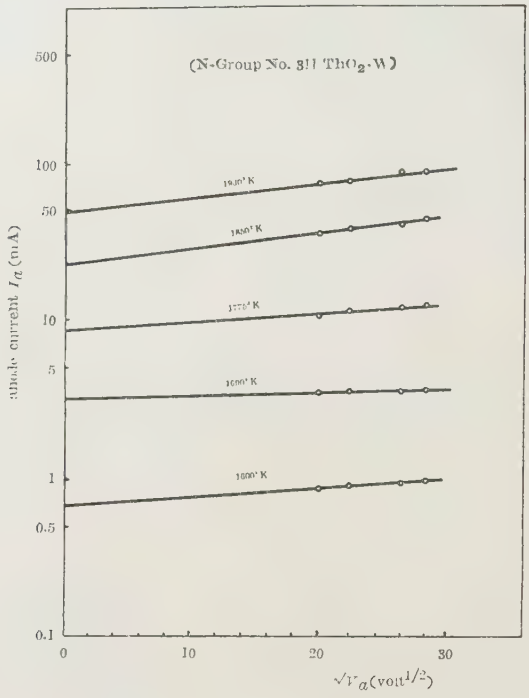

Fig. 3. Schottky lines: $\log I_a = \log I + \frac{300\sqrt{e \cdot 10^7}}{kT}\sqrt{V_a}$.

(11) *Experimental results and discussion*

Different from the thoriated tungsten filament, the thoria coated emitter is the so-called metallic excess type semi-conductor. Accordingly, both the number n_0 of excess thorium atoms and that N of crystal lattice vacancies or frozen-in holes produced by the thermal treatment, supply free electrons n in conduction band. In thermal equilibrium at certain temperature, the following relation is given from the theory of semi-conductor by Nijiboer (**6**):

$$\frac{n(n+N)}{n_0 - n} = \left(\frac{2\pi m kT}{h^2}\right)^{\frac{3}{2}} \exp\left(-\frac{eE}{kT}\right). \qquad (3)$$

The emission current will be as follows:

$$I = ne\rho D\left(\frac{kT}{2\pi m}\right)^{\frac{1}{2}} \exp\left(-\frac{e\chi}{kT}\right), \qquad (4)$$

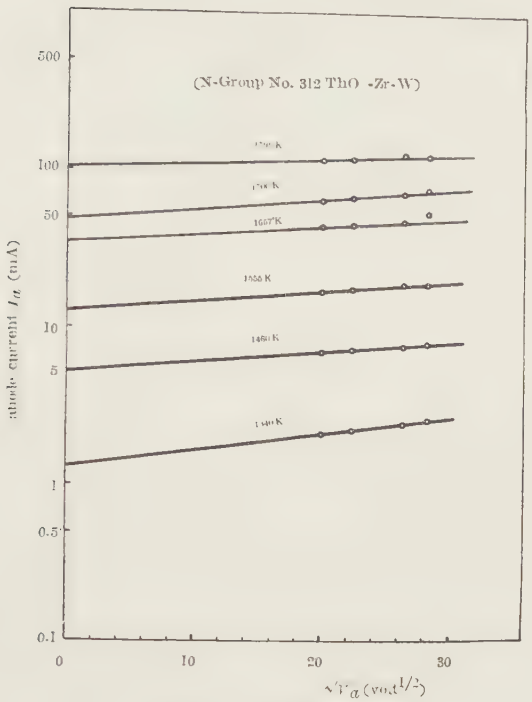

Fig. 4. Schottky lines.

where E denotes potential difference between the impurity level and the bottom of conduction band and χ that between the bottom of conduction band and the level outside of the crystal (see Fig. 5).

In case when $n \ll N$, Eqs. (3) and (4) become respectively

$$n = \frac{n_0}{N}\left(\frac{2\pi m kT}{h^2}\right)^{\frac{3}{2}} \exp\left(-\frac{eE}{kT}\right),$$

and

$$I = A_1 D_1 n_0 T^2 \exp\left(-\frac{e(E+\chi)}{kT}\right). \quad (5)$$

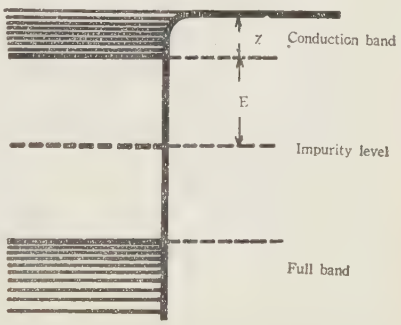

Fig. 5. Potential diagram of semiconductor.

In case when $n \ll N$, the corresponding equations are

$$n = n_0^{\frac{1}{2}}\left(\frac{2\pi m kT}{h^2}\right)^{\frac{3}{4}} \exp\left(-\frac{eE}{2kT}\right),$$

and

$$I = A_2 D_2 n_0^{\frac{1}{2}} T^{\frac{5}{2}} \exp\left(-\frac{e(E/2+\chi)}{kT}\right). \quad (6)$$

The value of n is small when low temperature prevents the full activation and large when activation is sufficiently carried out. It can be known from above equations that, in the medium cases, the work function distributes from $(E + \chi)$ to $(E/2 + \chi)$, according to the emitter's production process. Equation (6) is further modified to

$$\log(I/T^{\frac{n}{2}}) = \text{const} - \frac{e\phi}{kT}, \qquad (7)$$

or

$$\log_{10}(I/T^{\frac{n}{2}}) = \text{const} - 5040\,\phi/T, \qquad (7')$$

which represents the Richardson line. From the slope of the line, the work function can be calculated. (The difference between the values of ϕ obtained from equation (7) and those obtained from the equation (5) caused by the difference between the terms $T^{\frac{n}{2}}$ and T^2 is less than 10 %.) Figs. 6, 7, and 8 show the Richardson lines, where three groups N, S and T correspond to the different refining processes of thoria, and in one group the lines differ according to various exhaustion process.

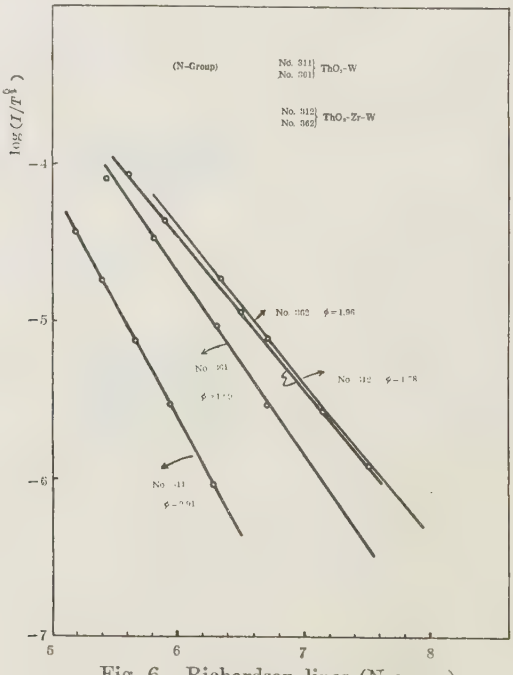

Fig. 6. Richardson lines (N-group).

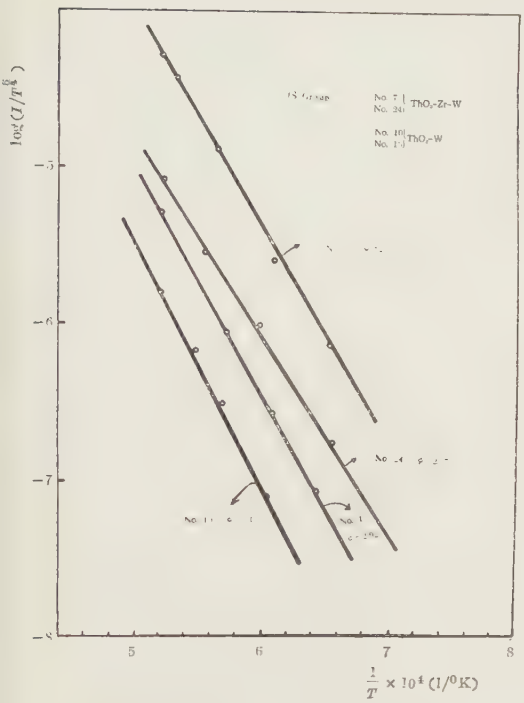

Fig. 7. Richardson lines (S-group).

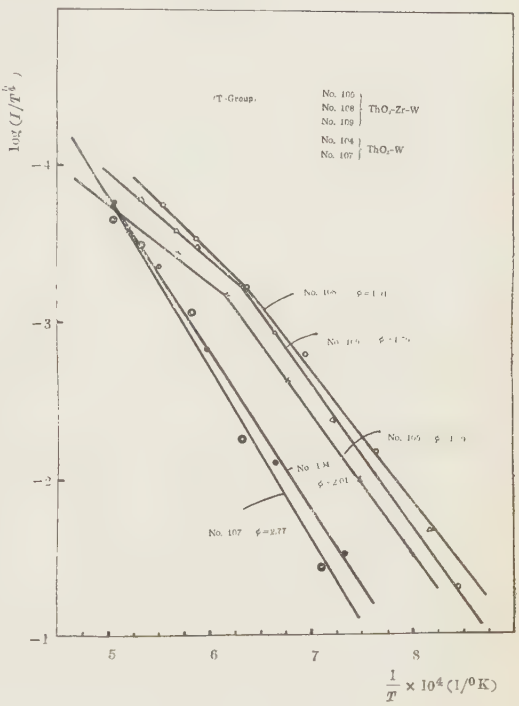

Fig. 8. Richardson lines (T-group).

Table I shows the summary of measured values of work function from these results.

TABLE I. Measured values of work function of "ThO_2—Zr—W" and "ThO_2—W".

Sample	"ThO_2–Zr–W"		"ThO_2–W"	Zr layer thickness	ThO_2 layer thickness
S group thorium oxarate	2.65	2.73 e.V.	2.92 e.V.	0.012 mm	0.11 mm
—(heating)—thoria	2.42		2.91	0.012	
	2.37	2.37	3.13		0.14
N group thorium nitrate	1.96		2.91	0.012	0.15
—thorium oxarate —thoria	1.78		1.99		
T group chemically pure thoria for sale	1.79		2.01	0.03	0.05
	1.99		2.70		
	1.91		2.77		

From this table we see that the measured values distribute over the region from $(E + \chi)$ to $(E/2 + \chi)$, when we take $E = 2.7$ ev and $\chi = 0.43$ ev.

The values of E and χ thus estimated from the values of the work function, however, are not accurate unless quite many measurements are made. Meanwhile, the fact that the resistance of semi-conductor is represented as a function of E and χ allows us another way to measure E and χ from both the resistance and the equation of thermal electron emission. By this method, Arizumi and Ezaki (4) estimated the values of E and χ of " ThO_2—W " emitter as

$$E = 2.5 \text{ ev}, \qquad \chi = 0.7 \text{ ev}.$$

As the existence of zirconium has no direct effect on the emission at the surface as will be seen in the following, these values should coincide.

Recently obtained values of work function of " ThO_2—W " by several experimenters are as follows:

2.6 ev		by Wright (1)
2.67 ,	2.55	by Nanley (2)
3.08 .	2.96	by Yabumoto (3)
1.9 ,	3.2	by Arizumi (4)

Number of samples used in these measurements are from one to three.

The author has found that while in case of " ThO_2—W " emitter the work function before the necessary heat-treatment is generally very large and is lowered only after that process, in case of " ThO_2—Zr—W " emitter, a large emission can be obtained without that process, and thus the work function is originally small. This problem will be discussed in detail in the following.

Another fact to be noticed about these measured values is that, in some cases, a break appears on the Richardson line as shown in Fig. 8. This fact indicates that above certain temperature, the activation proceeds sufficiently and the sample shows the state of the so-called Nijiboer-type represented by equation (6), but below this temperature, it is in a state of poor activation or the so-called Willson-type represented in equation (5). The same phenomenon occurs in case of Wehnelt cathode of (Ba Sr) O_2. This break whose temperature is T_c, is given by putting $n \fallingdotseq N$ in the foregoing theoretical formula (3). Thus,

$$n = N = \left(\frac{n_0}{2}\right)^{\frac{1}{2}} \left(\frac{2\pi m k T_c}{h^2}\right)^{\frac{3}{2}} \exp\left(-\frac{eE}{2kT_c}\right),$$

$$I = A_3 D_3 T_c^{\frac{3}{2}} \left(\frac{n_0}{2}\right)^{\frac{1}{2}} \exp\left(-\frac{e(E/2 + \chi)}{kT_c}\right).$$

3. The evaporation of thorium atoms

(1) *Experimental apparatus*

Excess thorium atoms in "ThO_2—Zr—W" emitter or "ThO_2—W" emitter lie in interphases of the crystal lattice points. Therefore their evaporation is easier than that of thoria locating at the crystal lattice points. Accordingly the evaporation of thorium atoms occurs at a relatively low temperature as compared with that of thoria, whose evaporation is scarcely seen below 2000° K. A test tube to measure the evaporation of thorium is illustrated in Fig. 9. To make a comparison between the cases of "ThO_2—W" and "ThO_2—Zr—W" emitters, both emitters were assembled together in a single tube. ④ is intended to prevent thorium atom evaporation from ① and ② from spattering on the both ends of the filament ③ where temperature is not uniform.

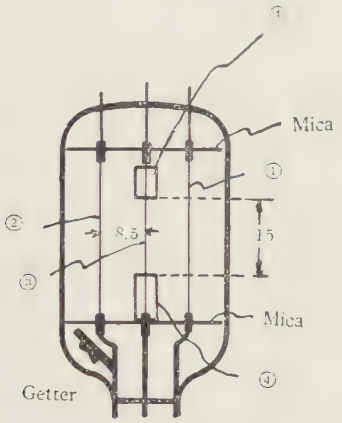

Fig. 9. Tube diagram for measuring the evaporation of thorium.
① ThO_2-Zr-W emitter (0.22 mm dia)
② ThO_2-W emitter (0.22 mm dia)
③ Tungsten probe filament (0.24 mm dia)
④ Screen plate (same potential as ③)

When ① or ② is heated and kept at a certain temperature T, the evaporating thorium atoms spatter on ③ which was heated beforehand at 2500° K for ten minutes to clean up its surface completely and is now kept at 1500° K so that the spattered thorium atoms can diffuse on the surface by surface migration and form uniform monoatomic layer. Thus formed layer of thorium atoms causes a thermal emission from tungsten filament. The quantity of the emission depends upon the surface area covered by the monoatomic thorium atoms. We denote the ratio of covered area to the whole area with θ corresponding to the emission current I and θ_m corresponding to the maximum emission current I_m. The relation of θ/θ_m *vs.* I/I_m as shown in Fig. 10 has been already given by Brattain and Becker (8). Using this relation, the measured values shown in Figs. 12 and 13 can be rewritten in the relation of θ/θ_m *vs.* time t as shown in Fig. 14.

On the basis of these data, we can estimate the time rate of evaporation of thorium atoms.

In practice, ① or ② is heated at a certain temperature T, and at the same time, the emission from filament ③ (1500° K) is measured by the circuit shown in Fig. 11.

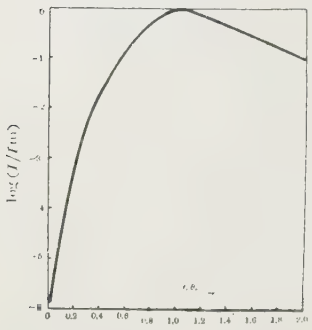

Fig. 10. Variation of electron emission from a thorium-covered tungsten filament as a function of θ, according to W. H. Brattain and J. A. Becker (8).

The emission grows larger in concert with the increase of the thorium atoms spattered on the filament ③ and reaches its maximum value I_m when filament ③ is coated almost entirely by thorium atoms. ($\theta_m \fallingdotseq 1$) Then we heat the filament ③ for five to ten minutes at 2500° K to clean it up, and repeat the measurements in the same way at different temperatures of ① or ②. Thus we obtained the rate of evaporation at different temperatures, as shown in Figs. 12—14.

In Fig. 14, though the plotted points at a certain temperature should be on a

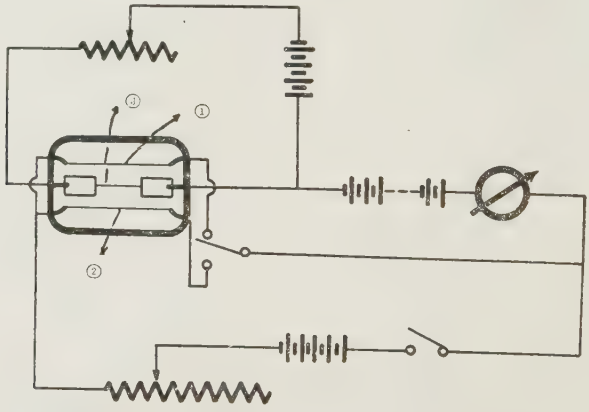

Fig. 11. Diagram of the measuring circuit for the evaporation rate.

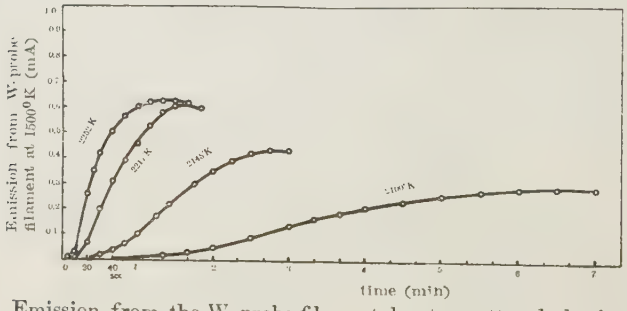

Fig. 12. Emission from the W-probe filament due to spattered thorium which evaporated from ThO_2-W emitter No. E 44 at several temperatures.

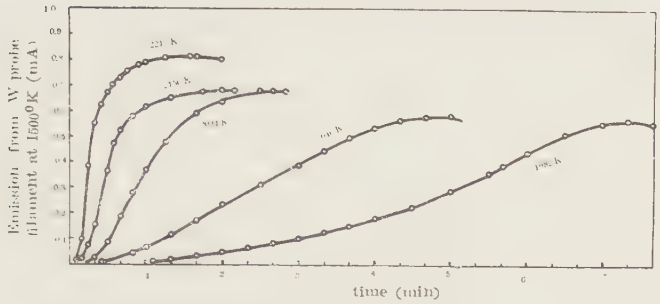

Fig. 13. Emission from the W-probe filament for the ThO_2-Zr-W emitter No. E 43.

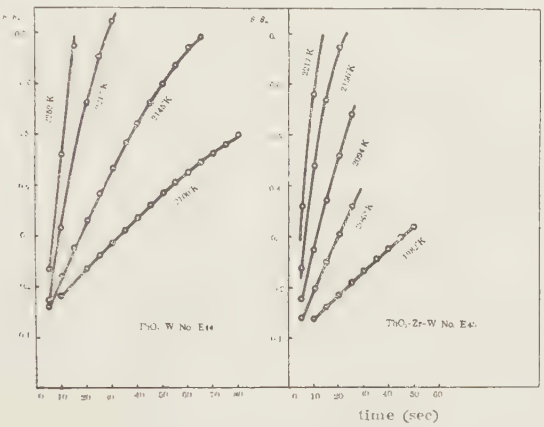

Fig. 14. Time variation of θ, indicated by θ/θ_m *vs.* t from Figs. 12 & 13.

straight line passing through the origin, the obtained values show some deviation. This is due to the insufficient purification of the surface of ③, and partly due to the fact that the thoria evaporating from the surface of ① or ② spatters on the surface of ③ and decreases its effective area for emission. The measurement was made at temperatures 1900° —2200° K at which the evaporation speed is relatively high, for if made at lower temperatuses the evaporation will be slow and the experiment will take so long time that chances of other errors may occur.

(2) *Experimental results*

The quantity of evaporation of thorium-atoms from the filament ① at the temperature $T°$ K, per unit area of the surface and per unit time, is given by

$$Q = Q_0 \exp\left(-\frac{eE_{ev}}{kT}\right), \tag{8}$$

where Q_0 is a constant, and eE_{ev} is the activation energy for evaporation.

When the surface area is covered by the spattered thorium atoms at the ratio θ, the increase $d\theta$ in time dt is related with Q by

$$Q\,dt = \alpha \frac{d\theta}{1-\theta}, \qquad (\theta < 1)$$

where α is a constant determined by the geometrical relation between the filament ③ and the filament ①. Then we have

$$Q = \frac{\alpha}{1-\theta}\frac{d\theta}{dt} = -\alpha \frac{d}{dt}\log(1-\theta). \tag{9}$$

From (9) and (8), we get

$$\log\left[-\frac{d\log(1-\theta)}{dt}\right] = \text{const} - \frac{eE_{ev}}{kT},$$

and differentiating this with respect to $1/T$, we have

$$E_{ev} = -1.97 \frac{\Delta \log_{10}\left[-\dfrac{d\{\log(1-\theta)\}}{dt}\right]}{\Delta\left(\dfrac{10^4}{T}\right)}, \text{ (ev)} \tag{10}$$

or

$$E_{ev} = -4.575 \times 10^4 \frac{\Delta \log_{10}\left\{-\dfrac{d\log(1-\theta)}{dt}\right\}}{\Delta\left(\dfrac{1}{T} \times 10^4\right)}. \text{ (cal/g-atom)} \tag{11}$$

If we calculate the quantity shown in equation (10) from the measured values in Fig. 14, we obtain Fig. 15, and the values of E_{ev} summarized in the following Table II.

The discrepancy among the values in Table II can be understood to have come from the fact that the activation energy for evaporation may be large or small in accordance with the attraction between thorium atoms at the surface and this attraction depends on the density of thorium atoms.

A similar case is seen in the measurement of the evaporation of thorium atoms from the thoriated tungsten filament performed by Andrew (**9**) and Langmuir (**10**), in which the former obtained the value

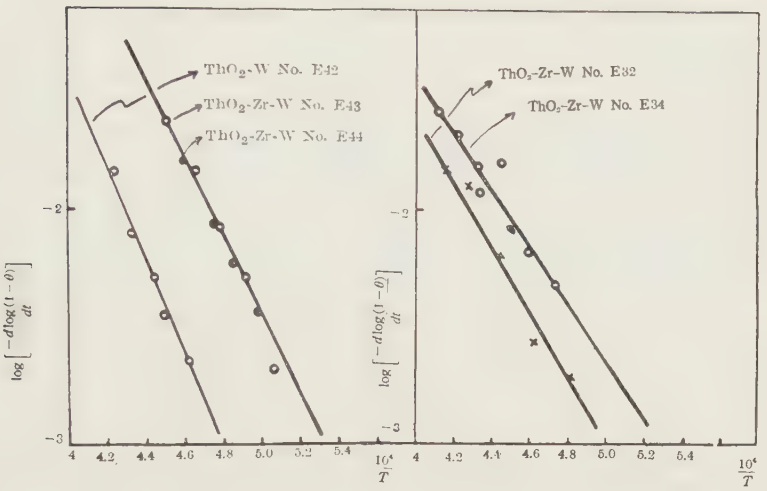

Fig. 15. Evaporation lines calculated from experimental data.

TABLE II.

Activation energy for evaporation of thorium from thoria emitter.

Emitter Sample number	"ThO_2—W" type	"ThO_2—Zr—W" type
E 43		3.34 ev (72,500) cal/g-atom
E 3.4		2.43 (56,400)
E 3.2		2.78 (64,400)
E 4.4	5.48 ev (127,000) cal/g-atom	3.4 (78,800)
E 4.2	4.02 (93,300)	
		(mean value)
		3.0 (69,500)

177000 cal/g-atom while the latter 204000 cal/g-atom. This difference is explained by them as attributable to the fact that in case when the value of θ is large, the attraction between thorium atoms weakens the adsorption of thorium atoms into the tungsten base metal.

In case of the thoria emitter, however, excess thorium atoms lie in interphases of the lattice points. Therefore the activation energy for evaporation may be lower. According to Fan's measurement (**11**), a smaller value of 466000 cal/g-atom was obtained for evaporation of thorium atom in case of sintered cathode made by mingling tungsten and thoria at the rate of 30 : 70 and then sintering them.

In case of barium atom in (Ba Sr) O_2, the values distribute from 3.1 ev to 2.75 ev and the mean value is 2.9 ev. These facts show that the value 3.0 ev we obtained is reasonable.

4. On the activation of thoria emitter by zirconium

(1) *Activation mechanism of thoria emitter*

In the process of electron emission from " ThO_2—Zr—W " emitter, the most remarkable feature is that any additional process for activation is unnecessary. We can imagine that this is because oxygen's affinity to zirconium is strong and oxygen easily makes absorbed diffusion into zirconium lattices and therefore the balance between oxygen in thoria and oxygen-free zirconium at the contact surface of thoria and zirconium is broken, and as a result a part of thoria supplies oxygen atoms into zirconium by absorption. Thus thorium atoms remain within thoria in a state of excess metal and the oxygen atoms diffuse into zirconium.

While in case of (Ba Sr) O_2 emitter oxygen atoms of Ba O fly into vacuum if vacuum is in a high degree and excess Ba atoms are produced on the surface, in case of thoria-emitter, however, such phenomenon does not occur because the dissociation of thoria is not easy. Accordingly, the reduction of thoria occurs only on the base metal. Thus produced thorium atoms diffuse towards the surface according to its concentration distribution. Meanwhile, the evaporation incessantly continues, and a steady state appears when the supply of thorium atoms by the diffusion and their consumption by evaporation balance. The quantity of emission is large or small depending on the number of thorium atoms in the steady state.

The speed of the thermal diffusion of oxygen into zirconium is very high (12). (Zirconium makes solid solution with oxygen atoms uniformly until the quantity of oxygen reaches 40 atomic percent.) Therefore, thoria which contacts with zirconium, is reduced and a very large number of thorium atoms is produced even at lower temperatures. Accordingly, in the case of " ThO_2—Zr—W " emitter it may be assumed that it is the thermal diffusion of thorium atoms in the thoria layer, that limits the supply of thorium for the evaporation. In case of " ThO_2—W " emitter, the situation is the same at high temperatures, but at low temperatures, it is not, as the reduction of thoria at the contact surface with tungsten becomes very difficult against the case of the contact with zirconium. (It has been said that below 2400° K reduction is quite difficult.) In the latter case we understand that the dissociation is the factor that limits the supply of thorium to the surface.

To ascertain our view, we proceed as follows. In the case of " ThO_2—Zr—W " emitter or high temperature " ThO_2—W " emitter, a steady state is brought about when the diffusion of thorium in thoria

and the evaporation of thoria at the surface balance. As the evaporation is proportional to the number n_0 of thorium atoms on the surface, we have

$$A \exp\left(-\frac{eE_{\text{diff}}}{kT}\right) = B n_0 \exp\left(-\frac{eE_{\text{ev}}}{kT}\right),$$

where A and B are constants, and eE_{diff} is the apparent activation energy for diffusion and eE_{ev} the activation energy for evaporation of thorium respectively. Thus, we get

$$n_0 = c \exp\left\{-\frac{e(E_{\text{diff}} - E_{\text{ev}})}{kT}\right\}. \tag{12}$$

n_0 can be measured by the instantaneous measurement at low temperature (1400° K), since the emission is proportional to n_0.

So we obtain

$$\log I = \text{const} - \frac{e(E_{\text{diff}} - E_{\text{ev}})}{kT}. \tag{13}$$

In the other case, the steady state is limited by the production of thorium atoms by the reduction of thoria. Denoting the activation energy for reduction of thoria on the tungsten surface with eE_r, in the same way as in equation (13), we obtain

$$\log I = \text{const} - \frac{e}{kT}(E_r - E_{\text{ev}}), \tag{14}$$

or

$$\log_{10} I = \text{const} - 5040\,(E_r - E_{\text{ev}}). \tag{15}$$

(2) *Experimental results and discussion*

Emitter of the emission test tube is kept at T° K, and when a steady state among the dissociation of thoria, diffusion and evaporation of thorium is almost reached, the temperature is suddenly lowered to 1400° K and emission is measured instantaneously. We repeat such measurement at intervals of three to five minutes and see that the emission settles at a certain value which shows that a steady state is reached. An example of the results of experiment is shown in Fig. 16 and in the form of $\log I$ *vs.* $1/T$ in Fig. 17.

The measurement is made at temperatures between 1400° K and 2200° K. Above 2300° K, both "ThO_2—Zr—W" and "ThO_2—W" make solid solution, and become inadequate as emitter.

It is obviously seen in Fig. 17 that in case of "ThO_2—W" emitter,

the emission curve consists of two straight lines which show that below 1700° K emission is scarce and over 1700° K emission increases rapidly and becomes useful as an emitter. This behavior is explained as follows. At 1700° K, reduction of thoria at the contact surface with tungsten begins and thorium atoms produced diffuse toward the surface and

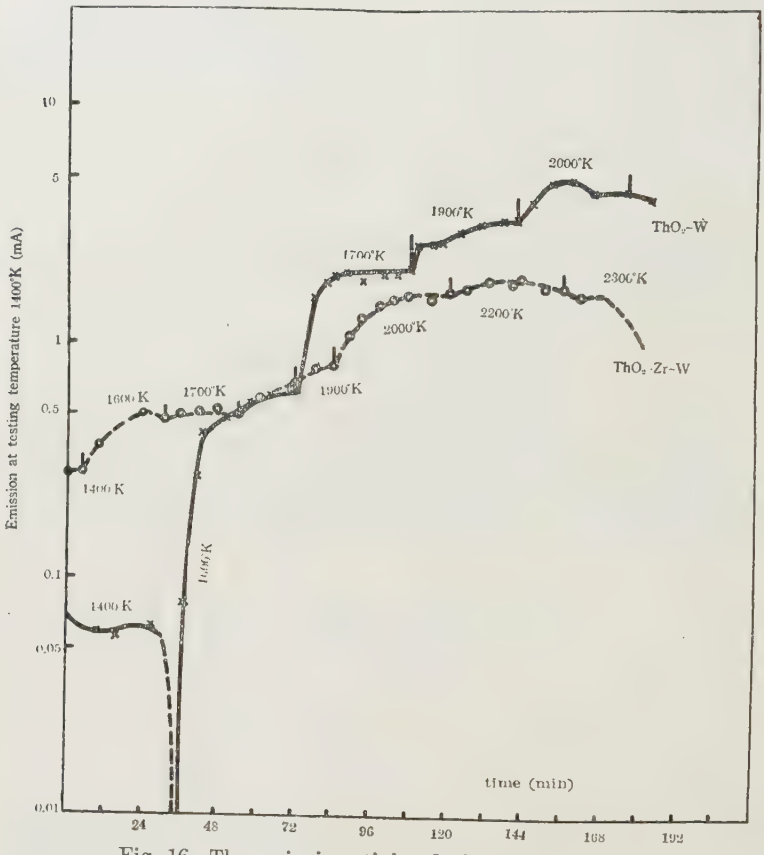

Fig. 16. Thermoionic activity during activation process.

constantly make up for the atoms consumed by evaporation and then the emission becomes stable. Above that temperature, alike in case of "ThO_2—Zr—W" emitter, the steady state is limited by the diffusion of thorium atoms in the thoria. This corresponds to the fact that the emission line in this region is parallel to that of "ThO_2—Zr—W" emitter.

Meanwhile, in case of "ThO_2—Zr—W" emitter the lines correspond to the fact that the steady states are limited by the diffusion throughout.

The results of the measurement thus well verifies our view. Table III has been summarized from Fig. 17, equation (13) and equation (15).

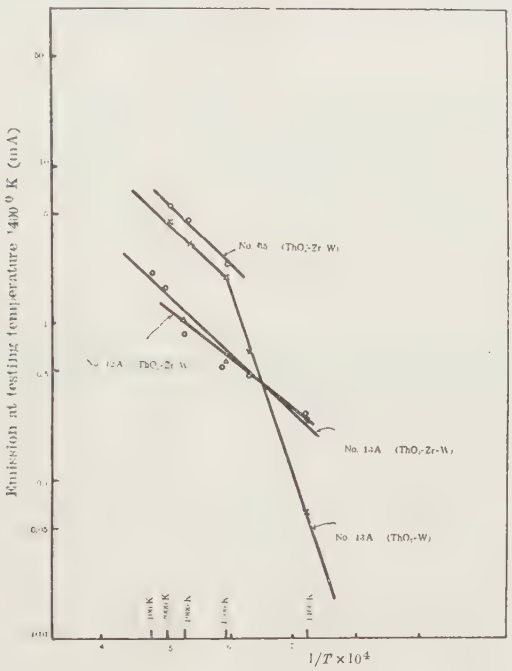

Fig. 17. Thermoionic emissivity of two types of emitter at various temperatures.
(T=temp. of emitter)

TABLE III. Activation energy for diffusion of Th in ThO_2 and that for reduction of ThO_2 on W.

Emitter's sample number	"Th O_2–Zr–W" emitter		"Th O_2—W" emitter			
	E_{diff}—E_{ev}	E_{diff}	E_{diff}—E_{ev}	E_r—E_{ev}	E_{diff}	E_r
N 1.3 A	0.788	3.788	0.785	2.345	3.785	5.345
1.2 A	0.636	3.638				
3.5	0.887	3.887				

$E_{ev} = 3.0$ (ev)

It can be considered that these values are generally smaller than those in case of diffusion in an ordinary crystal, because thoria has a semi-conductor structure with lattice defects. For instance, the values for diffusion of thorium atoms in tungsten obtained by Langmuir (13), Fonda (14) and others in case of body diffusion, surface diffusion and

intercrystalline surface diffusion are 120000, 66400 and 90000 cal/g-atom respectively. To obtain the activation energy for reduction of thoria on zirconium, instead of tungsten, the author is now carrying experiment by means of secondary electron emission.

5. Conclusion

In short, zirconium in "ThO_2—Zr—W" emitter has a great influence on the production of excess thorium atoms. By placing it under the thoria to supply impurity thorium atoms constantly, the operation of the emitter is stabilized at low temperature, without any special high temperature process which is indispensable for "ThO_2—W" emitter to make emission.

The most important application of "ThO_2—Zr—W" emitter will be found in magnetron or klystron which generates high peak power and requires the emitter of low resistance blocking layer and of high stability.

6. Acknowledgement

In concluding this paper, the author wishes to express his cordial thanks to Professors I. Takahashi and Y. Uchida for their kind advices. Also, the author wishes to express his deep gratitude to Mr. Masanori Hiraoka for his cooperation in this study. Lastly, the author's thanks are due to the members of the Committee of Electron Emission of Japan who held a discussion on these problems on Jan. 5th, 1949.

REFERENCES

1. Wright, Nature, **160** (1929), 47.
2. Nanley, J. App. Phys., **19** (1948), 583.
3. Yabumoto, J. Elect. Eng. Japan, **68** (1948), 319 (in Japanese).
4. Arizumi, Report read at the Commitees of Electron Emission of Japan (Nov. 1949).
5. Nanley, Appp. Phys., **19** (1948), 583.
6. Nijiboer, Proc. Phys. Soc., **51** (1938), 575.
7. Yabumoto, Report read at the Commitees of Electron Emission of Japan (Aug. 1946).
8. Brattain and Becker, Phys. Rev., **43** (1933), 428.
9. Andrew, Phys. Rev., **11** (1923), 454.
10. Langmuir, Z. allgem. Chem. **46** (1933), 719.
11. Fan, App. Phys., **20** (1949), No. 7.
12. Fukagawa and Nambo, Inst. Elect. Eng. Japan, **1** (1946), 12.
13. Langmuir, Z. allgem. Chem., **46** (1933), 719.
14. Fonda, Young and Walker, Physics **4** (1933), 1.

Japan Radio Co., Ltd.,
Mitaka, Tokyo.

Memoirs of the College of Science, University of Kyoto, Series A,
Vol. XXVI, Nos. 1 & 2, Article 6, 1950.

The Faraday Effect of Colored Rocksalts

By

Y. Uchida and **K. Fukuda**

(Received July 4, 1950)

1. Introduction

As is well known, the pure rocksalt crystals have the diamagnetic property in the magneto-rotatory power (**1**), but we found that colored rocksalt crystals, which contain F-centers, show a particular property in the rotation of the plane of polarization by the Faraday effect (**2**). This phenomenon results from the electrons captured in the lattice vacancies of Cl^- ions in rocksalt crystals. We believe that the results of our measurements on the magneto-rotatory power of F-centers for the light of Na D-lines, as well as its dispersion curve in the neighbourhood of F-band, give us some important informations about the intrinsic nature of F-centers, which has been discussed from every point of view.

2. Experiments

Colored rocksalt crystals were produced by applying the electric field of about 400 volts per cm between a plate anode and a point cathode to pure crystals heated at temperatures of 570—600° C in an electric furnace. The colored crystals thus obtained contain the density 10^{15}—10^{17} per cm^3 of F-centers. This density N_0 was optically determined from the absorption coefficient k_{max} at absorption maximum and the half-band breadth h of F-band, according to Smakula's formula (**3**):

$$fN_0 = 1.31 \times n_0/(n_0^2 + 2)^2 \times k_{max} h \times 10^{17} \quad \text{for NaCl},$$

where $n_0/(n_0^2 + 2)^2 \sim 0.079$, and f is oscillator strength and is equal to 0.7. The magneto-rotatory angle of polarized light for Na D-lines was measured on these colored crystals by means of "crossed Nicols method." Thus, it was found that this angle is smaller than that of pure transparent ones and that the difference of both angles is proportional to the density of F-centers contained in the colored crystals;

in other words, the Verdet constant of F-centers is negative and its absolute value is proportional to their density. For the specific rotation, $[V]$, of F-centers of Na D-lines we obtained the value of 1×10^3 min/Gauss·cm per gr/cm^3 (**4**), by giving the model of a neutral Na-atom to F-center.

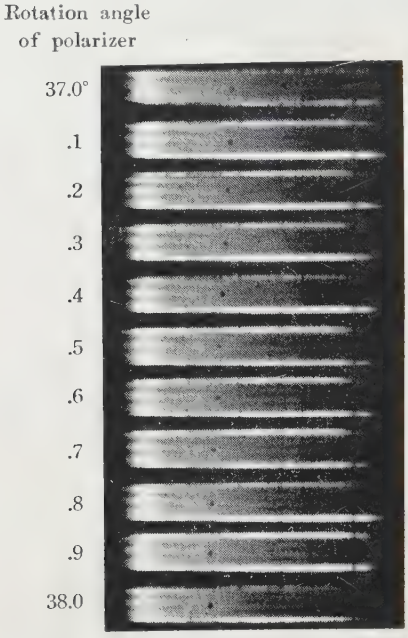

Fig. 1. Spectrograms of the interference fringes produced through Wild's polarimeter.

In succession to the above described experiment we measured the dispersion curve of magneto-rotatory power by taking spectrograms of the interference fringes as shown in Fig. 1 produced through Wild's polarimeter (**5**), which consists of polarizer, analyser and Savart plate, the latter being put just before the analyser (**6**). The place, where the fringes on spectrograms disappear, moves as the polarizer is rotated. It is indicated by a black point on each spectrogram of Fig. 1. The whole arrangement is shown in Fig. 2.

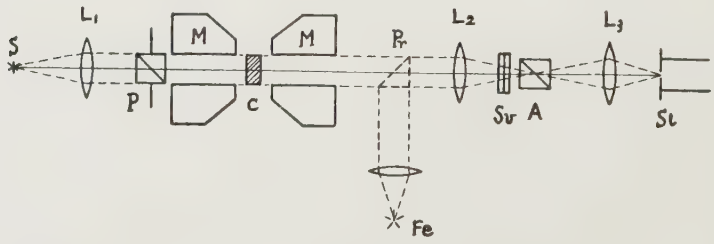

Fig. 2. The arrangement for measuring the rotatory polarization.
S: light source (100 V—500 W), L_1, L_2, L_3 and L_4: lenses, M: electromagnet (Weiss type), C: sample crystal, Pr: a small prism, P: polarizer, A: analyser, Sv: Savart plate, Sl: slit of spectrograph, Fe: Fe arc.

In this figure a small prism Pr is movable and pushed into the optical path to take spectra of Fe arc as comparison. An electromagnet M may be cooled by water and yields 7780 Gauss for the current of 10 Amp. This intensity of the magnetic field was determined by the

measurement on the magneto-rotatory angle of water for Na D-lines.* A Hilger Uviol Glass spectrograph was used in the near ultra-violet region.

Our measurement was carried out in the range from Na D-lines to about 390 mμ and the result is as follows: the magneto-rotatory angle (Verdet constant) of F-centers has negative signs on the longer wave-length side, while it happens the inversion of rotation at one point on the shorter wave-length side of the absorption maximum of the F-band and after that the rotation shows positive signs. In Table I the values of Verdet constants of F-centers are shown for various wave-lengths. In Fig. 3 the magneto-rotatory dispersion curve is shown (7).

TABLE I. The values of the Verdet constant of F-centers for various wave-lengths ($N_0 \sim 10^{16}$)

Wave-length in Å	Verdet constant in min/Gauss · cm
5893 (Na D)	-0.4×10^{-3}
5372	−0.8
5326	−1.5
5230	−1.5
5168	−2.6
5139	−2.2
5050	−2.7
4958	−2.8
4920	−2.9
4872	−3.0
4737	−2.3
4603	−2.2
4531	−2.2
4380	−1.9
4326	−1.7
4305	−0.5
4255	−0.2
4144	−0.1
4046	+0.8
4007	+0.7
3969	+0.8
3928	+1.1

* The Verdet constant of water for Na D-lines is

$$V_D = 0.01311\,(1 - 0.0000305\,t - 0.00000305\,t^2) \text{ for } 3° < t < 98° \text{C}.$$

Cf. J. W. Roger and W. Watson, Phil. Trans., A, **186** (1895), 621; ZS. f. Phys. Chem., **19** (1896), 323.

10. L. Rosenfeld, ZS. f. Phys., **57** (1930), 835.
R. Serber, Phys. Rev., **41** (1932), 489.
11. Z. Yamashita and M. Watanabe, Report Inst. Sci. and Techn., Tokyo Univ., **2** (1948), 4.

Institute of Physics,
Faculty of Science,
University of Kyoto.

Memoirs of the College of Science, University of Kyoto, Series A,
Vol. XXVI, Nos. 1 & 2, Article 7, 1950.

On the K-center in KCl Crystal

By

Masayasu Ueta

(Received July 4, 1950)

1. Introduction

Many interesting investigations on the color centers in alkali-halide crystals were made, both experimentally and theoretically, by Pohl(**1**), Mott and Gurney(**2**), Seitz(**3**), Muto(**4**) and others. Recently, new centers other than F, F′ and U bands have been discovered and called them V, M, R_1, R_2(**3**) and N(**5**) bands respectively. We have also discovered another new band in ultra-violet region in NaCl crystal which was colored by pushing electrons into from a pointed cathode, and have called it K-center(**6**). In our previous paper(**6**) it has been shown that several properties of K-center can be explained satisfactorily, if we make use of the model of F_2^+ which was already used by Seitz(**3**) for explaining Molnar's R_1, R_2 bands. Now that a center similar to K-center in NaCl crystal has been discovered in KCl crystal, the writer has investigated its properties, and to the description of the results of our investigations the present paper is mainly directed.

2. Production of K-center

When a single crystal of KCl ($10 \times 10 \times 20\,mm^3$) is held between a flat anode of platinum (or carbon) and a pointed cathode of platinum (or iron) at temperature of about 430° C, and electrons are pushed into from cathode, the crystal gives rise to a new absorption band ranging from $250\,m\mu$ to $350\,m\mu$ and its maximum absorption wave-length lies at $295\,m\mu$ at room temperature. We call it K-center, since this center has properties similar to K-center in NaCl crystal previously reported, i. e., (1) By irradiation of light lying in the absorption band, the crystal shows luminescence accompanied by photo-conduction ; (2) By heating it above 500° C for ten minutes, both the luminescence ability and K-absorption disappear ; (3) With the continuation of illumination, the luminescence gradually decays, its effect being prominent especially at 200° C.

The curve a in Fig. 1 shows K-absorption spectrum in KCl crystal measured with a Beckman-type quartz monochromator, a quartz photocell and an electrometer, while the curve b shows the absorption curve of the crystal which had lost the luminescence ability.

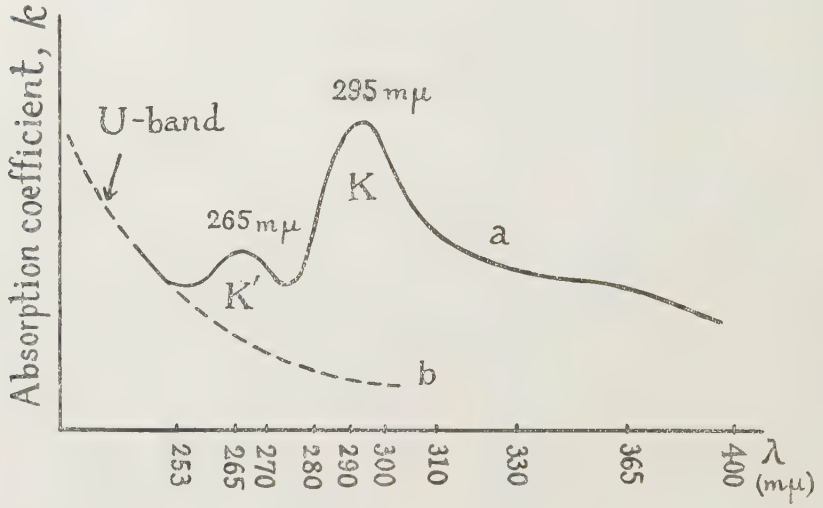

Fig. 1. Absorption spectra of K-center in KCl crystal.

3. Properties of K-center in KCl crystal

As mentioned above, the crystal having K-centers gives rise to photo-conduction when illuminated by the light lying in its absorption band. When the crystal containing K-centers is supported between two flat electrodes applied with an electric field of 1000 V/cm and is illuminated by the monochromatic light from a hydrogen discharge tube, through a powerful quartz spectrograph, then the photo-current flows, and it produces the potential drop across a high resistance ($10^9 \sim 10^{10}\,\Omega$) and causes a deflection of the electrometer. The relation between wave-length of exciting light and flowing photo-current is shown in Fig. 2. It will be seen that the wave-length corresponding to the maximum of the curve coincides with that of K-absorption maximum.

The wave-length region effective for exciting luminescence was photographed by the method of M. Hüniger and J. Rudolf(7). It was found that the maximum effective wave-length also coincides with that of K-absorption maximum.

K-centers are produced most prominently at 430° C and above this temperature the density of K-centers decreases, and F-centers begin to

appear. Above 500° C, however, K-centers are not produced at all in spite of intense coloration of F-centers. It was found that when a clear KCl crystal was heated once at 700° C, which is below its melting point by 50° C, and was then cooled rapidly to 430° C, the density of K-centers was considerably smaller as compared with the case when the crystal was heated to 430° C from room temperature. Thus, it is found that the formation of K-centers in KCl crystal has an intimate connection with the combination of positive and negative ion vacancies.

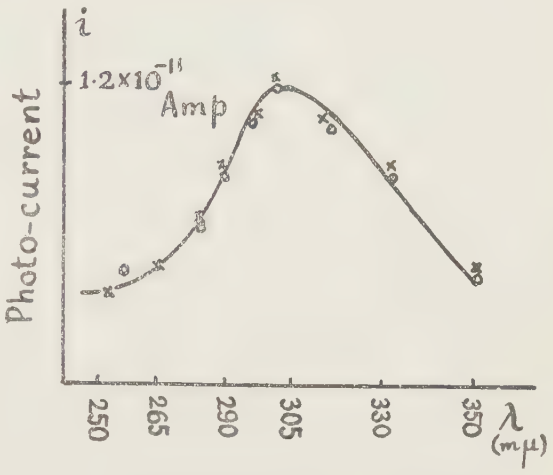

Fig. 2. The relation between photo-currents and wave lengths of excitation.

4. Displacement of K-center

It was previously mentioned that a crystal containing K-centers shows photo-conductivity just as a crystal containing F-center does. As is well known, the F-center moves towards the anode when an electric field is applied, and it is expected that the similar phenomenon would occur in the case of K-center.

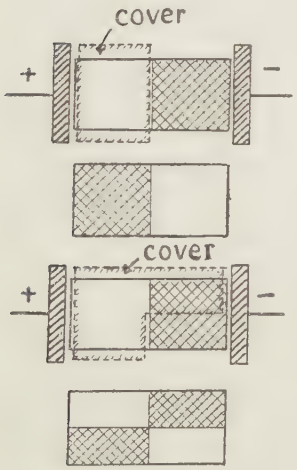

Fig. 3. Displacement of K-centers under the effect of illumination of light. Shadowed portion represents the existence of K-centers.

The crystal having K-centers in its one half was held between the two flat electrodes of carbon and was applied an electric field of 1000 V/cm. In Fig. 3 (a) the shadowed portion represents the existence of K-center. This crystal was heated at 300° C and illuminated by the light in K-absorption region for fifty minutes, on covering the other half of the crystal which does not contain any K-center.

After illumination, the crystal showed luminescence only in the covered portion, but not in the illuminated one (Fig. 3 (b)). The similar experiment was carried out in the case when only the lower half of K-containing portion was illuminated, and the remaining upper half of it as well as the half clear one of the crystal were covered (Fig. 3 (c)). After illumination, the K-containing portions became as shown in Fig. 3 (d). Thus, it has been found that K-centers move under the effect of illumination, but not due to the effect of an electric field only at this temperature.

5. Luminescence of K-center

Luminescence spectrum of K-center of KCl crystal was photographed with twenty minutes exposure and it was found that the spectral region extends from 600 mμ to 700 mμ, the maximum intensity being at 650 mμ. This luminescence does not decay so quickly during excitation at room temperature, but at 200° C, by the excitation of six hours the luminescence power decreases to half value of its initial intensity and at 250° C, K-centers disappear perfectly under this long excitation. At low temperatures, however, K-center does not decay so quickly, in spite of relatively strong emission. Thus, as for the mechanism of luminescence we must consider that electrons which had been raised to the excited state of K-center have to return ultimately to the ground state after emission. We consider that the model of K-center in KCl will be F_2^+ as in the case of NaCl, and since, according to Seitz, F_2^+ is analogous to H_2^+ molecule, the potential curve of F_2^+ (i. e., of K-center) may be as shown in Fig. 4. K-absorption occurs when electrons are raised from the ground state K to the upper excited state K* and then electrons transfer to the repulsion state on emitting the luminescence and ultimately return back to the original ground state.

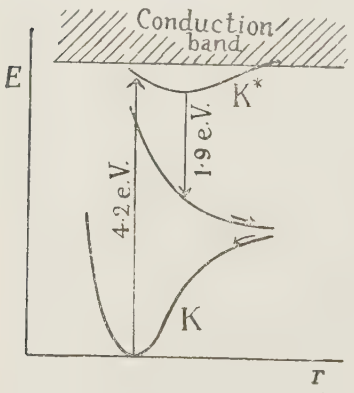

Fig. 4. Potential curve of F_2^+ molecule.

Considering in this way we can infer that the decay of K-center is not prominent at low temperatures, but at higher temperatures, on the other hand, electrons which are raised to the excited state K* move away into the conduction band by obtaining the lattice energy. When the K-center is thus ionized, the residual must be F_2^{++}, and these two negative ion

vacancies flight away from each other under the mutual repulsive force, and consequently the K-center vanishes.

6. Absorption band of 265 mμ in KCl crystal

In KCl crystal in which electrons have been pushed into from a pointed cathode at 560° C ~ 580° C, there is formed the F discoloration with density of $10^{17} \sim 10^{18}/cm^3$, but no K-center is formed at all at these high temperatures. When this crystal is irradiated by the light of shorter wave-length than the K-absorption band and successively by the light in the K-absorption band region, it shows the luminescence due to the K-center. This fact indicates that there exists another absorption band on the shorter wave-length side of K-absorption band. We shall call this K′-center.

As mentioned just in the above, the formation of K′-centers is accompanied by the formation of F-center, but we can also obtain such a crystal that contains K′-center only, in the following way. After the cystal had been colored with F-centers at high temperatures, it is quenched to 430° C, and at this temperature F-centers are driven away under the influence of an electric field. Then, the colored crystal becomes to contain K′-centers only and its maximum absorption lies at about 265 mμ, as will be seen from its absorption spectrum shown by curve a in Fig. 5. When this crystal is irradiated by the light in its absorption region, the K′-absorption will disappear and the K-absorption will be formed (cf, curve b in Fig. 5). If this crystal is again illuminated by the light lying in the K-absorption, it emits luminescence, and by continuing illumination, luminescence and consequently the K-absorption band will ultimately disappear (cf, curve c in Fig. 5).

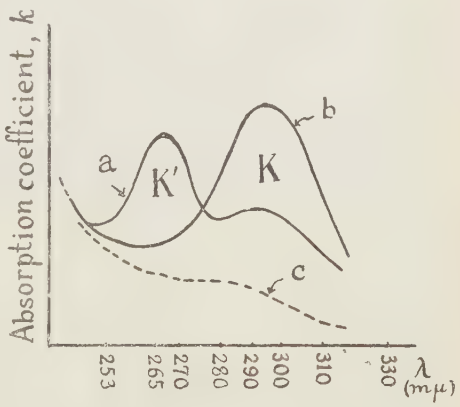

Fig. 5. Absorption spectra of K′-center.

When the crystal containing K′-centers together with F-ceners is irradiated, K′-centers disappear and there remain F-centers only in the crystal, but, by heating the crystal to 430° C, these F-centers are driven away perfectly under the influence of an electric field and the crystal

becomes again to contain K′-centers. Thus, it can be inferred that K′-centers are formed in the process of migration of F-centers.

Since several properties of K-centers in KCl crystal as well as in NaCl crystal can be explained satisfactorily by assuming the model of K-center to be F_2^+, it may be considered that K′-center has a model of F_2 from the K′→K light transformation.

On the other hand, Seitz has given F_2^+ model to Molnar's R_1 and R_2 centers in alkali-halide crystals colored by X-ray. If this model for R_1 and R_2 centers were correct, it may be expected that the same R_1 and R_2 bands should be formed in KCl crystal when it is F-colored additively. Thus, the writer has carried out experiments for the purpose of finding out the effect of visible light on F-centers in KCl crystal which had been colored additively and by electron bombardment or otherwise. But, the expected R_1 and R_2 centers could not be obtained except for one big band whose maximum wave-length is 710 mμ. This band may be considered to be due to the colloids.

In conclusion the writer wishes to express his best thanks to Professor Y. Uchida for his encouragement and guidance throughout the present work, and also to Mr. S. Ibuki for his assistance.

REFERENCES

1. R. W. Pohl, Proc. Phys. Soc. London (Sup.), **49** (1937), 3; Phys. Zeits., **39** (1937), 36.
2. N. F. Mott and R. W. Gurney, "*Electronic Processes in Ionic Crystals*" (1940).
3. F. Seitz, Rev. Mod. Phys., **18** (1946), 384.
4. T. Muto, Progr. Theor. Phys., 4 (1949), 181.
5. E. Burstein, Phys. Rev., **76** (1949), 1254.
6. Y. Uchida. M. Ueta and Y. Nakai, Journ. Phys. Soc. Japan, 4 (1949), 57.
7. M. Hüniger and L. Rudolf, Zeits. f. Phys., **117** (1940), 81.

Institute of Physics,
Faculty of Science,
University of Kyoto.

Memoirs of the College of Science, University of Kyoto, Series A,
Vol. XXVI, Nos. 1 & 2, Article 8, 1950.

Photoconduction of Alkalihalide Crystals which adsorb Dyes

By

Hisao Yagi

(Received July 4, 1950)

1. Introduction

It is well known that the adsorption of certain dyes on the surface of silver-halide crystals extends the spectral region of photo-chemical reactions towards the red and even into the infra-red. In practice, this principle has been applied to photographic emulsion and remarkable progress has been made in this field. The fundamental interpretation of this phenomenon was only given on a general idea by R. W. Gurney (1) and others. Recently it has been ascertained experimentally that the maximum of photographic sensitivity of dyed emulsion coincides with that of absorption of those dyes in adsorbed states, and that it moreover coincides with regions of photo-conductive effects of dyed silver-halides (2, 3).

Since all these experiments, spectroscopic or photo-effective, were carried out on powdered sample, the results obtained are not always sufficient for theoretical considerations. Obviously it seems better to carry out these experiments on large single crystals of silver-halide. But, since these were not obtained when our investigations started, artificial single crystals of rock-salt (4) were used in our experiment as the adsorbent, on which effective dyes were adsorbed, and photo-sensitized photoelectric effects appearing from this adsorption were studied. It has been found that all the facts found in silver-halide emulsion occur also in rock-salt. Thus, our interpretation of photo-sensitizing mechanism can stand on more concrete idea.

2. General principle

Dicyanine-A (E. Merck), Kryptocyanine, Phenosafranine (Fuji Photo.) were used as photo-sensitizing dyes. Artificial single crystals of rock-

salt prepared in our laboratory were used as the adsorbent. Absorption spectra of the photo-sensitizing dyes solved in absolute methyl alcohol (E. Merck) and in distilled water were measured and these spectra were compared with those of dyes which were adsorbed on rock-salt. The adsorption was effected by subliming dye molecules upon the surface of a rock-salt plate by means of evaporation in vacuum. It was noticed that the absorption maxima in adsorbed state was shifted towards the long wave-length side. Then the spectral sensitivity of photo-conductive effect of the rock-salt crystal which adsorbed these dyes, was measured. It was found that these photo-conductive regions almost coincide with the shifted absorption maxima of dyes adsorbed on rock-salt crystals (**3**).

The spectral sensitivity of photo-electric effect of these dyes were measured and the distance of electronic energy levels between stable state and zero-state of those dyes were determined. The photo-electric effects of rock-salt crystals containing F-centers were also measured and rough estimations of differences of electronic energy levels between ground state and zero state of F-centers were made. Thus, correlations of electronic energy levels between rock-salt and these dyes can be obtained.

If use is made of these correlations of electronic energy levels, relations between conduction levels of rock-salt and the lowest excited levels of these dyes can be obtained and mechanism of sensitized photo-conduction may be considered.

3. Experimental results

(1) Absorption of dyes in solution and in adsorbed states.

Absorption spectra of photo-sensitizing dyes solved in methyl alcohol and in water respectively were measured using a monochromator provided with a concave grating of 1 m. focus and a photo-cell (PG–65–G; Mazda) with an amplifier of DuBridge's type (**6**) using UX–54 tube. A 750 watt tungsten-filament projection lamp was used as a light source. The output of the amplifier was connected to the galvanometer (sensitivity : 10^{-10} Amp.) and its deflection was read by a scale 4 m. apart from the galvanometer. This arrangement can be used for the measurement of currents by about 10^{-14} Amp.

In order to investigate the absorption of these dyes in adsorbed state, dyes were evaporated in thickness of about 500 mμ on a rock-salt plate in vacuum and the absorption was measured.

TABLE 1. Absorption of dyes (Unit: mμ)

Dyes	Band	in Water	in Alcohol	on Rock-salt	Δ
Dicyanine-A	α	650	660	690	30
	β	580	615	638	23
Krypto-cyanine	α		705	725	20
	β			665	
	γ			601	
Pheno-safranine	α		558	590	32
	β		528	548	20

Wave-lengths of maximum absorption are shown in Table 1. Shifts (Δ) may be noticed in adsorbed states towards the long wave-length side in comparison with those of solution and their values decrease gradually as the thickness of dyes increases larger than 1 μ.

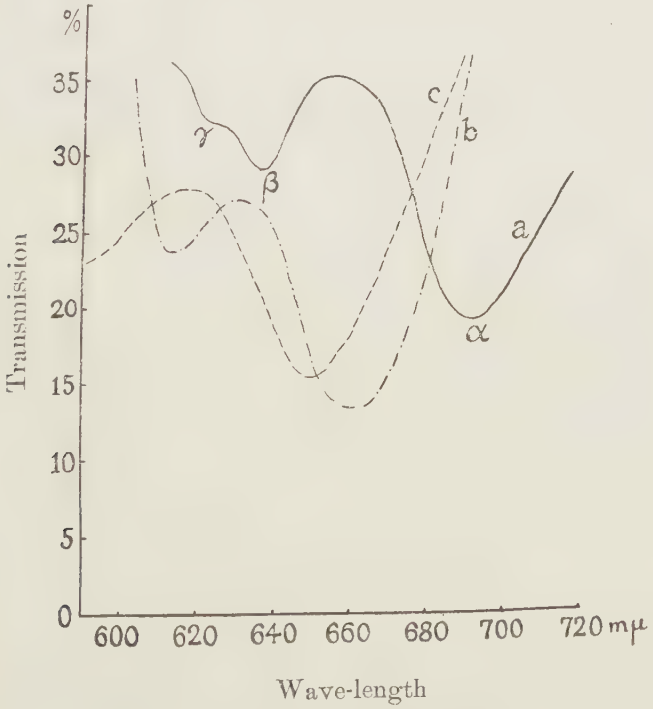

Fig. 1. Absorption curves of Dicyanine-A
a; on Rock-salt, b; in Alcohol, c; in Water.

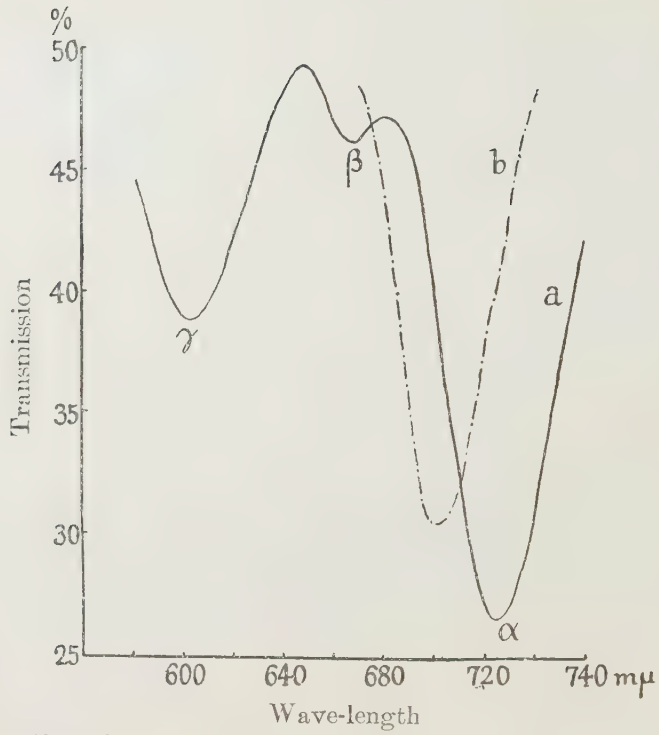

Fig. 2. Absorption curves of Kryptocyanine. a; on Rock-salt, b; in Alcohol.

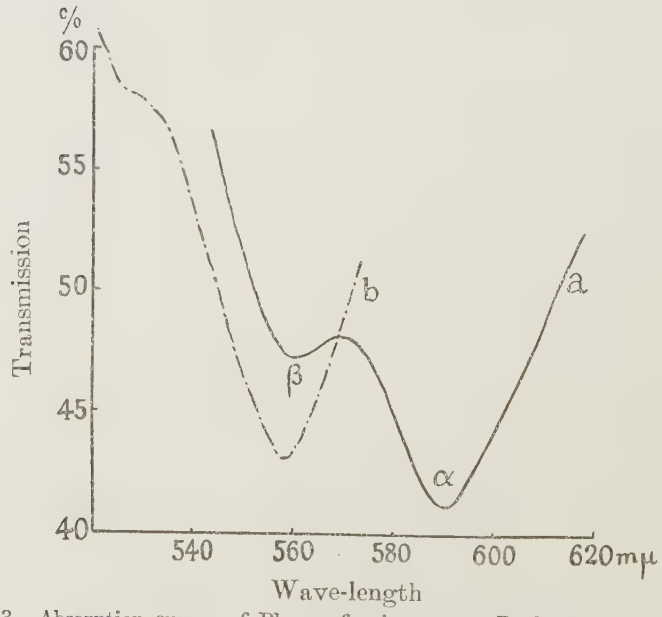

Fig. 3. Absorption curves of Phenosafranine. a; on Rock-salt, b; in Alcohol.

(2) **Photo-conductive effects**

Spectral sensitivity of photo-conductivity of rock-salt crystals which adsorbed these dyes, were measured by the arrangement shown in Fig. 4. In this case, suitable filters were used, instead of the above-mentioned grating monochromator, since intensities of light transmitted through the monochromator were too weak. A 750 watt projection lamp was set 30 cm. apart from the sample (D) and various filters were inserted between the lamp and samples successively. A photo-current produced in the dyed crystal (N) was led to the same amplifier used in the absorption experiment. The dark resistance of rock-salt crystals was found to depend on the humidity of the surrounding atmosphere, and the ease of measurement of the photo-currents depended on this resistance. As very low humidity was associated with high crystal resistance, a desiccative (A) was inserted inside the measuring apparatus and the electric resistance of the crystal was maintained to $10^{14} \sim 10^{15}\,\Omega$/cm. Since our measurements were performed at about 25° C, the amplifier was balanced initially to keep off the effects of electrolytic currents by these thermal influences.

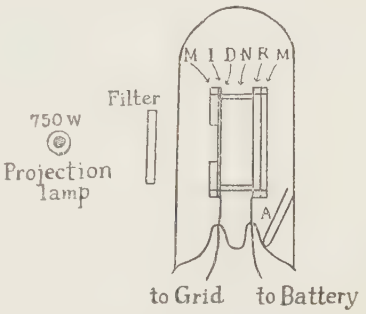

Fig. 4. Appratus measureing photo-conductive currents.
M; metal plate, I; mica insulator, D; dyes. N; rock-salt crystal, R; rubber, A; desiccative.

As the width and coefficient of transmmission bands are independent among each filter, photo-currents measured through these filters do not show absolute spectral sensitivity. Absolute amounts of energy of the light transmitted through these filters set in the position of the samples were measured by means of Moll's micro-thermopile which was calibrated against a standard Hefner lamp (7), the energy of Hefner lamp at 1 m. distance per cm^2 being 22.6×10^{-6} cal/sec.($=9.46 \times 10^2$ erg/sec). But, in our arrangement, the thermopile used produced 1.252×10^{-5} V which corresponded to 6.386×10^{-6} cal/sec $= 2.763 \times 10^2$ erg/sec considering its receiving area.

From these relations, photo-currents in the case when a unit energy is transmitted through each filter, may be calculated and spectral regions showing photo-current may be deduced. This is shown in Table 2. It is seen that photo-current increases in the regions of the filters VR1 and VR2 corresponding to the region of absorption bands α and β of Dicyanine-A in adsorbed states.

TABLE 2. Photo-conductive effect of rock-salt which adsorbs Dicyanine-A

Filters	Mazda				Wratten 740	
	VB1	VG1	VR2	VR1		
Energy transmitted through filters	687	702	1962	1526	1461	10^2 erg/sec.
	1962	3290	9198	7154	6847	μV/sec.
Rock-salt which adsorbs Dicyanine-A	2	2	20	20	5	Direct reading of galvanometer : 10^{-10}A.
	9.4	5.6	20	25.7	6.7	Relative amount of photo-current.
Photo-current	2	2	20	20	5	Absolute photo-current : 10^{-14} A.

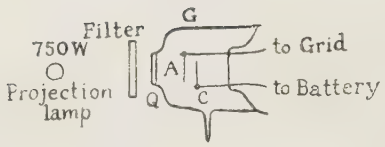

Fig. 5. Apparatus measuring photo-electric currents.
A; anode (molybdenum wire), C; cathode (silver plate coated with dyes), Q; quartz plate, G; glass bulb.

(3) Photo-electric effects

In order to measure the photo-electric effects of these dyes and of rock-salt crystals containing F-centers respectively, an arrangement shown in Fig. 5 was used. In the case of dyes, a silver plate on which these were evaporated thickly, was served as a cathode (C) and a molybdenum wire as an anode (A). The whole system was put in a glass bulb (G) which was evacuated and then tipped off. Then this arrangement was connected to the same amplifier used in the absorption experiment. Filtered light was sent on the sample through the quartz window (Q). Then photo-electric currents produced by these dyes were measured, and dividing photo-current by the number of incident photons, efficiency (8) was calculated for the case of Dicyanine-A. This amounts to 10^{-9}, which is very small in comparison with ordinary photocell, (which is about 10^{-4}).

Results are shown in Tables 3, 4, and 5. It is seen that maximum regions showing photo-electric effect are $430 \sim 440\,m\mu$ (corresponding to its absorption $420 \sim 430\,m\mu$) in the case of Dicyanine-A, $480 \sim 500\,m\mu$ in the case of Kryptocyanine and $230 \sim 240\,m\mu$ in the case of Phenosafranine.

TABLE 3. Photo-electric effect of Dicyanine-A

Filters	UVD1	Wratten 435	VP1	VB1	Wratten 500	VG1	
Energy transmitted through filters	401	2527	396	1178	2774	1203	10^2 erg/sec
	1880	11843	1857	3363	12999	5641	μV/sec
Photo-current by Mazda filters	2		9	8		4	Direct reading of galvanometer: $\frac{1}{4}\cdot10^{-10}$A
	6		28	13.2		4	Relative amount of photo-current
Photo-current by Wratten monochromatic filters		4.5			3.5		Direct reading of galvanometer: $\frac{1}{4}\cdot10^{-10}$A
		4.9			3.5		Relative amount of photo-current
Photo-current	0.5	1.1	2.25	2	0.9	1	Absolute photo-current: 10^{-14}A
Efficiency	225	39	1420	434	54	160	$10^{-12}/m\mu$ width
Half width of absorption curves of filters	50	30	90	100	30	100	$m\mu$

TABLE 4. Photo-electric effect of Kryptocyanine

Filters	VP1	VB1	Wratten 500	VG1	Wratten 546	
Energy transmitted through filters	56.0	105	383	174	418	10^2 erg/sec
	262	496	1798	817	1962	μV/sec
Photo-current by Mazda filters	0.5	2.5		1.5		Direct reading of galvanometer: $\frac{1}{4}\cdot10^{-10}$A
	4.3	8.3		3		Relative amount of photo-current
Photo-current by Wratten monochromatic filters			4.5		1.5	Direct reading of galvanometer: $\frac{1}{4}\cdot10^{-10}$A
			10		3	Relative amount of Photo-current
Photo-current	0.1	0.6	1.1	0.4	0.4	Absolute photo-current: 10^{-14}A

Photo-electric effects of rock-salt crystals have already been studied by P. Tartakowsky (9) and others (10). According to them, differences of energy between levels of zero state and ground state of F-center of rock-salt crystals is about 4.4 eV. We repeated experiments and verified their results: Photo-currents were not obtained by the light through filters transmitting longer than 300 mμ, but were obtained by the light through Br_2 gas filter transmitting 240～350 mμ region, thus showing the maximum sensitivity is at 4.9～4.4 eV in accordance with Tartakowsky.

TABLE 5. Photo-electric conductivity of Phenosafranine.

Filters	C_2H_5OH	CH_3OH	Glycerine	Mazda UV1
Shortest wave-length of transmitted light	210 mμ	220	240	250
Deflection of galvanometer	115 mm	210	210	20

Light source: Mercury lamp.

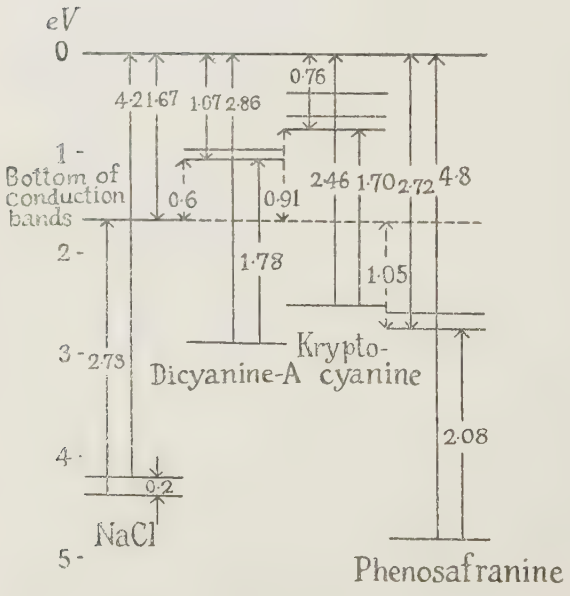

Fig. 6. Electronic energy levels.

4. Conclusion

According to these results, the electronic energy levels shown in Fig. 6 are obtained for rock-salt crystal, Dicyanine-A, Kryptocyanine and Phenosafranine, by taking their zero levels side by side. In terms of these levels, the mechanism of photo-sensitization of rock-salt crystals which adsorb Dicyanine-A or Kryptocyanine, may be explained as follows: since their lowest excited levels are situated above the lowest conduction level of rock-salt, electrons raised to their excited levels by absorption of light have some probability to fall down to the conduction band of rock-salt leading to

electric conduction in rock-salt crystals. Thus, the rock-salt crystal which adsorbs these dyes, becomes sensitive at only 1.8 eV corresponding to their absorption of light, while pure rock-salt crystal just becomes photo-sensitive at 9 eV, and that containing F-centers at 2.7 eV.

In the case of Phenosafranine, photo-conductivity does not occur. This may be understood from the electronic energy levels. For the lowest excited level of this dye is situated lower than the conduction level of rock-salt by about 1 eV and electrons may not be transferred from this excited level of the dye molecule to the conduction band of the rock-salt. Next, when Dicyanine-A and Phenosafranine are used in mixture, photo-conductivity is not found. The reason may be that electrons transferred to excited levels of Dicyanine-A are directly transferred to those of Phenosafranine and may be difficult to be transferred to the conduction levels of rock-salt.

Probably, the above-described mechanism of sensitization and desensitization of photo-conduction applied to rock-salt crystals, may be extended to silver-halides in photographic emulsion. For the fundamental process of latent image formation in silver-halides is a production of conduction electrons in silver-halides and in the case of dyed emulsion this may be effected by electrons of the dye molecules by the same mechanism shown in the case of rock-salt. In this connection, experiments on large single crystals of silver-halides are anticipated in future.

In conclusion, the writer wishes to express his hearty thanks to Prof. Y. Uchida, under whose guidance this work was accomplished. This investigation was supported by the grant from the Ministry of Education.

Institute of Physics,
University of Kyoto.

REFERENCES

1. R. W. Gurney, Proc. Roy. Soc. London, A, **164** (1938), 152.
2. N. Kameyama, J. Soc. Chem. Ind. Japan, **42** (1939), 244.
3. W. West, J. Chem. Phys., **15** (1947), 529.
4. Y. Uchida and H. Yagi, Oyobutsuri, **16** (1947), 65.
5. S. E. Sheppard, J. Chem. Phys., **9** (1941), 96.
6. J. Strong, Proc. Exper. Phys., (1938), 418.
7. W. Gerlach, Phys. ZS., **14** (1913), 577.

8. S. E. Sheppard, J, Chem. Phys., **7** (1939), 426.
9. P. Tartakowsky, ZS. f. Phys., **96** (1935), 191; **90** (1934), 504; **58** (1929), 394.
10. N. Kalabuchow, ZS. f. Phys., **75** (1932), 282.
11. N. I. Fisher, Proc. Roy. Soc. London, A, **154** (1936), 703.
12. B. Beclenson, Proc. Roy. Soc. London, A, **163** (1937), 138.

Memoirs of the College of Science, University of Kyoto, Series A,
Vol. XXVI, Nos. 1 & 2, Article 9, 1950.

The (γ, n) Reaction of Molybdenum produced by the Li (p, γ) γ-Rays

By

Sakae Shimizu, Shinjiro Yasumi, Yoshio Saji and **Jiro Muto**

(Received July 7, 1950)

ABSTRACT

The (γ, n) reaction of molybdenum produced by the irradiation of Li (p, γ) γ-rays was observed. The radioactivities induced in molybdenum samples were measured precisely by an end-window type β-ray counter with a thin mica window. While we determined the absolute number of γ-ray quanta by a specially constructed Geiger-Mueller counter with a thick lead wall, of which counting efficiency was computed theoretically. By measuring the intensities of activities produced in a set of molybdenum samples of various thickness and the number of γ-ray quanta concerned, we could determine the apparent cross section of this reaction for the sample with different thickness. Extrapolating the curve of apparent cross section *versus* the thickness of irradiated sample to zero thickness, we could determine the absolute cross section of the $Mo^{92}(\gamma, n)Mo^{91}$ reaction for the Li (p, γ) γ-rays as 9.9×10^{-26} cm^2. Some discussions on the results obtained are also given.

1. Introduction

The (γ, n) type photo-disintegration of heavier nuclei can be induced only by the high energy quanta having the energy larger than neutron binding energy of a neutron in these nuclei. In recent years many works on thresholds and excitation functions of these reactions by the high energy X-rays from betatrons and synchrotrons were reported. Since, however, the continuous energy spectra of the X-rays used have been scarcely known, it is very difficult to determine the absolute cross sections for the photo-induced reactions by these experiments. And there are so far a few works concerning the experimental determination of the absolute cross sections with high energy γ-rays produced by the Li (p, γ) reaction (1).

One of the authors has recently reported the experimental determination of the cross section for $Cu^{63}(\gamma, n)Cu^{62}$ reaction produced by these γ-rays (2). After this work, with the intention to find out any relation, if it exist, between cross sections and nuclear structures, we

have further continued the studies on (γ, n) reactions of heavier elements by the irradiation of Li (p, γ) γ-rays. The present report describes a similar work with molybdenum.

2. Apparatus

The apparatus and experimental arrangements were essentially the same as those of the previous work. But it is profitable to give some simple descriptions about the apparatus used.

For the production of Li (p, γ) γ-rays we used a high voltage machine of Cockcroft-Walton type equipped in our laboratory. The proton beam of about 460 Kev was directed on the target of metallic lithium placed on the bottom of a thin brass tube 0.2 mm thick. It was focused to a spot of about 1.5 mm in diameter.

The number of γ-ray quanta was counted by a Geiger-Mueller counter with a lead wall 6.5 mm thick, the inside diameter and the effective length of which are 2 cm and 2 cm respectively. The counting efficiencies of this lead counter for high energy quanta were recently computed theoretically by M. Sonoda (3) by taking the knowledges of the shower theory into account. Since the rigorous determination of the counting efficiency by accurate experiments is yet difficult, we used presumably these theoretical values. In actual arrangements the lead counter was placed at a fixed position 29.4 cm apart from the Li-target and usually shielded by a lead cylinder 1.05 cm thick. The practical absorption coefficient of this lead cylinder was measured as $\mu_\gamma = 0.53\ \mathrm{cm}^{-1}$. The absolute number of γ-ray quanta concerned was easily obtained from the data of net counts as described in the following section.

The samples irradiated were a set of molybdenum circular discs of various thicknesses. The diameter of all the discs was precisely equal to 22.8 mm, while the thickness was chosen as listed in Table I. The purity of molybdenum was examined spectroscopically and the density of samples was measured and was found to be $\rho = 9.67\ \mathrm{g/cm}^3$.

TABLE I. Thickness of molybdenum samples.
(Diameter of each sample = 22.8 mm)

Sample No.	Thickness		
	in mm (δ)	in mg/cm^2 (w)	in mg/cm^2/Z^2
1	0.05	48.0_5	7.4_1
2	0.08	77.0_3	11.8_9
3	0.12	117.8_5	18.1_8
4	0.16	153.1_7	23.6_3

In the present experiment we used also copper activation monitors of 40 mm in diameter and 801.3 mg/cm^2 in thickness in order to avoid the effects due to the fluctuation of γ-ray irradiation, which may introduce some errors into the final results.

For the measurements of the positron activities induced in these samples we used two Geiger-Mueller counters of 2π-type (end-window type) with same dimensions except that the thickness of mica window of the sample counter is 5.2 mg/cm^2 while that of the monitor counter is 6.1 mg/cm^2. The details of these counters were described in the previous paper (2). The pulses of the counters, after amplification, were counted by a decade scaler and two scale-of-4 scalers.

3. Experimental procedures

Cross section

When the irradiation of γ-rays of constant intensity is made for one minute in the geometry shown in Fig. 1, the number of the active nuclei produced in the sample, N, is given by the following expression:

$$N = \frac{\sigma m N_\gamma (1 - e^{-\lambda})}{\lambda} \left[\frac{1}{4} \int_a^{a+\delta} \log \left(\frac{x^2 + r^2}{x^2} \right) dx \right], \qquad (1)$$

where

σ : reaction cross section,
m : number of the parent Mo-nuclei per c.c. in molybdenum sample,
λ : decay constant of the active nuclei produced,
N_γ : total number of γ-ray quanta emitted from the Li-target for one minute,
a : distance between the γ-ray source and the upper surface of the sample disc,
δ : thickness of the sample disc,
r : radius of the sample disc.

Since, in actual experiments, γ-ray intensity fluctuated gradually while the sample was irradiated during about $20 \sim 50$ minutes, γ-ray counts were measured for each one minute, for which the intensity was assumed to be constant. The activities of the active Mo-nuclei produced were measured from just one minute after the end of irradiation for the following 15 minutes. Then the net counts, N_s, obtained by this procedure can be given, according to Eq. (1),

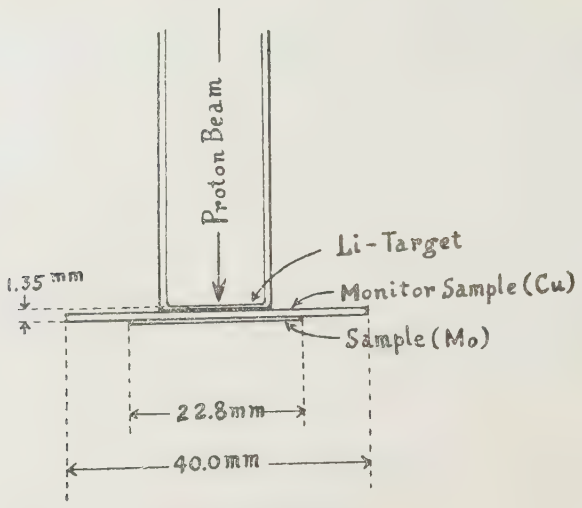

Fig. 1. Standard geometry of irradiation of samples.

$$N_s = \frac{\sigma A_s m}{2 C_g C_\beta} \frac{1 - e^{-\lambda}}{\lambda} \left[\frac{1}{4} \int_a^{a+\delta} \log \left(\frac{x^2 + r^2}{x^2} \right) dx \right] \times (1 - e^{-15\lambda}) \sum_{i=1}^{T} N_{\gamma_i} e^{-(T-i+1)\lambda}, \qquad (2)$$

where

T : time of irradiation in min.,

N_{γ_i} : absolute number of γ-ray quanta emitted from the Li-target during each one minute interval,

C_g : correction factor concerning the geometrical condition of activity measurements of the sample,

C_β : correction factor for the absorption of β-particles in a mica window of the β-ray counter,

A_s : factor concerning the self-absorption in the sample.

From Eq. (2) we obtain

$$A_s \sigma = \frac{2\lambda C_g C_\beta}{(1 - e^{-\lambda})(1 - e^{-15\lambda}) \sum_{i=1}^{T} N_{\gamma_i} e^{-(T-i+1)\lambda}} \times \frac{N_s}{\frac{1}{4} \int_a^{a+\delta} \log \left(\frac{x^2 + r^2}{x^2} \right) dx} \frac{1}{m}. \qquad (3)$$

The value of $A_s\sigma$ is the apparent cross section for the sample of thickness δ. We prepared four kinds of molybdenum samples as listed in

Table I, and for these samples the values of $A_s\sigma$ were obtained. Now the true cross section means the value of $A_s\sigma$ when the sample thickness tends to zero. Hence we could easily obtain the true cross section, σ, by extrapolating the curve of $A_s\sigma$ *versus* w (weight of sample per unit area) to zero thickness $w = 0$.

Absolute number of γ-ray quanta

In order to obtain the absolute number of γ-ray quanta, N_{γ_i}, from the observed net counts of the γ-ray Geiger-Mueller counter used, n_{γ_i}, the following relation was used:

$$N_{\gamma_i} \frac{\omega}{4\pi} \varepsilon_{ff} e^{-\mu_\gamma x} = n_{\gamma_i}, \tag{4}$$

where ω is the solid angle subtended by the effective volume of the γ-ray counter at the γ-ray source, and $e^{-\mu_\gamma x}$ is the factor for the absorption of γ-rays by the lead cylinder (thickness $x = 1.05$ cm) shielding the γ-ray counter. The efficiency of this counter used, ε_{ff}, was calculated theoretically by M. Sonoda (3), obtaining the result that $\varepsilon_{ff} = 0.23_8$ for 17.6 Mev γ-ray quanta. By numerical computation we obtained

$$n_{\gamma_i} / N_{\gamma_i} = 8.28_1 \times 10^{-5}. \tag{5}$$

Correction factors concerning the β-ray measurements

The geometrical correction, C_g, was carefully determined by a series of experiments using Ag-sample activated by a neutron source (50 mg Ra + Be), and was found to be $C_g = 1.89$. In the case of Cu^{62}, as one of the authors previously reported (2), the correction factor C_β for the absorption of β-rays in a mica window of the sample counter was determined by inserting a set of thin mica sheets between the sample and the counter. Since the maximum energy of β-rays of the active molybdenum seemed to be about 2 Mev, as described in the following section, we could also in the present case adopt the same value as that in the case of Cu^{62}, namely $C_\beta = 1.06_6$.

Copper monitor

The irradiation was monitored by the measurements of Cu^{62} activities induced in the monitor sample of copper, mounted directly under the bottom of the Li-target together with Mo-samples in the geometry shown in Fig. 1. After the irradiation the similar measurements were made for the Cu-monitor as for the Mo-samples. For each run of measurements, the value

$$\frac{N_M}{\sum_{i=1}^{T} N_{\gamma_i} e^{-(T-i+1)\lambda_{Cu}}} \tag{6}$$

was computed, where N_M is the total net counts of Cu-monitor for 15 minutes. We regarded the value of (6) as an index for the condition of γ-ray irradiations. In practice, however, throughout whole series of measurements data of only one run was excluded according to this point of view.

Stability of the β-ray counter

Stability of the β-ray counters used was daily examined by a standard KCl-sample placed at the fixed position in front of a mica window of the counter. The errors which may be introduced by small day-to-day variations in counter sensitivity were excluded by measuring the ratio of the net counts of KCl-sample in every day.

4. Results

Cross section

The apparent cross section for each sample is shown in Table II and Fig. 2. The observed value corresponding to the No. 1-sample could not be adopted, since the intensity of the β-activities induced in this sample was much weaker than the others. By the calculation using the least square method, we obtained the following empirical relation between the apparent cross section, $A_s\sigma$ (in cm^2), and the thickness of samples, w (in mg/cm^2):

$$A_s\sigma = (-0.0125_2 w + 15.7_6) \times 10^{-27}/\zeta\,, \qquad (7)$$

where ζ is the abandance ratio of the parent Mo-isotope concerned. Extrapolating w to zero, then A_s tends to 1 (cf. Fig .2). Hence, we obtained a value of the true cross section as

$$\sigma = (15.7_5 \times 10^{-27})/\zeta\ cm^2\,. \qquad (8)$$

Therefore we obtained the following results:

(a) If the observed reaction is assigned to $Mo^{92}(\gamma, n)\,Mo^{91}$, then
$\sigma = 9.9 \times 10^{-26} cm^2$ for Li (p, γ) γ-rays,
since ζ of Mo^{92} is 0.1586 (4).

(b) If the observed reaction is assigned to $Mo^{94}(\gamma, n)\,Mo^{93}$, then
$\sigma = 17.3 \times 10^{-26} cm^2$ for Li (p, γ) γ-rays,
since ζ of Mo^{94} is 0.0912 (4). (9)

But, we can affirm that the reaction observed in the present experiment is assigned to Mo^{92} (γ, n) Mo^{91}, since the recent work of Duffield and Knight (5) indicated that the activity with a half-life of 15.5 minutes was observed by the use of molybdenum oxide enriched in Mo^{92} under the irradiation of 23 Mev betatron X-rays.

TABLE II. The apparent cross section for each sample.

Sample No.	Thickness w in mg/cm^2	Apparent cross section × abundance ratio $A\,\sigma\zeta$ in cm^2
2	77.0_3	$14.3_9 \cdot 10^{-27}$
3	117.8_5	$15.1_5 \cdot 10^{-27}$
4	153.1_7	$13.3_7 \cdot 10^{-27}$

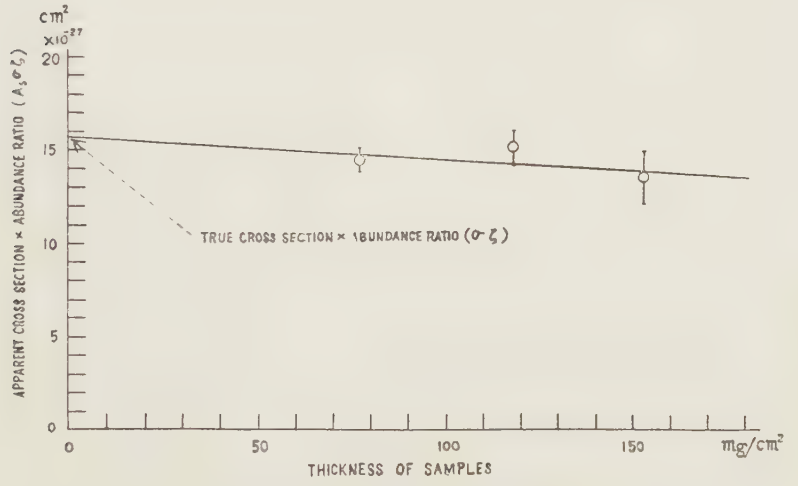

Fig. 2. Apparent cross section *versus* thickness of samples.

Half-life

In order to obtain half-life, T, or decay constant, λ, of the active Mo-nuclei, Mo-samples of 40 mm in diameter were prepared. Data obtained from the counting measurements of 12 separate runs are plotted in Fig. 3. From these data T and λ were determined by applying the rigorous method of Peierls (6) as follows:

Half-life $T = 14.2$ min., and decay constant $\lambda = 0.0487\ \text{min}^{-1}$.

These values were used in the calculation of the cross section.

Transmission of β-rays

If we assume that the extrapolated value obtained by the empirical formula (7) corresponding to the transmission of β-rays is 100 per cent, the per cent transmission of the Mo-samples used is obtained as follows:

93.9 % for No. 2-sample (11.8_9 mg/cm^2/$Z^{\frac{1}{2}}$),

90.6 % for No. 3-sample (18.1_8 mg/cm^2/$Z^{\frac{1}{2}}$),

87.8 % for No. 4-sample (23.6_8 mg/cm^2/$Z^{\frac{1}{2}}$).

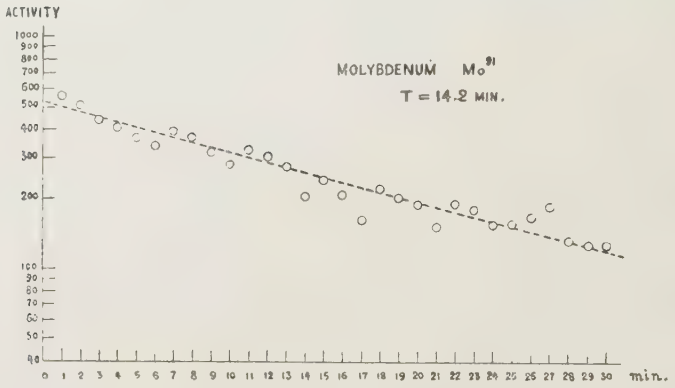

Fig. 3. Decay curve of active molybdenum.

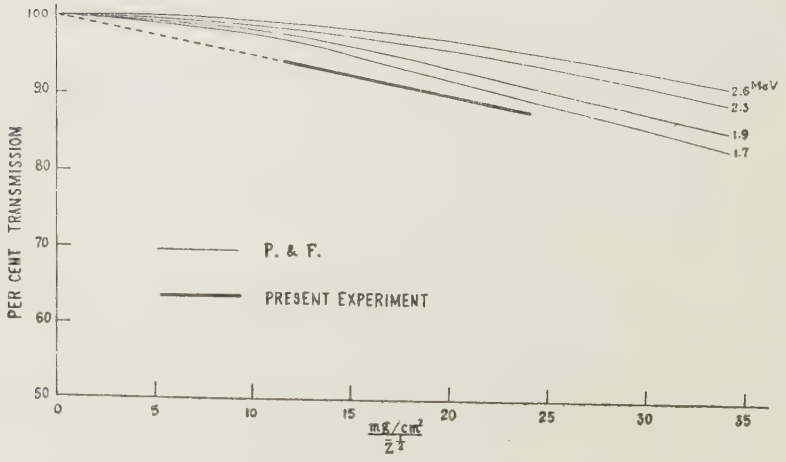

Fig. 4. Self-absorption of β-rays of various energies (Mev). Thin curves are quoted from the results obtained by Perlman and Friedlander (Phy. Rev. **74** (1948), 442). Thick curve is obtained by the present experiment.

In Fig. 4 self-absorption curve—transmission *versus* mg/cm^2/$Z^{\frac{1}{2}}$—obtained by the present experiment is shown together with the curves given by Perlman and Friedlander (7). It seems probable, from Fig. 4, that the gradient of the curve obtained for β-rays of Mo-sample lies between those of 1.9 Mev and 2.3 Mev. For this reason it is concluded that the maximum energy of β-rays emitted from the active molybdenum may be about 2 Mev.

5. Discussions

From the preliminary experiments using a neutron source (50 mg Ra + Be) with and without paraffin, we could ascertain that the neutrons which might be emitted from the Li-target by the natural content of deuterons in the proton beam were incapable of causing any observable activities in the Mo-sample.

Since the decay measurements of active molybdenum were commenced from one minute after the end of irradiation, it could not be concluded whether much shorter half-lives* than that we observed exist or not. We observed 14.2-min. half-life, while other investigators reported that the active molybdenum produced by (γ, n) reaction had 17-min. half-life (8). Recently, however, Duffield and Knight (**5**) observed 15.5-min. half-life, which is in considerable agreement with the determination of the present experiment.

Since there are many stable isotopes of molybdenum, the assignment of the observed active molybdenum seems to be difficult. It is, however, probable that the present reaction is assigned to either $Mo^{92}(\gamma, n)\,Mo^{91}$ or $Mo^{94}(\gamma, n)\,Mo^{93}$. But, the recent work of Duffield and Knight (**5**) using the molybdenum samples enriched in Mo^{92} and Mo^{94} established the assignment of this reaction, and namely the intensity of the reaction was found to be proportional to the Mo^{92} content of the irradiated samples, confirming its assignment to Mo^{92}. Therefore, as mentioned in the preceding section, the cross section of $Mo^{92}(\gamma, n)\,Mo^{91}$ determined by the present experiment is

$$\sigma_{Mo} = 9.9 \times 10^{-26}\,\mathrm{cm}^2 \quad \text{for Li}\,(p, \gamma)\,\gamma\text{-rays.} \qquad (9')$$

* Besides 17-min. half-life a shorter period of about one min. was observed by Baldwin and Koch using the X-rays of above 14 Mev (Phys. Rev. **67** (1945), 1) and Duffield and Knight (**5**) using the X-rays of 23 Mev.

Now comparing this value with the cross section for $Cu^{63}(\gamma, n)Cu^{62}$ reaction, $\sigma_{Cu} = 8.5_0 \times 10^{-26}\,cm^2$*, obtained by the previous work (2), we obtain :

$$\sigma_{Mo}/\sigma_{Cu} = 1.1_6 \text{ for } Mo^{92} \text{ and } Cu^{63} \text{ for } Li(p, \gamma)\,\gamma\text{-rays.} \qquad (10)$$

Taking into consideration the fact that the gradient of self-absorption curves for β-rays with various energies becomes smaller as the value of $mg/cm^2/Z^{\frac{1}{2}}$ decreases,** as shown in Fig. 4, it appears that the extrapolation of w to zero according to the linear relation (7) may give a little larger value of the cross section than the true one, however, the error introduced by this procedure is not larger than 5 per cent. The probable error of the results obtained by the present work, derived from the whole course of the experiments, is estimated to be about 15 per cent. But the result (10) seems to be more accurate, since the apparatus and experimental arrangements adopted in both works are essentially same.

Now, by the measurements of Perlman and Friedlander (7) it was made clear that the (γ, n) yields for the target nuclei with masses between 60 and 120 were in the same order for 50 Mev X-rays and, further, the same trend was also valid for 100 Mev X-rays. This fact, however, only suggests that the integrated cross sections for these X-rays are nearly equal. But from the present experiment we can conclude that the absolute cross section for copper and molybdenum are in the same order for lithium γ-rays.

The value of cross section above mentioned has been obtained on the assumption that the lithium-γ-rays constitute themselves of the quanta of 17.6 Mev monochromatically. But, according to the recent measurements of Walker and McDaniel (**9**) using a γ-ray spectrometer there are two lines instead of a single line, and namely a line at 17.6 Mev and another line at 14.8 Mev. And the ratio of intensities of the lower energy line to the higher energy line was found to be approximately 0.50 for the protons of 460 Kev bombarding energy. Then, it is proper that the effect due to the quanta of 14.8 Mev should be taken into account, since the observation by Baldwin and Koch (**10**) indicated that

* This value is, however, about 10 per cent larger than that previously obtained, $\sigma_{Cu} = 7.7_5 \times 10^{-26}\,cm^2$. This discrepancy is due to the difference of the counting efficiency adopted in both works, and namely $\varepsilon_{ff} = 0.21_7$ in the previous work while $\varepsilon_{ff} = 0.23_8$ in the present work. The difference of two values results from the difference of calculating procedures of efficiency. At present we can not ascertain, from the experiments, which value is more accurate.

** This effect was also observed in the previous work with Cu^{62}.

the threshold for Mo (γ, n) reaction was 13.5 ± 0.4 Mev. By simple considerations, it is clear that all corrections for 14.8 Mev quanta can be made, multiplying by a factor α which is given by

$$\alpha = \left(1 + \frac{\varepsilon_{14}}{\varepsilon_{17}} R\right) \Big/ \left(1 + \frac{\sigma_{14}}{\sigma_{17}} R\right),$$

where R is the ratio of intensities of the line at 14.8 Mev to that at 17.6 Mev, and ε_{17} and ε_{14} are the counting efficiencies of the γ-ray counter for 17.6 Mev and 14.8 Mev quanta respectively, and are given by M. Sonoda (3) theoretically as $\varepsilon_{17} = 0.23_8$ and $\varepsilon_{14} = 0.18_4$ respectively. σ_{17} and σ_{14} are the cross section for 17.6 Mev and 14.8 Mev quanta respectively. Since, however, at present the ratio σ_{14}/σ_{17} has been scarcely known, it is difficult to determine precisely the cross section for each of two lines of lithium-γ-rays.

Further work on the cross sections of photo-nuclear reactions with various nuclei is clearly necessary. In particular, the high yield of $Re^{187}(\gamma, n)$ reaction observed by Perlman and Friedlander (7) tempts us to investigate (γ, n) reactions for the nuclei with masses above 120. Further studies on the dependence of cross section on nuclear structure are now in progress.

6. Acknowledgments

The authors wish to express their sincere appreciation for the encouragement and helpful discussion given them by Professor B. Arakatsu. We wish further to acknowledge Professor K. Kimura, Professor M. Sonoda, Dr. Y. Uemura and the other members of our laboratory for their interests and suggestions throughout the course of the experiment. We are very thankful to Dr. T. Arizumi of Kobe Kogyo Corp. for the kindful present of the molybdenum samples which made the present work possible. This work was financially supported by the special fund of the Ministry of Education for the Advancement of Science.

In connectin with the happy circumstance that this paper will appear in the number of this "Memoirs," issued in memory of Professor Arakatsu's 60th birthday, it is a great pleasure for us to express our most profound admiration for his important contribution to the development of nuclear physics in Japan.

REFERENCES

1. W. Bothe and W. Gentner, Zeits. f. Phys., **106** (1937), 236.
H. Wäffler and O. Hirzel, Helvetica Phys. Acta, **21** (1948), 200.

2. S. Shimizu, Mem. Coll. Sci., Univ. of Kyoto, A, **25** (1950), 193.
3. M. Sonoda, Journ. Phys. Soc. Japan, now in press.
4. D. Williams and P. Yuster, Phys. Rev., **69** (1946), 556.
5. R. B. Duffield and J. D. Knight, Phys. Rev., **76** (1949), 573.
6. R. Peierls, Proc. Roy. Soc., A, **149** (1935), 467.
7. M. L. Perlman and G. Friendlander, Phys. Rev., **74** (1948), 442.
8. W. Bothe and W. Gentner, Naturwiss., **25** (1937), 191; Zeits. f. Phys., **106** (1937), 236.
   This period was also observed by $(n, 2n)$ reaction of molybdenum, (M. L. Pool, J. M. Cork, and R. L. Thorton, Phys. Rev., **52** (1937), 239; R. Sagane, S. Kojima, G. Miyamoto, and M. Ikawa, Phys. Rev., **54** (1938), 542.)
9. R. L. Walker and B. D. McDaniel, Phys. Rev., **74** (1948), 315.
10. G. C. Baldwin and H. W. Koch, Phys. Rev., **67** (1945), 1.

Nuclear Research Laboratory,
Department of Physics,
Faculty of Science,
University of Kyoto.

Memoirs of the College of Science, University of Kyoto, Series A,
Vol. XXVI, Nos. 1 & 2, Article 10, 1950.

The Photo-disintegration of Beryllium by the High Energy Gamma-Rays

By

Bunsaku Arakatsu, Masateru Sonoda, Yoshiaki Uemura, Shinjiro Yasumi, and **Yoshio Saji**

(Received July 11, 1950)

1. Introduction

After the discovery of Chadwick and Goldhaber, the phenomenon of the photo-disintegration of Beryllium was studied both experimentally and theoretically by several workers (1) for the γ-rays of comparatively low energies up to about 3 Mev. There are, however, no literatures known to us concerning the investigation for the γ-rays of higher energies.

In our laboratory, it was previously studied (2) that the α-particles may be suspiciously ejected from various nuclei when they are irradiated by the high energy γ-rays of (Li–p) and (F–p) reactions. However, owing to the lack of the observed number of pulses and cloud chamber tracks, no decisive conclusion was given there. We have recently repeated the experiments under the improved conditions and obtained some conclusive results. In the present paper, the results of observation with Beryllium will be given.

2. Apparatus

The γ-rays of 17.6 Mev and 6.13 Mev were produced by bombarding thick target of Lithium metal and Calcium fluoride with protons of energy of 500 Kev and 350 Kev respectively. The hydrogen ion beam amounting to 30～50 microamperes was, in this case, directed upon the target unseparatedly.

Two proportional counters of methane gas flow type (3), which are made of brass cylinder 3.6 cm in diameter and 20 cm in effective length, are placed parallel at the distance of 6.5 cm from the target as shown in Fig. 1. The inner surface of one of the counters is coated with thick layer of Beryllium oxide and the other is uncoated. The γ-ray

counter of lead wall 6.5 mm in thickness (4) is placed at 29.5 cm from the target, being shielded by a lead cylinder of 1.05 cm in thickness.

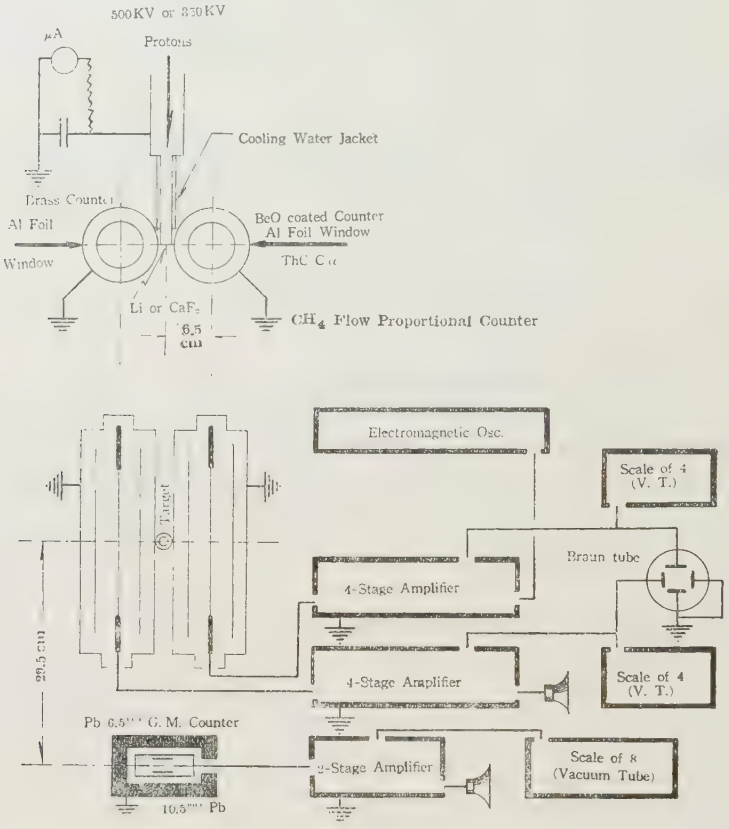

Fig. 1.

The pulses due to the α–particles ejected from the walls of the counters were counted usually by two scale-of-4 scalers, after having been amplified by the respective 4–stage linear amplifier. In order, however, to discriminate a spurious count due to an accidental electromagnetic induction from the accelerating tube, special cares were taken to the device. The pulses from each of the counters were fed respectively into the vertical and horizontal deflectors of a Braun-tube oscilloscope (Fig. 1), so as the spurious pulse which took place simultaneously in both counters appeared as an oblique pulse on the oscilloscope screen and the number of these kicks were subtracted from the counts. It was found that in general the spurious pulses were seldom in winter,

when the conditions of the high tension apparatus and the accelerating tube system were good.

The linearity of the counter and amplifier system was ascertained by observing the integrated Bragg curve in the methane gas (5), for the various distances of a sample of Thorium deposit from the counter window.

3. Experiments

(i) When the counters were irradiated by the γ–rays, many pulses due to α–particles were observed in the Be-coated counter, but very few in the uncoated one. Moreover, the number of observed pulses from the Be-coated counter was found to be exactly proportional to that of the γ–ray counter. A part of the experimental data is shown in Table I for the case of (Li–p) γ–rays.

TABLE I.

	Number of pulses by Be-coated counter		Number of pulses by uncoated counter
Proton energy	500 Kev	375 Kev	500 Kev
γ–counts	119804	1643	28449
α–counts	2800	36	39
$\frac{\alpha\text{–counts}}{\gamma\text{–counts}}$	2.34×10^{-2}	2.19×10^{-2}	1.37×10^{-3}

These facts show that the observed pulses from the Be-coated counter are definitely to be attributed to the α–particles ejected from Beryllium irradiated by the γ–rays, but not to the particles emitted by $(n\text{–}\alpha)$ reaction induced by the neutrons which might be produced by the (D–D) and (Li–D) reactions at the target. During the course of our experiments, it was found that the height of the pulses in this case were found most frequently to be nearly equal on the screen of the Braun-tube oscilloscope. This aspect may be attributed to the fact that the range of the emitted α–particles are in most cases sufficiently long to pass across the tube diameter and reach the opposite surface of the counter wall.

(ii) Another counter of larger diameter was therefore constructed and the similar experiments were repeated. The inner diameter of the new counter is 6 cm, while the effective length of which is 20 cm as before. Beryllium oxide is coated in the inner surface to the

thickness of 7.49 mg/cm^2. The linearity of the counter and amplifier system was ascertained as previously. After having been amplified, the output pulses were counted by the scalers and at the same time observed on the oscilloscope screen as in the previous experiments. Furthermore, an electromagnetic oscillograph (**6**) was used to record the pulses on the printing paper. The pulse-height distribution was in this way carefully determined for each case. Fig. 4 is a part of the oscillograph records for the case of (Li–p) γ–rays. The pulse-height was daily calibrated by comparing with that of the α–particles from a Thorium deposit. An example of the calibration curve is shown in Fig. 2, in

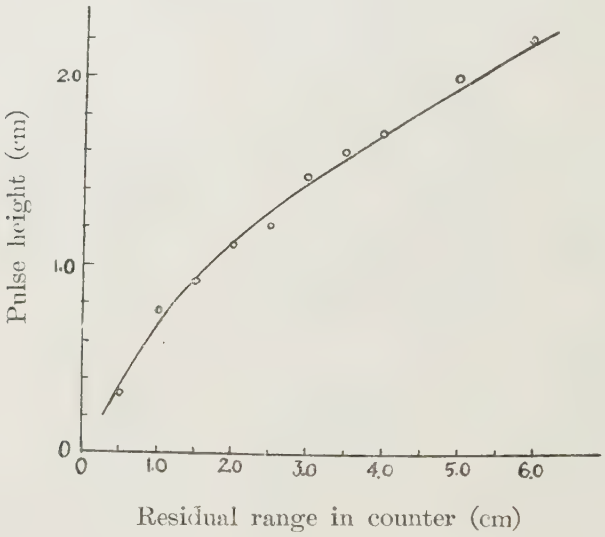

Fig. 2.

which the abscissa is the residual range in the counter and the ordinate is the pulse-height on the oscillograph record. The solid curve is the integrated Bragg curve calculated from Tayler's data (**5**), and the conformity with experiments (a series of dotted marks) is taken to be sufficiently good.

By using this calibration curve, the range distribution was obtained for the α–particles emitted by the photo-disintegration process. The results are shown in Fig. 3 for the cases of (Li–p) and (F–p) γ–rays, in which the number of pulses having the range greater than r is plotted against r.

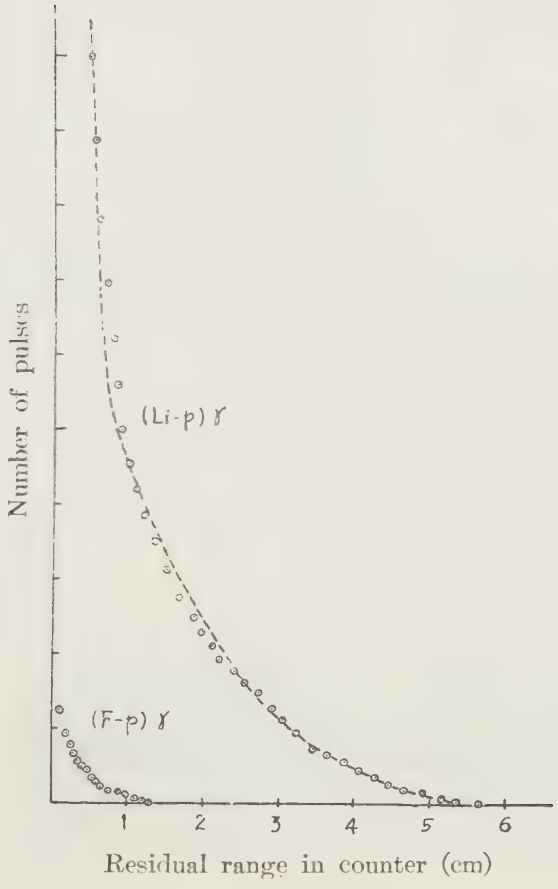

Fig. 3.

4. Explanation of the phenomena, together with discussions

Let us now try to give the explanation of the disintegration processes occurred in Beryllium nucleus irradiated by these γ–rays and estimate their cross-sections by analysing the range distribution curves shown in Fig. 3.

(i) From the figure, we see that the maximum range is about 5.8 cm in the case of (Li–p) γ–rays. And so, from the consideration of mass and energy, the following processes are taken to be possible, namely :

$$\left.\begin{aligned} \mathrm{Be}^{9} + (\mathrm{Li\text{–}p})\gamma &\rightarrow \mathrm{Be}^{8*} + n\,, \\ \mathrm{Be}^{8*} &\rightarrow 2\alpha\,, \end{aligned}\right\} \qquad (1)$$

where the residual nucleus Be^{8*} is considered to be remained either in the ground state or in an excited state of energy 3.0, 4.8, or 7.0 Mev (7). If we assume the process (1) to be the case, the maximum range of the emitted α-particle is expected by simple calculations to be as shown in the second and third columns of Table II for each of the above-mentioned states of recoiling Be^{8*} nucleus.

TABLE II. Maximum range of α-particles calculated for different energy states of Be^{8*} excited by γ-rays of various energies.

Energy of excited state of Be^{8*} (Mev)	Maximum range of α-particle in cm		
	(Li-p) γ-rays		(F-p) γ-rays
	$h\nu$=17.6 Mev	$h\nu$=14.8 Mev	$h\nu$=6.13 Mev
0	0.70	0.64	0.33
3.0	2.84	2.47	1.25
4.8	4.05	3.52	——
7.0	5.49	4.71	——

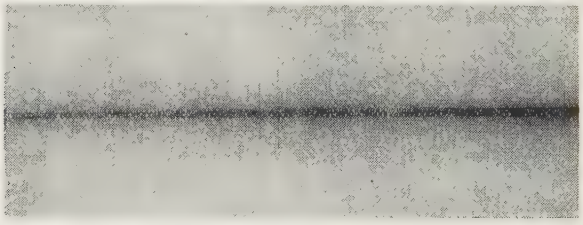

Oscillo. No. 130

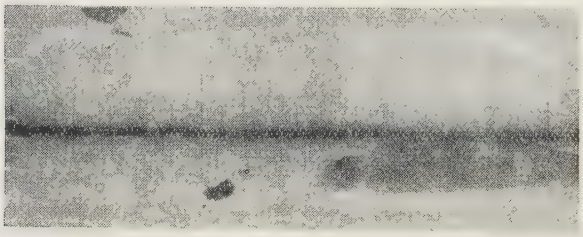

Oscillo. No. 132

Fig. 4. Oscillograph records for Be^{9}+17.6 Mev γ (29/VI 1950).

Both of the alternative considerations, namely the splitting reaction:

$$Be^{9} + (\text{Li-p})\gamma \rightarrow 2\alpha + n\,, \qquad (2)$$

and the simple fission process:

$$Be^9 + (Li\text{–}p)\gamma \rightarrow He^4 + He^5, \qquad (3)$$

followed by

$$He^5 \rightarrow \alpha + n \qquad (3')$$

are considered to be energetically impossible, since the observed maximum range is 5.8 cm in air.

Indeed, however, when the energy of the γ–rays is 14.8 Mev, the reaction (3) seems to be possible (maximum range = 5.99 cm). But, if it were the case, it had to appear a steep step in the observed curve in Fig. 3 at the range of 4.59 cm due to the homogeneous group of α–particles.

Now, by the reaction (1), Be^{8*} is considered to split up into two α–particles with the mean life of about $10^{-15} \sim 10^{-17}$ seconds (8). If the spherical symmetry in the center of gravity system is assumed in the splitting up of Be^{8*}, the number $n(\theta)$ of the α–particles emitted from unit volume of sample at an angle θ with the direction of recoil of Be^{8*}, will be given by

$$n(\theta)\,d\theta = \frac{\sigma N n_\gamma}{4\pi} 2\pi \sin\theta\, d\theta\,, \qquad (4)$$

where σ is the cross-section of photo-disintegration, N the number of Be^9 nuclei per unit volume, n_γ the number of γ–ray quanta falling on the unit area of Be layer, and θ is measured in the center of gravity system. The range of the emitted α–particle is determined as a function of θ and it is denoted by $R(\theta)$.

When the homogeneous α–particles of the range $R(\theta)$ are emitted from a thick target, the probability that the residual range in the counter volume is greater than r is given by a simple calculation as

$$\frac{R - r}{4s}\,,$$

where s is the stopping power of BeO relative to air. Then the total number of the α–particles having the residual range greater than r will be

$$N_\alpha = \frac{\Omega'}{4\pi} \frac{\sigma N N_\gamma}{8s} \int_0^{\theta_0} (R - r) \sin\theta\, d\theta\,, \qquad (5)$$

where N_γ is the total number of γ–ray quanta emitted from the source, θ_0 the value of θ corresponding to r in the R–θ relation, and Ω' the

solid angle, modified by taking the oblique incidence of γ-quanta into account.

We can now analyse the observed range distribution curve by using equation (5). Unfortunately, however, since the effects by the two components of (Li–p) γ–rays, namely 17.6 and 14.8 Mev lines (**9**), could not be separated by the observed curve in our experiments, we have to consider the whole effect presumably as solely due to the 17.6 Mev line.* Then we can explain the portion of the longer and shorter range of the observed distribution curve as due to

$$\left.\begin{aligned} &\mathrm{Be}^{9} + 17.6\ \mathrm{Mev}\ \gamma \rightarrow \mathrm{Be}^{8*} + n\,, \quad (7\ \mathrm{Mev\ excited}) \\ &\mathrm{Be}^{8*} \rightarrow 2\alpha\,, \end{aligned}\right\} \tag{6}$$

and

$$\left.\begin{aligned} &\mathrm{Be}^{9} + 17.6\ \mathrm{Mev}\ \gamma \rightarrow \mathrm{Be}^{8} + n\,, \quad (\mathrm{ground\ state}) \\ &\mathrm{Be}^{8} \rightarrow 2\alpha\,, \end{aligned}\right\} \tag{7}$$

respectively.

The range distribution curve calculated under the assumption of the processes (6) and (7) is shown by the dotted line in the figure. The conformity with the observed curve is fairly satisfactory for the range longer than about 2.5 cm. It seems, however, that there remains a small deviation for the range smaller than the value, which cannot be explained by any process shown in Table II. It may probably be attributed to the fact that the pulses of smaller height are observed more frequently than they are theoretically expected, because of the effect of the cylindrical shape of the counter. A more precise experiment will be necessary to derive conclusion as to this point.

To obtain the cross-section for each process, it is necessary to know the counting efficiency of the γ–ray counter. This quantity was previously calculated by one of the authors (**10**) and found to be

23.8 % for 17.6 Mev γ–rays,

18.1 % for 14.8 Mev γ–rays,

and 3.2 % for 6.13 Mev γ–rays,

respectively, for the lead-walled counter used in our experiments.

* According to Walker and McDaniel (**9**), the ratio of intensities of the lower energy line to the higher energy line is found to be 0.50 at 0.46 Mev protons.

The practical absorption coefficient of the lead cylindrical shield covering the γ–ray counter was carefully measured for both of the γ–rays and was found to be

$$\mu_{\text{Li-p}} = 0.53\ \text{cm}^{-1},$$

and

$$\mu_{\text{F-p}} = 0.40\ \text{cm}^{-1},$$

respectively.

The actual readings of the γ–counts were corrected thereby in computing the absolute number of γ–quanta emitted from the target. Using these values, the cross-section with which the Be^{8*} nucleus is produced by the γ–rays could be estimated and it is given as

$$\sigma_{17.6} = 2.15 \times 10^{-27}\ \text{cm}^2 \quad \text{for the 7 Mev excited state,} \tag{8}$$

and

$$\sigma_{17.6} = 5.1 \times 10^{-26}\ \text{cm}^2 \quad \text{for the ground state,} \tag{9}$$

respectively.

(ii) For the (F–p) γ–rays, the observed number of α–particles is very small compared to the case of (Li–p) γ–rays. The maximum range was found to be about 1.5 cm and the process shown in the last column of Table II seems therefore to be possible. We may interpret the observed curve as the superposition of the following two processes:

$$\left.\begin{aligned} &Be^9 + 6.13\ \text{Mev}\ \gamma \rightarrow Be^8 + n\,, \qquad \text{(ground state)} \\ &Be^8 \rightarrow 2\alpha\,, \end{aligned}\right\} \tag{10}$$

and

$$\left.\begin{aligned} &Be^9 + 6.13\ \text{Mev}\ \gamma \rightarrow Be^{8*} + n\,, \quad \text{(3 Mev excited).} \\ &Be^{8*} \rightarrow 2\alpha\,. \end{aligned}\right\} \tag{11}$$

Now, as shown in Table II, the maximum range of α–particle is about 0.33 cm and 1.25 cm respectively for the cases expressed in (10) and (11). We may explain in this way the part of range longer than 0.33 cm presumably by the process (11).* However, the shape of the range distribution curve calculated for this process is found to change more rapidly with the range than that of the observed one.

* Recently, Miller and Cameron (**11**) have reported that the 3 Mev excited state of Be^{8*} appears in the photo-disintegration of C^{12} by the X–rays from a 24 Mev betatron. This is not consistent with our results, though no decisive conclusion could be derived owing to the lack of their number of observed pulses.

On the other hand, we see that the part of range smaller than 0.33 cm is nearly consistent with process (10). There will therefore remain a small unexplained part of the range from 0.33 to 1.5 cm similarly to the case of (Li–p) γ–rays.

Now, for the sake of simplicity, if the process (10) is solely considered in the case of (F–p) γ–rays, we obtain

$$\sigma_{6.13} = 1.62 \times 10^{-27}\,\mathrm{cm}^2 \tag{12}$$

as the roughly estimated value of the cross-section for the ground state of Be^8.

From (9) and (12), it can be concluded that the cross-sections of the process

$$Be^9 + h\nu \rightarrow Be^8 + n \quad (Be^8 \text{ in the ground state})$$

are 5.1×10^{-26} and $16.2 \times 10^{-28}\,\mathrm{cm}^2$ for the 17.6 and 6.13 Mev γ–rays respectively.

According to the theoretical calculation by Guth and Mullin (1), the cross-section is about $15 \times 10^{-28}\,\mathrm{cm}^2$ for the 6.13 Mev γ–rays and it decreases monotonously with the energy of the γ–rays in the energy range under consideration.* The observed value is, in the case of 6.13 Mev γ–rays, nearly equal to the theoretical one, but it increases with the energy of the γ–rays in our energy range, which is contradictory to the theoretical expectation. This discrepancy may probably be ascribed to the fact that the assumptions made by Guth and Mullin do not hold for the γ–rays of such high energies, in which the Be^9 nucleus is taken to consist of the inert Be^8 core and a " valence " neutron moving around it in the ground $P_{\frac{3}{2}}$ state and the electric dipole transitions take place when it is irradiated by the γ–rays.

It is to be noted that the excited states of Be^{8*} of 4.8 Mev and probably also 3.0 Mev which were observed in the nuclear reactions by high speed ions (7) seem to have no contribution in the photo-disintegration process.

From the above consideration, it may be concluded that the Be^9 nucleus emits a neutron when irradiated by the γ–rays and then the residual Be^8 nucleus splits up into two α–particles. We previously observed (12) that a fission process took place in the nucleus of Uranium or Thorium irradiated by the high energy γ–rays. Comparing the photo-fission process of Uranium and Thorium to the photo-

* Miller and Cameron (11) found one event which may be explained as the photo-disintegration of C^{12} via the ground state of Be^8.

disintegration of Be^9 nucleus, it may be presumably considered that the nucleus of Uranium or Thorium emits at first a neutron when irradiated by the γ-rays and then splits up into two nuclei of intermediate mass.

More precise experiments are now in progress by using a photographic emulsion and a deep ionization chamber with a grid.

In conclusion, the authors acknowledge their indebtedness to the financial support given by the Special fund for the Advancement of Science of the Ministry of Education.

REFERENCES

1. J. Chadwick and M. Goldhaber, Proc. Roy. Soc., A **151** (1935), 479.
   H. v. Halban, C. R., **206** (1938), 1170.
   K. Kimura, Memo. Coll. Sci. Kyoto Imp. Univ., **22** (1940), 237.
   J. E. Meyer and I. A. Van Atta, Phys. Rev., **61** (1942), 19.
   F. G. Hontermans and I. Bartz, Physik. Zeits., **44** (1943), 167.
   L. G. Elliott, M. Deutsch and A. Roberts, Phys. Rev., **63** (1943), 386.
   M. L. Wiedenbeck and C. J. Marhoefer, Phys. Rev., **67** (1945), 54.
   K. Siegbahn, Phys. Rev., **70** (1946), 127.
   B. Russell, D. Sachs, A. Wattenberg and R. Fields, Phys. Rev., **73** (1948), 545.
   B. Hamermesh, M. Hamermesh and A. Wattenberg, Phys. Rev., **76** (1949), 611.
   V. I. Mamasachilisow, Phys. Zeits. Sowjetunion, **10** (1936), 214.
   E. Guth and C. J. Mullin, Phys. Rev., **74** (1948), 833; **76** (1949), 234, 682.
2. B. Arakatsu and others, Proc. Phys.-Math. Soc. Japan, **25** (1943), 173; Journ. Phys. Soc. Japan, **1** (1946), 24.
3. M. Sonoda, Memo. Coll. Sci. Kyoto Univ., **25** (1949), 187.
4. M. Sonoda, Memo. Coll. Sci. Kyoto Univ., **25** (1949), 177.
5. T. S. Tayler, Phil. Mag., **21** (1911), 571; **24** (1912), 296; **26** (1913), 402.
   M. G. Holloway and M. S. Livingston, Phys. Rev., **54** (1938), 18.
6. K. Kimura and Y. Uemura, Memo. Coll. Sci. Kyoto Imp. Univ., **23** (1940), 1.
7. W. F. Hornyak and T. Lauritsen, Rev. Mod. Phys., **20** (1948), 191.
8. J. A. Wheeler, Phys. Rev., **59** (1941), 27.
9. R. L. Walker and B. D. McDaniel, Phys. Rev., **74** (1948), 315.
10. M. Sonoda, Journ. Phys. Soc. Japan, in press.
11. C. H. Miller and A. G. W. Cameron, Phys. Rev., **78** (1950), 78.
12. B. Arakatsu and others, Proc. Phys.-Math. Soc. Japan, **23** (1941), 440, 623.

Nuclear Research Laboratory,
Institute of Physics,
University of Kyoto.

Memoirs of the College of Science, University of Kyoto, Series A.
Vol. XXVI, Nos. 1 & 2, Article 11, 1950.

Measurement of the Branching Ratio of Thorium C by a Photographic Method

By

Senzo Tokunaga

(Received July 15, 1950)

1. Introduction

It is well known that in the radioactive series of Thorium families a branching takes place in Thorium C; ThC may decay with the emission of either an α- or β-particle. The latest experiment to determine the branching ratio of the dual decay was performed by A. F. Kovarik and N. I. Adams (1) with an ionization chamber and a linear amplifier. They used specimens which were in radioactive equilibrium, and by counting the number, N_1, of α-particles from ThC′ and that, N_2, of all kinds of α-particles from the same specimens (α-rays from RdTh, ThX, Tn, ThA and Th(C + C′)) in the same interval of time, they obtained the results that the ratio $N_1/\frac{1}{5}N_2$, i. e., ThC′/Th(C + C′) was 0.663. From this, we can see that 66.3 per cent of ThC nuclei decays with the emission of β-particles, while the remaining 33.7 per cent with the emission of α-particles.

2. Results of experiment

We performed an experiment to measure the branching ratio of ThC by a photographic method. One of the methods with photographic emulsions may be done by counting the number of Thorium stars* with five prongs, distinguishing the tracks of α-rays from ThC and ThC′. (One of the Thorium stars is shown in Fig. 1.) But there appear so many particles which pass out of the emulsion that the method requires much labour and moreover is not easy. So we turned to the following method.

* After we soak a plate in a solution of Thorium acetate or nitrate in water (1 per cent by weight) for ten minutes, and dry, leave in the dark for three days, and then develop, we can find in the plate many star-like tracks.

Fig. 1. Thorium stars (×1000)

(a)	RdTh	22.0 μ
(b)	ThX	23.6 μ
(c)	Tn	27.7 μ
(d)	ThA	31.2 μ
(e)	ThC′	47.2 μ

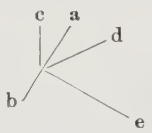

The method is to count the number of tracks of α-rays from ThC and ThC′ respectively in the same emulsion exposed to a specimen. We used a nuclear emulsion plate, Eastman Kodak NTB (50 microns thick), and a specimen of Thorium deposit which was formed on the surface of a copper disc and in which radioactive equilibrium had been established between ThB and ThC. After putting the emulsion face to face on the surface of the copper disc for some minutes, we developed. Thus, we could obtain many tracks of α-rays in the emulsion emitted only from ThC and ThC′. If we observe the tracks in the emulsion with a microscope, it is liable to miss some of the tracks. So we took photomicrographs of them magnifying 200 times. One of the photomicrographs is shown in Fig. 2. With this magnification we could photograph all of the tracks because of its deep focal depth. Then, the classification of these tracks was made possible from the following points of view.

In the first place, the stopping power of the emulsion being 1800, all the α-particles from ThC and ThC′ are considered to have their

whole ranges in the emulsion. And as α-particles enter the emulsion with various angles, the tracks in the photomicrographs are their projections in the direction parallel to the surface of the emulsion. The range of α-particle from ThC in the photomicrograph being 0.52 cm (26.1 microns in the original emulsion), the tracks longer than 0.52 cm are attributed to ThC′ and all the other tracks to Th (C + C′) α-rays.

Fig. 2. Tracks of α-particles of ThC and ThC′ ($\times$200)

In the second place, the angular distribution of α-particle emission is spherically symmetric. We have ascertained the fact by estimating the angle of dip of α-particle (the angle between the direction of the particle and the normal to the surface of the emulsion), measuring the length of each track longer than 0.52 cm in the photomicrographs. So, if the angle of dip is θ, when the length of ThC′ α track is 0.52 cm, the number of α-particles the tracks of which are not longer than 0.52 cm will be proportional to the solid angle $2\pi(1-\cos\theta)$ and that of longer $2\pi\cos\theta$. Therefore, the ratio of the number of tracks of ThC′ longer than 0.52 cm to that of not longer than 0.52 cm would be $(1-\cos\theta)/\cos\theta$. Since $\sin^{-1}26.1/47.3 = 33.4^\circ$ (the range of ThC′ being 47.3 microns in the emulsion), if the number of tracks longer than 0.52 cm is x, the number of α-rays from ThC′ may be given as $[1+(1-\cos\theta)/\cos\theta]x$, numerically $(1+0.198)x$.

We examined 27 sheets of photomicrographs the size of which was 6 cm $\times$ 10 cm, and counted 6792 tracks in total, of which 3739 tracks were longer than 0.52 cm. So, the number of ThC′ would be 4484 and the ratio of ThC′ to Th(C + C′) 0.6601 ± 0.0028. The results are nearly equal to that of Kovarik et al.

The characteristic of the photographic method is that we can count the number of tracks of α-particles emitted only by ThC and ThC′ in the same emulsion in the same interval of time.

Finally the author expresses his gratitude to Eastman Kodak Co. for their kind offer of the nuclear emulsion plates and Dr. B. Arakatsu and Prof. K. Kimura for their important advice, and Miss K. Ishii for her help in this work. This work is indebted to the Ministry of Education for research grant.

REFERENCES

1. A. F. Kovarik and N. I. Adams, Phys. Rev., **54** (1938), 413.

Memoirs of the College of Science, University of Kyoto, Series A,
Vol. XXVI, Nos. 1 & 2, Article 12, 1950.

1.5 cm Wave-length Microwave Spectroscope*

By

Isao Takahashi, Akira Okaya, Toru Ogawa, and **Tsuneo Hashi**

(Received June 30, 1950)

1. Introduction

In U. S. A., the field of microwave spectroscopy has grown with tremendous rapidity in post war years, but in our country, the researches in this field have been scarce so far.

In compliance with the physical importance of this field, we have designed and constructed the 1.5 cm wave-length spectroscope, whose general view is given in Fig. 1. With this set, we observed the absorption line of Methyl Bromide (CH_3Br). Our observed wave-length of maximum absorption coincides with the theoretical value within the

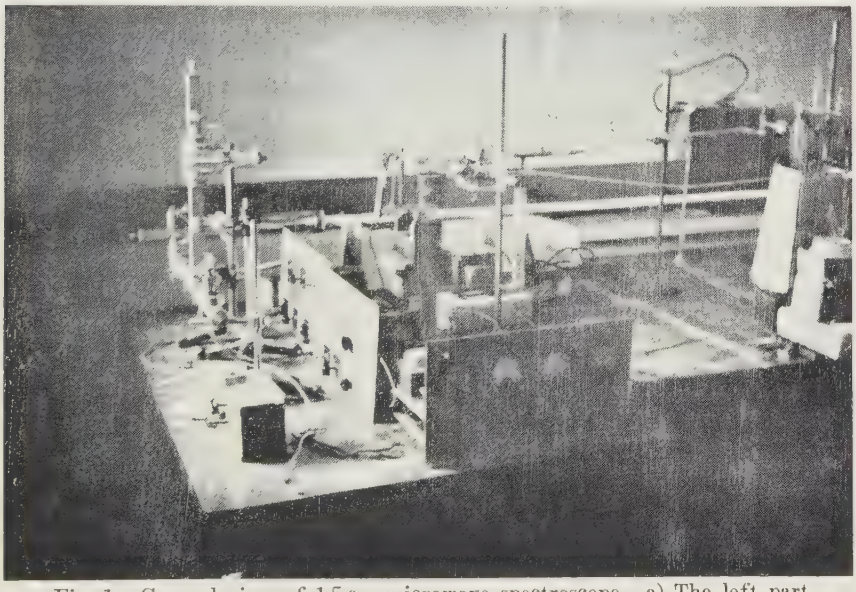

Fig. 1. General view of 1.5 cm microwave spectroscope. a) The left part

* Read on May 1, 1950, at the meeting of Microwave Physics Branch of the Physical Society of Japan.

error of our cavity wave meter and we confirmed the hyperfine structure of spectral line due to the presence of the quadrupole moment of Br nucleus.

Several accurate measurements about Methyl Bromide have already been reported by others (**11, 12, 13, 14, 15**). Methyl Bromide was used in our measurement too, since it is appropriate for checking our set and in our country no experimental report about centimeter wave spectrum has hitherto been given.**

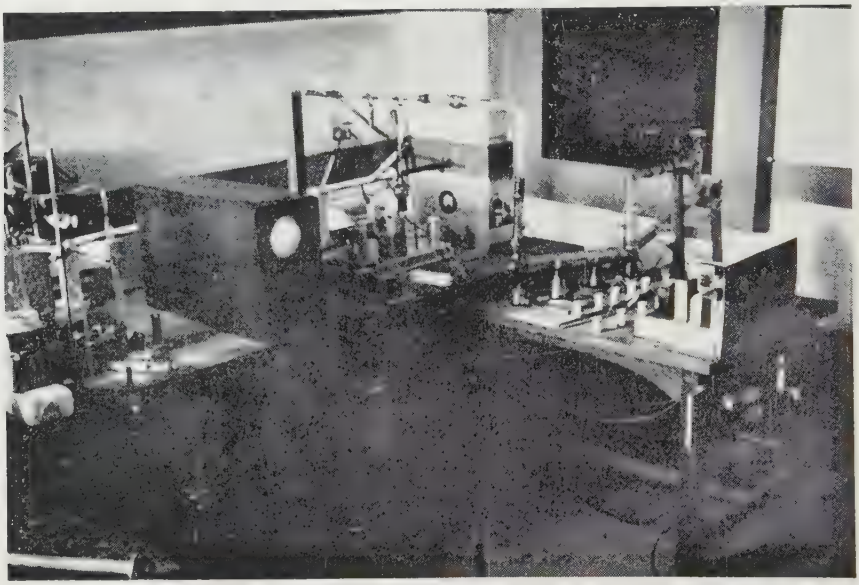

Fig. 1. General view of 1.5 cm microwave spectroscope. b) The right part

2. Description of the set and its components

The block diagram of our microwave spectroscope is shown in Fig. 2. A part of 3 cm microwave energy from the signal oscillator, passing through T-junction and attenuator A, is converted to 1.5 cm energy by the frequency converter. This converted energy is then led into the absorption cell formed by a circular cylinder and transparent mica windows at its both ends.

The original 3 cm energy is frequency-modulated by the saw-tooth generator and consequently the 1.5 cm is so also. Thus, if the frequency of the converted energy is tuned to the absorption frequency of

** We are aware of only Prof. Kojima's spectroscopic researches with 12 cm wavelength microwave which are carried on at Tokyo Educational University. He also has read his paper on May 1, 1950.

the sample in the cell, the energy going out from the cell is much damped.

The output energy amplitude-modulated corresponding to the degree of absorption of the sample in the cell is detected by the crystal detector and the detected power which represents the absorption character of the sample is amplified and applied to the vertical axis of the oscillograph whose horizontal axis is swept by the voltage of the saw-tooth generator. Thus, the absorption character of the sample is visualized on the screen of the oscillograph.

In our set, the amplification of detected power is carried out in two ways. One way is the direct amplification by the video amplifier, and the other consists in modifying the signal generator with 463 kc/sec source modulator in addition to the saw-tooth generator and amplifying and detecting by means of 463 kc/sec narrow band receiver.

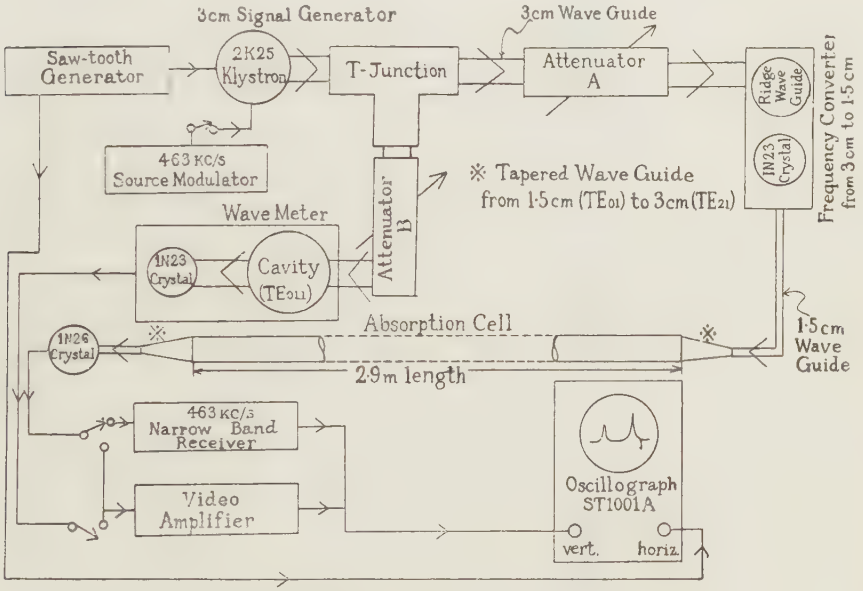

Fig. 2. Block diagram of 1.5 cm microwave spectroscope.

In the following, the main components of the set are described.
(1) *Signal Generator*: The well-known klystron tube 2K25 is used and its frequency range is from 8.5 to 9.8 kMc/sec.
(2) *Frequency Converter*: As shown in Fig. 3, it is composed of ridge type wave guide, coaxial line and silicon crystal 1N23. To design the ridge type wave guide, some papers (**2, 3**) were referred to, and this is the matching device between 50 ohm coaxial line and 3 cm wave guide.

To check its behavior, we measured the voltage standing wave ratio (V. S. W. R.) in 3 cm wave guide when the ridge type wave guide is inserted between 3 cm wave guide and 50 ohm coaxial line, and reasonable results were obtained as shown in Table I below.

TABLE I. Some results concerning ridge type wave guide.

Wave meter scale "L"	Converter crystal current	V.S.W.R. in 3cm wave guide	Impedance calculated from V.S.W.R. "Z"
23.68 mm	2.50 m A	1.335	698 Ω
23.93	3.50	1.284	671
24.25	5.12	1.333	696
24.62	4.12	1.285	671

The characteristic impedance of 3 cm wave guide $z_0 = 523\ \Omega$

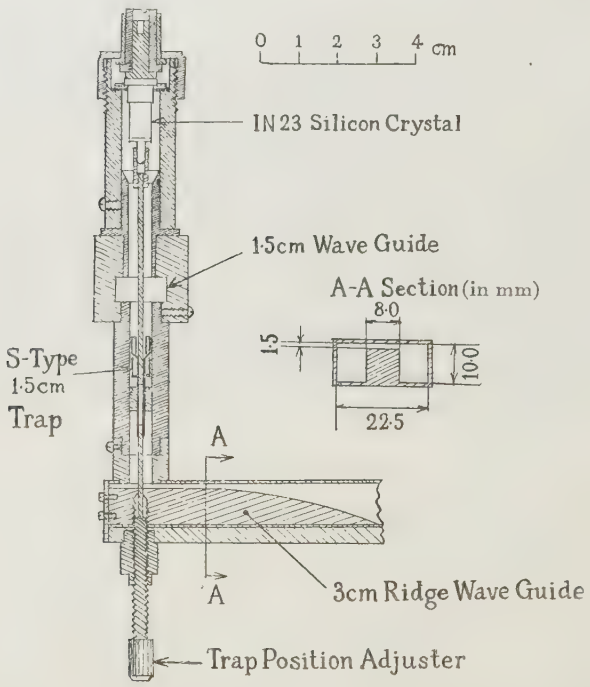

Fig. 3. Schematic sketch of frequency converter.

(3) *Attenuator*: Vane type variable attenuator is used. The vane is a thin bakelite plate coated with the mixture of graphite powder and binder consisting of polystyrene and benzol solvent. Maximum attenuation is about 20 db.

(4) *Wave meter*: A transmission type cavity wave meter utilizing

TE_{011} mode is used in 8.5—9.8 kMc/sec range. To suppress TM_{111} mode, behind its piston is inserted the link of thin nickel plate which is used because of unavailableness of polyiron. This wave meter is self-calibrating and can afford the frequency measurement to the accuracy of $\pm$ 5 Mc/sec.

The output from the crystal detector attached to the cavity is led through the video amplifier and used as a frequency marker pip on the oscillograph screen.

(5) *Crystals*: 1N23 silicon crystals are used for converter and 1N26 for detection of 1.5 cm wave. We remove 1N26 from the wave guide for its safety except in case of experiment being carried on.

(6) *Absoption cell*: The absorption cell is constructed from brass circular wave guide of 2.9 m length, 2.29 cm inner diameter and 2.59 cm outer diameter. Of course, we know that the rectangular wave guide is better for our purpose, but since it is not available for us under the present circumstances, we have employed the following procedure: The section of 1.5 cm wave rectangular guide is gradually changed from rectangle of 13.0 mm $\times$ 6.5 mm to the circle of 22.9 mm diameter through elliptic section tapered along 22 cm length. The surface finishing of this tapered part is most carefully done and so expected symmetry and inconsiderable reflection is attained.

The mica window of about 1/20 mm thickness is fixed at each end to seal the cell by means of red beeswax and brass ring to clamp and some cares are taken to minimize the reflection from these junction points. But we cannot yet succeed to suppress completely such reflection, as some ghosts have appeared which, however, can be clearly distinguished from absorption lines.

We suppose that the mode in the cell is mainly TE_{21} but some other modes can be anticipated to occur at the same time, which we are now planning to suppress.

(7) *Saw-tooth generator*: The saw-tooth generator of frequency range from 1.5 c/sec to 150 c/sec is used. Its circuit is similar to that of A. H. Sharbaugh (5). Low sweep rates serve to better resolution and to more accurate production of the absorption line shape. 50 volt sweep voltage applied to the reflector electrode of klystron suffices to sweep the 100 Mc/sec band width at 1.5 cm wave.

The sweep frequency is 60 c/sec when the video amplifier is used, and 2 c/sec when the narrow band receiver is.

(8) *Narrow band receiver*: A handmade single band receiver with crystal filter is used. The selection of frequency 463 kc/sec is made for

convenience only. The gain is about 140 db, the band width can be changed from 500 c/sec to 10 kc/sec on five steps, and for input stage, low noise tube 6AC7 is used.

(9) *Video amplifier*: The gain is about 100 db. The frequency response is sufficient for our purpose.

(10) *Oscillograph*: The type ST1001A of Matsuda Mfg. Co. is used, some additional measures to adapt for our set being taken.

(11) *Vacuum system*: The block diagram of vacuum system is shown in Fig. 4. Phillips gauge was used for measuring pressure of the gas, since it has fairly good sensitivity and moreover is not spoiled by gases. Its measuring limit is about 10^{-5} mmHg.

In order to obtain greater accuracy at lower pressure, however, a more sensitive ionization gauge with L. N. Ridenour stabilization circuit (6) was used. We have thus obtained the minimum pressure as low as 10^{-6} mmHg in wave guide cell.

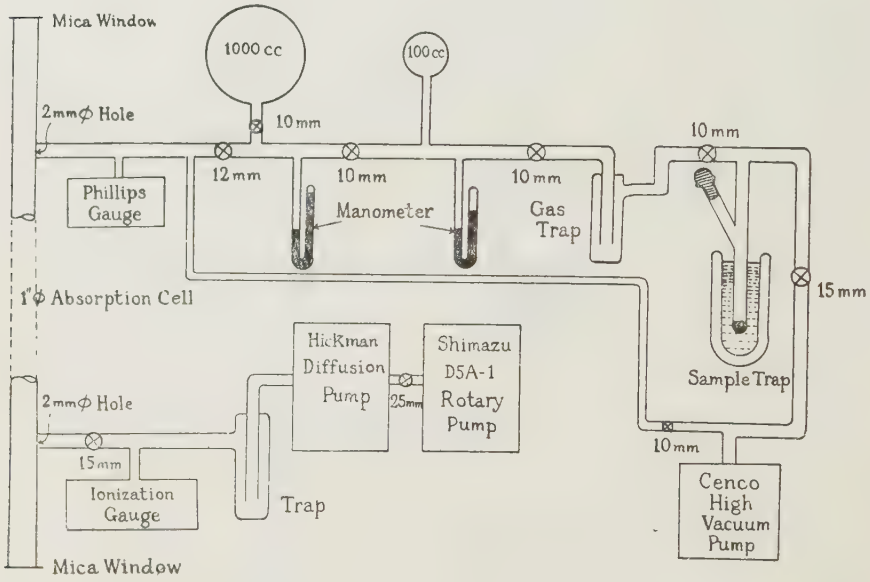

Fig. 4. Block diagram of vacuum system.

3. Absorption spectra of methyl bromide

With our microwave spectroscope, we observed the rotational transition $J, K(0, 0) \rightarrow J, K(1, 0)$ of CH_3Br^{79} and CH_3Br^{81}. The absorption frequencies were measured with the cylindrical cavity wave meter operating in TE_{011} mode. The resonant frequencies are given by the following formula: $f = (c/2)\,[(7.6634/\pi D)^2 + (1/L)^2]^{\frac{1}{2}}$,

where c is the light velocity, and D and L are the diameter and length of the cylinder respectively.

Our measuring system can afford the accuracy of ± 5 Mc/sec at 3 cm wave. The satellite structure of rotational line of CH_3Br is caused by the interaction of nuclear quadrupole moment of Br with molecular field. The theoretical formula for the interaction (**7, 8, 9, 10**) is

$$E_0 = eQ\frac{\partial^2 V}{\partial z^2}\left(\frac{3K^2}{J(J+1)} - 1\right)\frac{\frac{3}{4}C(C+1) - I(I+1)J(J+1)}{2(2J+3)(2J-1)I(2I-1)},$$

with

$$C = F(F+1) - I(I+1) - J(J+1),$$

$$F = J + I, J + I - 1, \cdots\cdots, |J - I|,$$

where I is the spin of the interacting nucleus, e the electronic charge, Q the nuclear quadrupole moment, and $\partial^2 V/\partial z^2$ is the divergence along the molecular axis of the molecular field at the interacting nucleus.

For the case of CH_3Br, we performed calculations, by putting the following values (**15**)

$$eQ\,\partial^2 V/\partial z^2 = 577.3 \text{ Mc/sec for } CH_3Br^{79},$$

$$= 482.4 \text{ Mc/sec for } CH_3Br^{81},$$

$$I = 3/2 \text{ for both } Br^{79} \text{ and } Br^{81},$$

and using selection rules

$$\Delta J = +1, \quad \Delta K = 0, \quad \Delta F = 0, \pm 1.$$

Our observed values and calculated values are summarized in Table II.

TABLE II. Absorption frequencies of CH_3Br.

	Transition	Frequency (obs.)	Frequency(calc.)
CH_3Br^{79}	$F = 3/2 \rightarrow 1/2$	1899_1 Mc/sec	18992 Mc/sec
	$3/2 \rightarrow 3/2$	1926_2	19252
$\nu_0 = 19197$ Mc/sec	$3/2 \rightarrow 5/2$	1910_8	19108
CH_3Br^{81}	$3/2 \rightarrow 1/2$	1896_0	18943
	$3/2 \rightarrow 3/2$	1917_0	19160
$\nu_0 = 19064$ Mc/sec	$3/2 \rightarrow 5/2$	1906_8	19040

(ν_0: frequency of the unsplit rotational line)

The calculated and observed values agree well with each other within the error of our present frequency measuring system, whose accuracy is ± 10 Mc/sec at 1.5 cm wave.

Several accurate measurements for CH_3Br have been already reported (**11, 12, 13, 14, 15**). Among them, however, 1.5 cm wave-length spectrum was observed only by A. H. Sharbaugh and J. Mattern (**15**).

Two absorption lines accompanied by one ghost are shown in Fig. 5.

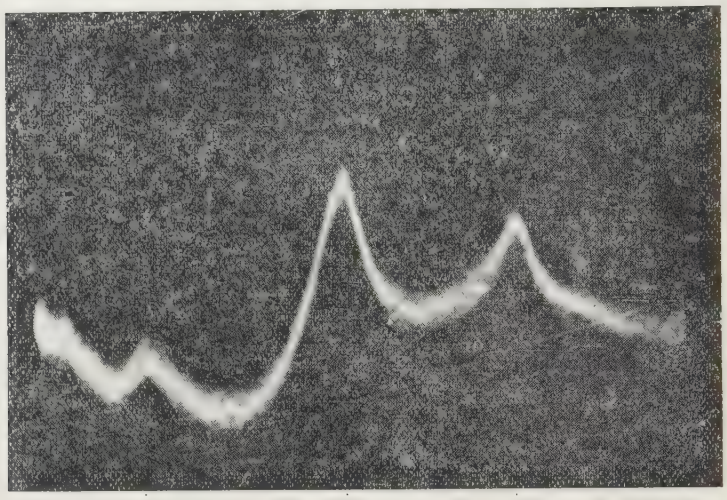

Fig. 5. The absorption lines of CH_3Br.

The intensity comparison among absorption lines was not made this time, because it was difficult to adjust all circuit components for each line into the same conditions, especially so for the lines lying in the different electronic tuning ranges of klystron, and further the output power of klystron could not be kept constant without any necessary procedure over the range of electronic tuning.

The more accurate frequency measuring system utilizing harmonics of 100 kc/sec crystal controlled oscillator which makes zero beat with the standard wave of the Standard Frequency Station JJY is now under construction by us.

4. Acknowledgements

The authors express their heartfelt thanks to Prof. R. Nozu, Dr. R. Goto, and Mr. H. Shakutsui for the preparation of the sample, and

we owe deep thanks to Dr. O. Cary who helped us to get klystron and silicon crystals. Also, much credit is due to Messrs. H. Narumi and H. Takeyama and several members both in Arakatsu Laboratory and in our Laboratory. We thank further to Messrs. D. Nakayama and H. Iwata for their cooperation in constructing wave meter and other components used in our research.

REFERENCES

1. W. Gordy, Rev. Mod. Phys., **20** (1948), 668.
2. S. B. Cohn, Proc I. R. E., **35** (1947), 783.
3. T. G. Mihran, Proc. I. R. E., **37** (1949), 640.
4. C. G. Montgomery, *Technique of Microwave Measurements*, Rad. Lab. Series **11**, (McGraw-Hill, 1947), 322.
5. A. H. Sharbaugh, R. S. I., **21** (1950), 120.
6. L. N. Ridenour, and C. W. Lampson, R. S. I., **8** (1937), 162.
7. H. B. G. Casimir, *On the Interaction between Atomic Nuclei and Electrons* (Teyler's Tweede Genootschap, E. F. Bohn, *Haalem*, 1936); Physica, **2** (1935), 719.
8. D. K. Coles, and W. E. Good, Phys. Rev., **70** (1946), 979.
9. J. H. Van Vleck, Phys. Rev., **71** (1947), 468.
10. B. P. Dailey, R. L. Kyhl, M. W. P. Strandberg, J. H. Van Vleck, and E. B. Wilson, Jr., Phys. Rev., **70** (1946), 984.
11. W. D. Hershberger, J. Appl. Phys., **17** (1946), 495.
12. W. Gordy, J. W. Simons, and A. G. Smith, Phys. Rev., **72** (1947), 249, 344.
13. J. W. Simons, W. Gordy, and A. G. Smith, Bull. Amer. Phys. Soc., **23** (1948), No.3.
14. W. Gordy, J. W. Simons, and A. G. Smith, Phys. Rev., **74** (1948), 243.
15. A. H. Sharbaugh, and J. Mattern, Phys. Rev., **75** (1949), 1102.

Memoirs of the College of Science, University of Kyoto, Series A,
Vol. XXVI, Nos. 1 & 2, Article 13, 1950.

On the Effect of a Conducting Screen with Concentric Aperture in the Circular Wave Guide *

By

I. Takahashi, T. Watanabe and **K. Tanimoto**

(Received June 30, 1950)

1. General description

When there is a thin conducting screen with a concentric circular aperture in the circular wave guide (see Fig. 1), the screen behaves like a shunt reactance inserted in the transmission line. We shall discuss the behaviour of such a screen in the present paper.

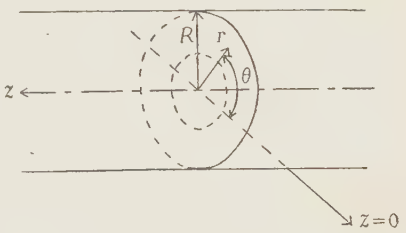

Fig. 1.

Now, the symmetrical E-type wave is taken to be incident waves in the circular wave guide of inner radius R, i. e., we assume that the incident waves are given, in M. K. S. units, by

$$\left.\begin{aligned} E_z^{\pm m} &= J_0(\lambda_m r)\, e^{i(\omega t \mp h_m z)}, \\ E_r^{\pm m} &= \pm i \frac{h_m}{\lambda_m} J_1(\lambda_m r)\, e^{i(\omega t \mp h_m z)}, \\ E_\theta^{\pm m} &= 0, \\ H_z^{\pm m} &= 0, \\ H_r^{\pm m} &= 0, \\ H_\theta &= \mp \frac{\varepsilon_0 \omega}{h_m} E_r^{\pm m}, \end{aligned}\right\} \qquad (1)$$

* Read at the meeting of Electric Waves Branch of the Physical Society of Japan (Oct. 1949).

where J's are cylinder functions of the first kind and $\lambda_1 = \xi_1/R$, $\lambda_2 = \xi_2/R, \cdots\cdots$, ($\xi_1$, ξ_2, $\xi_3, \cdots\cdots$ being the roots of $J_0(x) = 0$), while $h_m^2 = k^2 - \lambda_m^2$ with $\omega^2 \varepsilon_0 \mu_0 = k^2$.

In compliance with the mth mode of incident waves and with the axial symmetry of this transmission system, E_{0m} waves are supposed to be excited and therefore E_r depends upon r alone in the aperture. Hence, we can assume in the aperture, which is situated at $z = 0$, that

$$(E_r)_{z=0} = \psi(r), \tag{2}$$

while on the screen outside the aperture, we have

$$E_r = 0.$$

Therefore we obtain the following equations at $z = 0$; namely, on the incident waves side of the screen ($z < 0$),

$$E_r^{(-)} = E^{+m} + \sum_{n=1}^{\infty} a_n^{(-)} E_r^{-n}, \tag{3}$$

and, beyond the screen ($z > 0$),

$$E_r^{(+)} = \sum_{n=1}^{\infty} a_n^{(+)} E_r^{+n}. \tag{4}$$

Now, making use of the orthogonality of $J_1(\lambda_n r)$, $a_n^{(\pm)}$ are expressed in terms of $\psi(r)$ by (3) and (4). Particularly, when $n = m$,

$$a_m^{(-)} = \frac{\lambda_m}{\gamma_m h_m}\left(\frac{h_m \gamma_m}{\lambda_m} + i\varphi_m\right), \tag{5}$$

and when $n \neq m$,

$$a_n^{(-)} = i\varphi_n \frac{\lambda_n}{\gamma_n h_n}, \tag{6}$$

$$a_n^{(+)} = -i\varphi_n \frac{\lambda_n}{\gamma_n h_n}, \tag{7}$$

where

$$\gamma_n = \int_0^R (J_1(\lambda_n r))^2 r\, dr, \qquad \varphi_n = \int_0^\rho \psi(r) J_1(\lambda_n r) r\, dr.$$

Next, $H_\theta^{(+)}$ and $H_\theta^{(-)}$ are expressed in terms of (5), (6) and (7) as follows (in the following, field quantities represent the values at $z = 0$):

$$H_\theta^{(-)} = -\frac{\varepsilon_0\omega}{h_m}E_r^{+m} + \sum_{n=1}^{\infty} a_n^{(-)}\frac{\varepsilon_0\omega}{h_n}E_r^{-n}$$

$$= -i\varepsilon_0\omega\left\{\frac{J_1(\lambda_m r)}{\lambda_m} + \sum_{n=0}^{\infty}\frac{a_n^{(-)}}{\lambda_n}J_1(\lambda_n r)\right\}$$

$$= -i\varepsilon_0\omega\left\{2\frac{J_1(\lambda_m r)}{\lambda_m} + i\int_0^{\rho}\psi(r')\,G(r', r)r'\,dr'\right\}, \qquad (8)$$

and

$$H_\theta^{(+)} = -\varepsilon_0\omega\int_0^{\rho}\psi(r')\,G(r', r)r'\,dr', \qquad (9)$$

with

$$G(r', r) = \sum_{n=1}^{\infty}\left\{J_1(\lambda_n r')J_1(\lambda_n r)\right\}/\gamma_n h_n .$$

Since the screen is thin, it has been assumed in the above that the relation $E_r^{(+)} = E_r^{(-)}$ holds in the region $0 \leqq r \leqq \rho$, where ρ is the radius of the aperture.

Similarly, we have the relation $H_\theta^{(+)} = H_\theta^{(-)}$ only in the region $0 \leqq r \leqq \rho$. Then, we obtain, in the interval $0 \leqq r \leqq \rho$,

$$\frac{iJ_1(\lambda_m r)}{\lambda_m} = \int_0^{\rho}\psi(r')\,G(r', r)r'\,dr'. \qquad (10)$$

Multiplying both sides with $\psi(r)$, and intergrating from 0 to ρ, we have

$$\int_0^{\rho}\frac{i\psi(r)J_1(\lambda_m r)}{\lambda_m}r\,dr = \int_0^{\rho}\int_0^{\rho}\psi(r')\,G(r', r)\psi(r)r'dr'rdr . \qquad (11)$$

If the solution $\psi(r)$ of the integral equation (10) be found, we can compute $a_n^{(-)}$ and $a_n^{(+)}$, and obtain the field quantities exactly. But it is very difficult to find the exact solution $\psi(r)$ and its numerical integration is also troublesome (**1**). Mayer (**2**) has calculated the proper frequency of the nosed-in cavity, by a method somewhat similar to ours. Hansen (**3**) has also treated the similar problem about the cylindrical cavity, his expression corresponding to our expression (10) being however somewhat different from ours. It is because of the fact that we deal with the progressive and reflected waves in the guide, while Hansen considered the stationary waves in the cavity.

2. Behavior of a small aperture

For arbitrary magnitude of ρ, it is difficult to solve (10) either analytically or numerically. We shall therefore discuss the case of $\rho \ll 2\pi/k$. In such a case, it will be seen by analogy in the electrostatic case that $\psi(r)$ will have a singularity like $1/\sqrt{\rho^2 - r^2}$ in the neighbourhood of the periphery of the aperture, and due to the axial symmetry, we have

$$\psi(0) = 0.$$

Hence it will be justified to put

$$\psi(r) = br/\sqrt{\rho^2 - r^2},$$

where b is the unknown constant to be determined by (11).

Substituting this into (11), we obtain

$$b = \frac{i}{\lambda_m}\alpha_m \Big/ \sum_{n=1}^{\infty} \frac{{\alpha_n}^2}{\gamma_n h_n}, \tag{12}$$

with

$$\alpha_n \equiv \int_0^{\rho} \frac{r^2}{\sqrt{\rho^2 - r^2}} J_1(\lambda_n r)\, dr\,.$$

Hence, if follows that

$$\varphi_n = \frac{i}{\lambda_m}\alpha_m\alpha_n \Big/ \sum_{n'=1}^{\infty} \frac{{\alpha^2}_{n'}}{\gamma_{n'} h_{n'}}\,. \tag{13}$$

The convergency of series in (12) and (13) will be discussed later.

Now, we assume that the mode of the incident waves is $m = 1$ and other modes in both reflected waves and transmitted waves are cut off. Then, we obtain the reflection coefficient $a_1^{(-)}$ and the transmission coefficient $a_1^{(+)}$ by the expressions:

$$a_1^{(-)} = 1 + i\frac{\lambda_1}{h_1 i_1}\varphi_1 = 1 - \left(\frac{{\alpha_1}^2}{\gamma_1 h_1} \Big/ \sum_{n=1}^{\infty} \frac{{\alpha_n}^2}{\gamma_n h_n}\right)$$

$$= 1 \Big/ \left\{1 + i\left(-\frac{A}{B}\right)\right\}, \tag{14}$$

$$a_1^{(+)} = i\left(-\frac{A}{B}\right) \Big/ \left\{1 + i\left(-\frac{A}{B}\right)\right\} \tag{14'}$$

respectively, where

$$A = \alpha_1^2/\gamma_1 h_1, \qquad B = \sum_{n=2}^{\infty} \alpha_n^2/h_n'\gamma_n,$$

h_2', h_3',..... being positive numbers and connected with h_2, h_3,..... as $h_2 = -ih_2'$, $h_3 = -ih_3'$,.....

Comparing (14) and (14′) with the case of transmission line, it will be seen that they correspond to the reflection and transmission coefficients in the transmission line with the shunt reactance iX_p inserted as shown in Fig. 2, where z_0 is its characteristic impedance.

From the comparison, we get

$$-A/B = 2X_p/z_0 = 2\xi_p,$$

and so the relative impedance is

$$\xi_p = -A/2B, \qquad (15)$$

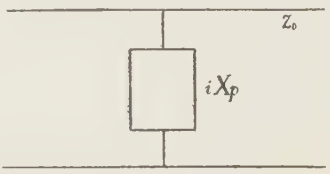

Fig. 2.

or the corresponding relative susceptance is

$$\eta_p = 2B/A. \qquad (15')$$

As A and B are both positive, it follows that $\xi_p < 0$. Therefore, it is found that the small circular aperture behaves like a capacitive reactance.

3. Detailed calculations

We shall estimate the series in the denominators of (12) and (13). The expression α_n is expressed by Sonine's first integral (4), by putting $\nu = -\frac{1}{2}\ \mu = 1$:

$$\alpha_n = \rho^3 \frac{J_{\frac{3}{2}}(\lambda_n\rho)\,\Gamma(\frac{1}{2})}{(\lambda_n\rho)^{\frac{1}{2}}\sqrt{2}} = \rho^3 \sqrt{\frac{\pi}{2\lambda_n\rho}} J_{\frac{3}{2}}(\lambda_n\rho) = \rho^3 j_1(\lambda_n\rho),$$

where

$$j_1(x) = \sqrt{\pi/2x}\, J_{\frac{3}{2}}(x) = \sin x/x^2 - \cos x/x.$$

Since $h_n^2 = k^2 - (\xi_n/R)^2$ and $\gamma_n = \frac{1}{2}R^2\{J_1(\xi_n)\}^2$, the following approximate formulas are obtained, when $\xi_n \to \infty$,

$$h_n \sim -i\xi_n/R, \qquad (16)$$

and

$$J_1(\xi_n) \sim \sqrt{\frac{2}{\pi\xi_n}} \cos\left(\xi_n - \frac{1}{2}\pi - \frac{1}{4}\pi\right). \qquad (17)$$

Therefore, we get

$$\frac{\alpha_n^2}{\gamma_n h_n} = \frac{2\rho^6}{R^2}\frac{1}{h_n}\left\{\frac{j_1(\xi_n \rho/R)}{J_1(\xi_n)}\right\}^2 \sim \frac{i\pi\rho^4 R}{\xi_n^2}. \tag{18}$$

Since $\xi_n \sim n\pi$ (when $n \to \infty$),

$$\frac{\alpha_n^2}{\gamma_n h_n} \sim i\frac{\rho^4 R}{\pi}\frac{1}{n^2}.$$

From this consideration, it has been proved that the denominator of (13) converges as the series $\sum 1/n^2$.

When we approximate (14) by the sum of finite number of terms, the order of magnitude of the remainder can be estimated by use of the relation $\sum_{n=1}^{\infty} 1/n^2 = \pi^2/6$, as shown in the following table:

n_0	$\sum_{n=n_0}^{\infty} 1/n^2$	$\sum_{n=1}^{n=n_0-1} 1/n^2$
2	0.64	1.0
3	0.39	1.25
4	0.28	1.36
5	0.24	1.40
6	0.22	1.42
7	0.20	1.44
8	0.18	1.46
9	0.17	1.47
10	0.16	1.48

Next, we shall compute the η_p of (15′), which becomes

$$\frac{1}{2}\eta_p = \frac{B}{A} = \sum_{n=2}^{\infty}\frac{1}{h_n'}\left\{\frac{j_1(\xi_n \rho/R)}{J_1(\xi_n)}\right\}^2 \Big/ \frac{1}{h_1}\left\{\frac{j_1(\xi_1 \rho/R)}{J_1(\xi_1)}\right\}^2. \tag{19}$$

We substitute (16)$\sim$(18) into the above expression, and remembering that $\rho/R \ll 1$, we replace the denominator $\{j_1(\xi_1 \rho/R)\}^2$ in the expression (19) for $\frac{1}{2}\eta_p$ by $\{\frac{1}{3}(\xi_1 \rho/R)\}^2$. Then, we obtain

$$\frac{1}{2}\eta_p \fallingdotseq \sum_{n=1}^{\infty}\frac{9\pi h_1 R}{2\xi_1^2 x^2}\{J_1(\xi_1)\}^2\left(\frac{\sin \xi_n x}{\xi_n^2 x^2} - \frac{\cos \xi_n x}{\xi_n x}\right)^2, \tag{20}$$

where $\rho/R \equiv x$. To the right-hand side we have added a term with $n = 1$, but this term can give only negligibly small contribution.

Since $\xi_n \sim n\pi$, we may write

$$S \equiv \sum_{n=1}^{\infty}\left(\frac{\sin \xi_n x}{(\xi_n x)^2} - \frac{\cos \xi_n x}{\xi_n x}\right)^2 = \sum_{n=1}^{\infty}\left(\frac{\sin n\pi x}{(n\pi x)^2} - \frac{\cos n\pi x}{n\pi x}\right)^2.$$

Splitting S up into three parts S_{I}, S_{II} and S_{III} as

$$S_{\mathrm{I}} = \sum_{n=1}^{\infty}\frac{\sin^2 n\pi x}{(n\pi)^4 x^4} = \frac{1}{(\pi x)^4}\sum_{n=1}^{\infty}\frac{\sin^2 n\pi x}{n^4},$$

$$S_{\mathrm{II}} = \sum_{n=1}^{\infty}\frac{\sin n\pi x \cos n\pi x}{(n\pi)^3 x^3} = \frac{1}{(\pi x)^3}\sum_{n=1}^{\infty}\frac{\sin n\pi x \cos n\pi x}{n^3},$$

$$S_{\mathrm{III}} = \sum_{n=1}^{\infty}\frac{\cos^2 n\pi x}{(n\pi)^2 x^2} = \frac{1}{(\pi x)^2}\sum_{n=1}^{\infty}\frac{\cos^2 n\pi x}{n^2},$$

and modifying them a little, we get

$$S_{\mathrm{I}} = \frac{1}{2(\pi x)^4}\left\{\sum_{n=1}^{\infty}\frac{1}{n^4} - \sum_{n=1}^{\infty}\frac{\cos 2n\pi x}{n^4}\right\},$$

$$S_{\mathrm{II}} = \frac{1}{2(\pi x)^3}\left\{\sum_{n=1}^{\infty}\frac{\sin 2n\pi x}{n^3}\right\},$$

$$S_{\mathrm{III}} = \frac{1}{2(\pi x)^2}\left\{\sum_{n=1}^{\infty}\frac{1}{n^2} + \sum_{n=1}^{\infty}\frac{\cos 2n\pi x}{n^2}\right\}.$$

Using Bernoulli's polynomials

$$B_{2m}(x) = (-1)^{m+1}2(2m)!\sum_{n=1}^{\infty}\frac{\cos 2n\pi x}{(2n\pi)^{2m}},$$

$$B_{2m+1}(x) = (-1)^{m+1}2(2m+1)!\sum_{n=1}^{\infty}\frac{\sin 2n\pi x}{(2n\pi)^{2m+1}},$$

we obtain

$$S_{\mathrm{I}} = \frac{1}{6x^4}(x^4 - 2x^3 + x^2),$$

$$S_{\mathrm{II}} = \frac{1}{3x^3}\left(x^3 - \frac{3}{2}x^2 + \frac{3}{6}x\right),$$

$$S_{\mathrm{III}} = \frac{1}{2x^2}(x - x^2).$$

Since $x \ll 1$, the predominating terms in S_{I} and S_{II} are both of the order of $1/x^2$, and that in S_{III} is of the order of $1/x$. Hence,

$$S_{\mathrm{I}} \fallingdotseq \frac{1}{6x^2}, \qquad S_{\mathrm{II}} \fallingdotseq \frac{1}{6x^2}, \qquad S_{\mathrm{III}} \fallingdotseq \frac{1}{2x}.$$

Therefore, we get $S \fallingdotseq 1/(3x^2)$ and consequently

$$\frac{1}{2}\eta_p \fallingdotseq \frac{3\pi h_1 R}{2{\xi_1}^2}\left\{J_1(\xi_1)\right\}^2 \frac{1}{x^4}.$$

If we let λ_g and λ_c represent the guide wave-length and the cut off wave-length of the incident waves E_{01} respectively, i. e., $h_1 = 2\pi/\lambda_g$ and $\xi_1 = 2\pi R/\lambda_c$, the above expression can be written as follows:

$$\eta_p \fallingdotseq \frac{3}{2}\frac{\{J_1(\xi_1)\}^2\lambda_c}{\lambda_g R}\frac{1}{x^4}.$$

Since $J_1(\xi_1) \fallingdotseq 1/2$,

$$\eta_p \fallingdotseq \frac{3}{8}\frac{{\lambda_c}^2}{\lambda_g R}\frac{1}{x^4}.$$

Thus, it is clearly seen that η_p tends to infinite as $1/x^4$.

REFERENCES

1. K. Hidaka, *Theory of Integral Equations* (in Japanese), 292.
2. E. Mayer, Resonant frequency of the nosed-in cavity, Journ. Appl. Phys. **17** (1946), 1046.
3. W. W. Hansen, Disk loaded wave-guide, Journ. Appl. Phys. **20** (1949), 280.
4. G. N. Watson, *A Treatise on the Theory of Bessel Functions* (1922), 373.

Memoirs of the College of Science, University of Kyoto, Series A,
Vol. XXVI, Nos. 1 & 2, Article 14, 1950.

Researches on the Activation Energy of (Ba, Sr) O by Electron Bombardment

By

Kyozo Ohira

(Received July 31, 1950)

ABSTRACT

When (Ba, Sr) O is bombarded by electrons, it is found that the resistance *versus* accelerating voltage curve shows a trough at some accelerating voltage. From the estimation of the kinetic energy of an incident electron which causes the trough change, it has been found that the optical activation energy required to remove an electron from the impurity level to the conduction band is about 3.35 ev. This agrees with the value as estimated roughly from thermionic data.

By this method may be obtained the energetic structure of such a substance that cannot be investigated by spectroscopic method.

To get more accuracy, however, the results obtained by this method must be compared with those obtained by the spectroscopic method for the well-known substances.

Moreover, it has been found that the impurity level plays an important role in the phenomenon of secondary emission of excess type impurity semiconductor.

1. Introduction

The thermionic work function of (Ba, Sr) O has been measured by many workers since 1924 (1). But the thermal activation energy $\Delta\varepsilon$ has not been measured because it is not distinct whether the value obtained from the temperature dependence of conductivity is $\Delta\varepsilon/2$ or $\Delta\varepsilon$. Also, optical activation energy has not yet been measured because of the difficulty in the treatment of a sample. Thus we have attempted to get its activation energy by electron bombardment.

2. Experiment

(1) *Apparatus*

The apparatus used in our experiment is shown in Fig. 1. The sample was made by winding 16 turns of each of two tungsten wires, about 0.01 cm in diameter, on the cylinder of insulating material about 0.2 cm in diameter and about 3.5 cm in length, and coating with (Ba,

Sr) O between the wires (Fig. 2). The heater was inserted within the cylinder. The dark resistance of the sample was $10^5 \sim 10^6$ ohms.

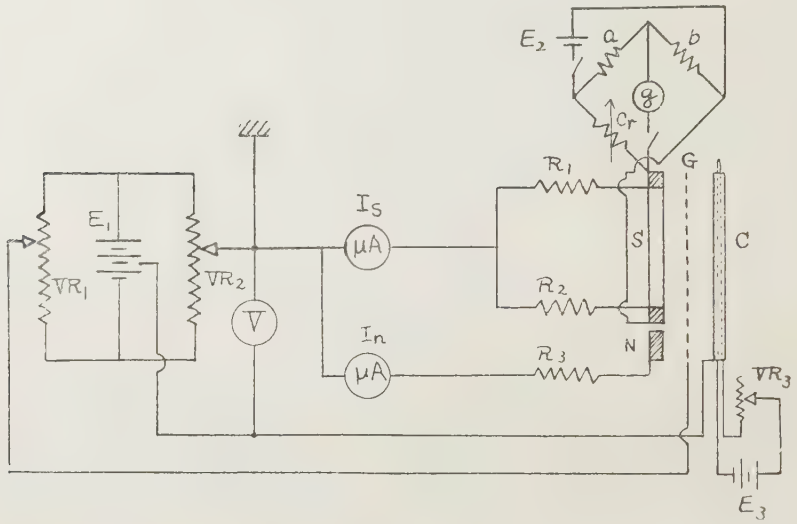

Fig. 1.

S	: sample	$6\,I_n$	: incident current	VR_1	: 100 KΩ	1 W	R_3	: 500 KΩ
G	: grid	E_1	: 200 volts	VR_2	: 100 KΩ	//	a	: 10 Ω
C	: emitter	E_2	: 0.2 volts	VR_3	: 8 Ω	2 A	b	: 2000 Ω
N	: nickel plate	E_3	: 18 volts	R_1	: 1 MΩ		c_r	: 1000~10000 Ω
I_s	: sample current			R_2	: 1 MΩ			

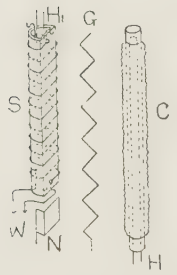

Fig. 2.
W : electrodes
H_1, H_2: heater

As the emitter of the bombarding electrons use was made of direct heating ThW wire in the first case and indirect heating nickel cylinder coated with (Ba, Sr) O in the second case.

The voltage between the sample and the emitter could be varied from a potentiometer connected with a storage battery. An adjustable voltage on the grid, mounted between the sample and the emitter, regulated the incident current without altering the filament current.

The sample was inserted in one arm of a Wheatstone bridge in parallel with a known resistance r, whose midpoint was connected through the voltage supply to the emitter, a galvanometer serving to read the conducting current and a voltage meter

indicating the sample potential, i. e. accelerating voltage. The parallel resistance was inserted so that none of the incident current did flow through the bridge circuit. All the measuring instruments were supported with insulating materials in order to prevent the leakage current.

(2) *Procedure*

Emitter's filament was fired after biasing the grid -30 volts so that none of the electron beam was incident. After the resistance of the sample, that was decreased by radiation from the emitter, had reached to equilibrium state, the sample was bombarded by electron beam for two minutes. Since it required 15～25 seconds to measure the resistance of the sample, the value after 30 seconds was recorded. The bridge circuit was open, during the bombardment, not to scale out. The same procedure was repeated by altering sample voltage after the resistance of the sample reached to equilibrium state. Thus it required 90～120 minutes for one series of observation to be finished. The vessel was kept evacuated at about 10^{-6} mm Hg by means of a liquid air trap.

(3) *Results*

(i) The resistance of the sample *versus* the accelerating voltage curve shows a minimum at about 1.5 volts in the case of ThW emitter (Fig. 3) and at about 0.2 volts in the case of Oxide emitter (Fig. 4) and then increases up to the value in the case of non-bombardment with increasing accelerating voltage. Above 2.0 volts in the former case, and above 0.7 volts in the latter one, the resistance does not change by the electron bombardment.

This trough of the resistance curve seems to depend upon the excitation of electrons from a bound state to the conduction band. And the kinetic energy of an incident electron which causes the trough gives approximately the optical activation energy from the bound state to the conduction band. We shall call this quantity $h\nu_{\max}$ (cf. Discussion). Now $h\nu_{\max}$ is given by substituting the observed value of V into the following equation (2):

$$h\nu_{\max} \equiv \frac{1}{2}mv^2 = V - i_s r_A - i_s r + \Psi_A - \Psi_C \text{ , (ev)} \qquad (1)$$

where V : reading (in volt) of accelerating voltage meter when the trough occurs,

i_s : sample current (ampere) (cf. Results (ii)),

r_A : internal resistance of ammeter $= 1013\,\Omega$,

r : series resistance $= 0.5 \times 10^6\,\Omega$,

Ψ_A: work function of sample = 4.54 ev (cf. Discussion),
Ψ_C: work function of emitter : 3.00 ev for ThW and 1.35 ev for Oxide (cf. Discussion).

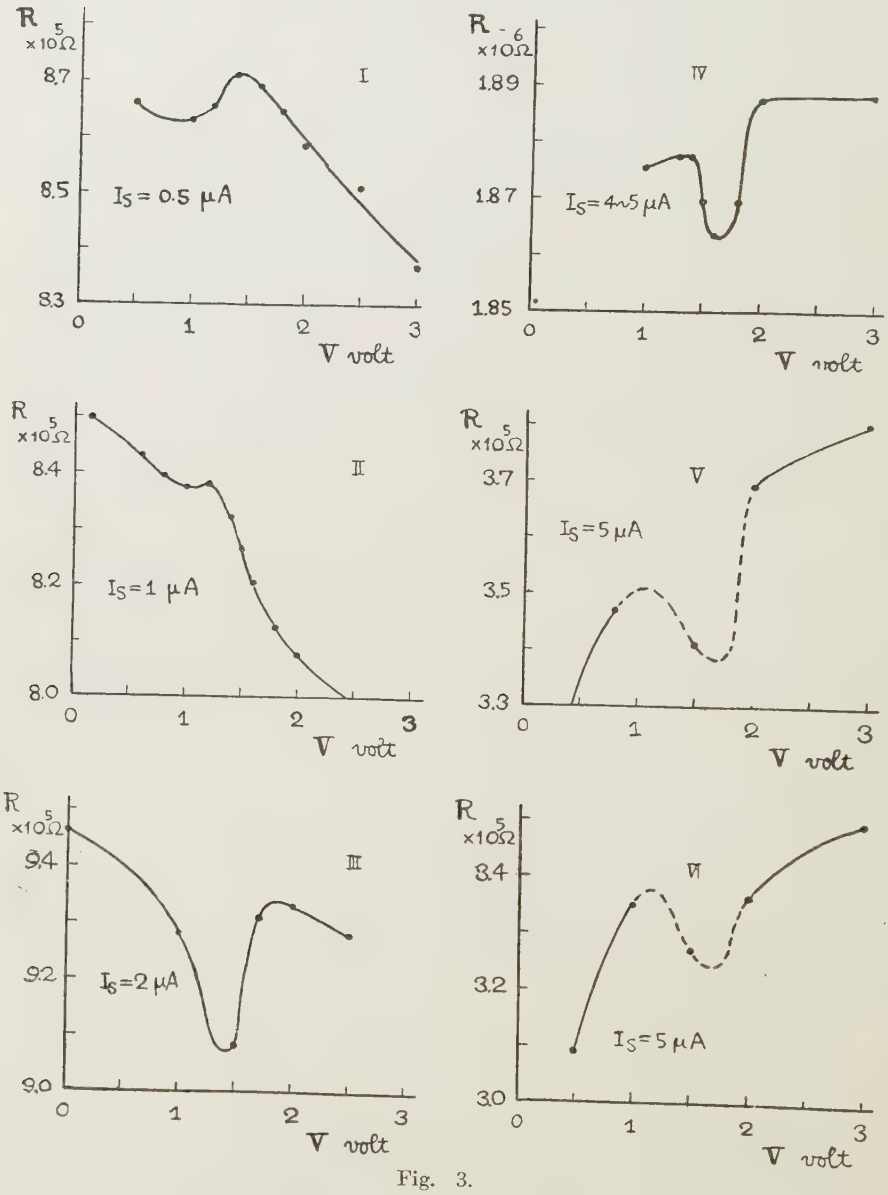

Fig. 3.

R: resistance of the sample.
V: reading of accelerating voltage meter.
I_s: incident current through the sample.

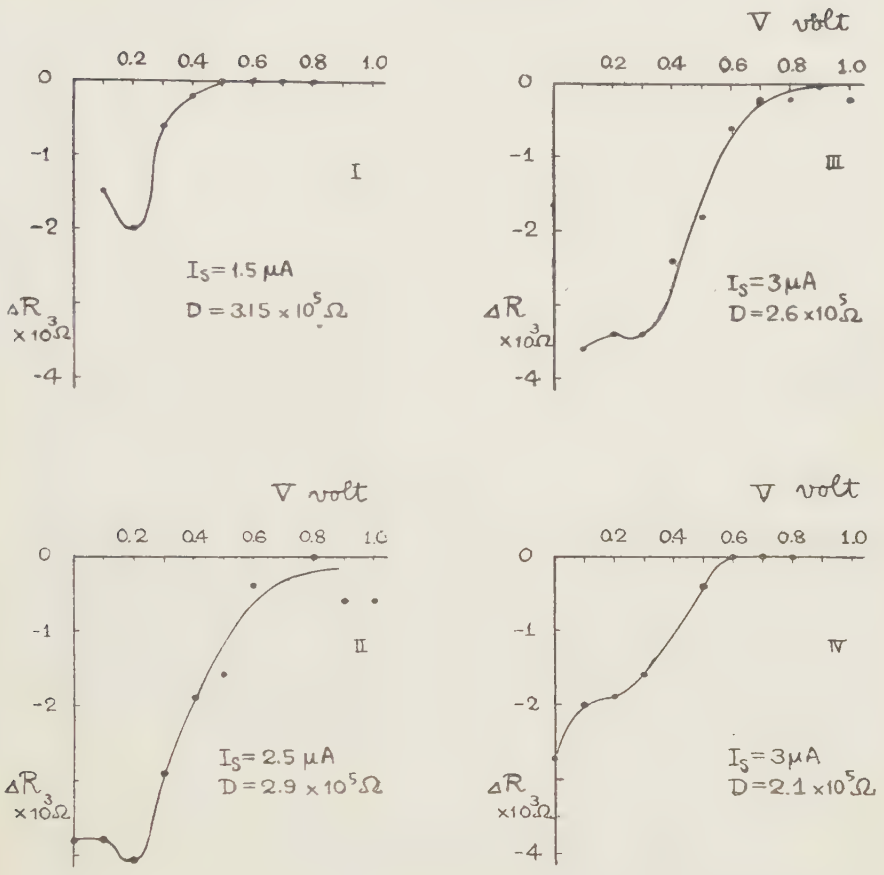

Fig. 4.

ΔR: decrement of the resistance.
D: dark resistance of the sample.

The observed values of V and the calculated values of $h\nu_{max}$ are given in the following Table I.

TABLE I.

Emitter	i_s ($\times 10^{-6}$ A)	Observed values of V (volt)	$h\nu_{max}$ (ev) (calculated)
Th W	0.5	0.9	2.19
〃	1.0	1.0	2.04
〃	2.0	1.45	1.99
〃	4.0~5.0	1.65	1.19
〃	5.0	1.7	0.74
Oxide	1.0	0.18	2.87
〃	1.5	0.2	2.64
〃	1.7	0.2	2.54
〃	2.5	0.2	2.14
〃	3.0	0.23	1.91

The curve of $h\nu_{max}$ *versus* the sample current decreases with increasing sample current both in the cases of ThW emitter and of Oxide emitter (Fig. 5). By extrapolation from this curve we have obtained the value $h\nu_{max} \sim 3.35$ ev in the latter case (cf. Discussion).

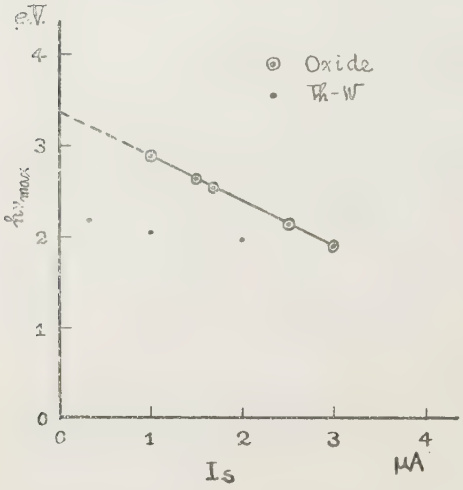

Fig. 5.

(ii) In order to explain the question why the resistance does not change above 2.0 volts (ThW) or 0.7 volts (Oxide), we observed the resistance and secondary emission against the accelerating voltage simultaneously.

The blackened nickel plate, whose area is 1/6 of that of the sample, was placed in the same plane of the surface of the sample and perpendicular to the incident beam. The plate current i_n in case when the same voltage as the sample voltage was supplied, was measured together with the sample current i_s. Thus, we have obtained the results that

(a) $6i_n > i_s$,

(b) $\delta = \dfrac{6i_n - i_s}{6i_n}$ *versus* accelerating voltage curve shows the same behaviour as the resistance curve (Fig. 6).

Thus the reason why the resistance does not change above the given voltage is that bound electrons are not excited to the conduction band but emitted as secondary electrons. It seems therefore that the impurity level (cf. the next section) plays an important role for the secondary electron emission from (Ba, Sr) O.

(iii) After two or three series of the bombardment the resistance begins to decrease monotonously and is independ-

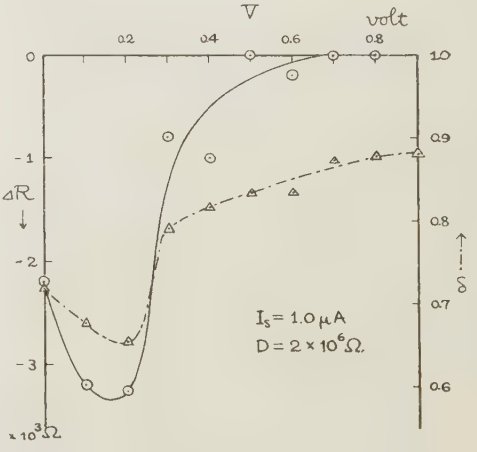

Fig. 6. δ = yield of secondary electron.

ent of the accelerating voltage and then the surface of the sample has been blackened.

Also, as soon as a liquid air vessel is removed, it is immediately blackened. Therefore it seems that adsorbed diffusion pump oil on the surface is carbonized by the electron bombardment.

(iv) In spite of the fact that the dark resistance of the sample ranges over $10^5 \sim 10^6$ ohms, the decrement of resistance is about the same quantity in each case and depends only upon the incident current. It seems that this phenomenon depends only upon the energetic structure of surface layers.

3. Comparison with the optical activation energy estimated from thermionic data

It has been known that the thermal activation energy, required to excite thermally an electron from the impurity level to the conduction band, is about 1.4 ev. Therefore the optical activation energy, roughly estimated from the above value, is about 3.5 ev. This agrees approximately with the value 3.35 ev which have been obtained in the present experiment. Thus we conclude that the trough of resistance curve depends upon the excitation of electrons from the impurity level to the conduction band by the electron bombardment.

For the work function of (Ba, Sr) O, various different values have been obtained by many workers. Nijboer (3) attempted to explain this fact by assuming that the number of impurity levels is greater than that of electrons available. He obtained the equilibrium state of crystal from the condition that the free energy of crystal is minimum. According to his results work functions ψ_1 and ψ_2 corresponding respectively to the cases of good activation and bad one, are given as follows:

$$\psi_1 = \frac{\Delta\varepsilon}{2} + \phi\,, \qquad \psi_2 = \Delta\varepsilon + \phi\,,$$

where $\Delta\varepsilon$ is the thermal activation energy and ϕ is the width of the conduction band. Adopting the same model, we obtained the same results by the entirely statistical method (cf. Appendix below).

Kawamura (1) has found, by the method of Richardson's line, that the work function of (Ba, Sr) O ranges over 1.0$\sim$1.7 ev in various cases. Thus, putting

$$\left.\begin{aligned} \Delta\varepsilon/2 + \phi &= 1.0 \quad (\text{ev})\,, \\ \Delta\varepsilon + \phi &= 1.7 \quad (\text{ev})\,, \end{aligned}\right\}$$

he has obtained the results that

$$\left.\begin{aligned} \Delta\varepsilon &= 1.4 \quad (\text{ev}), \\ \phi &= 0.3 \quad (\text{ev}). \end{aligned}\right\} \tag{2}$$

Now it has been observed (4) that the surrounding ions do not move during an electron's removal from an impurity center by the absorption of kinetic energy of an incident electron. Also this fact has been predicted from the probability calculated by the quantum theory of molecules (5). Therefore, we have (6)

$$h\nu_{\max} - \Delta\varepsilon \fallingdotseq \frac{e^2}{2R}\left(\frac{1}{\kappa_0} - \frac{1}{\kappa}\right),$$

where κ_0 is the dielectric constant for high frequency, κ the dielectric constant for electrostatic field, and R the radius of impurity atom.

Since the depth of the potential hole with this model is $e^2/\kappa_0 R$ we shall have

$$h\nu_{\max} \sim e^2/2\kappa_0 R\,,$$

$$\Delta\varepsilon \sim e^2/2\kappa R\,.$$

Assuming that $\kappa_0 \sim 4$, $\kappa \sim 10$ for (Ba, Sr) O which seem to be probable, we obtain

$$h\nu_{\max} \sim \frac{10}{4}\Delta\varepsilon\,. \tag{3}$$

Substituting Eq. (2) into Eq. (3) we have

$$h\nu_{\max} \sim 3.5 \quad (\text{ev})\,. \tag{4}$$

4. Discussion

(1) We assumed that the value of $h\nu_{\max}$, i. e. the kinetic energy of an incident electron which causes the trough change gives approximately the optical activation energy. To know the more strict meaning of $h\nu_{\max}$ we must take into account the fact that incident electrons distribute according to the Maxwellian distribution law and that the conduction band has its width. Thus we shall have a quantitative relation among the short wave edge, the long wave edge and $h\nu_{\max}$. The discussion on such a relation is now in progress.

(2) In calculating $h\nu_{\max}$ by Eq. (1), the following three assumptions are made:—

(a) Initial velocity distribution of incident electrons is assumed to show a maximum at zero velocity. Since incident electrons actually distribute according to the Maxwellian distribution law the maximum would be at about 0.0869 ev. This, however, is of the order of lattice vibration, i. e., the order of $1/40 \sim 1/20$ ev and so can be neglected.

Also the hump of surface barrier that accelerates the emitted electrons is neglected. But it seems to have an appreciable height in the case of ThW emitter, as we shall show later.

(b) The work function of tungsten electrodes (4.54 ev (7)) is taken as that of the sample, since the electrodes expose from the Oxide surface. Otherwise the reasonable value of $h\nu_{\max}$ cannot be obtained simultaneously both in the cases of ThW and Oxide emitters.

The work function of ThW emitter (3.00 ev) is taken from the table (7). It corresponds to the case of $\theta \fallingdotseq 0.812$. That of Oxide (1.35 ev) is the intermediate value of Kawamura's data (cf. the previous section). Therefore, the obtained value of $h\nu_{\max}$ has uncertainty of about $\pm$ 0.35 ev in both cases. To obtain the more accurate value, the contact potential difference between the sample and the emitter should be measured.

(c) The effect of charging up the sample is neglected. It, however, should be estimated as for the well-known substances.

(3) It seems to depend upon the hump of surface barrier and direct heating voltage that the value of $h\nu_{\max}$ is smaller in the case of ThW than in the case of Oxide. Therefore the data in the latter case are used to get $h\nu_{\max}$.

(4) The decrease of the $h\nu_{\max}$ *versus* the incident current curve is more rapid in the case of Oxide than in the case of ThW. The fact shows that this decrease cannot be explained only by the lattice vibration of the sample. It seems to be probable that, externally applied voltage is decreased in the case of Oxide, since the mean work function of the sample is increased by the production of WO ($\psi = 9.2$ ev (8)) on the sample electrodes. And it seems that the oxygen which produces WO, becomes to be dissociated from the CO_2 gas, that is evaporated from the Oxide emitter, and adsorbed on the electrodes. According to this assumption it seems to be reasonable that $h\nu_{\max}$ decreases with the increasing incident current, since the production of WO increases with the increasing incident current. This should be tested by measuring the actual contact potential difference in the above case.

(5) The fact that the resistance curve closely agrees with the secondary emission curve, seems to suggest how interactions occur between the

low velocity electron and the crystal. From this point of view, it seems to be naturally comprehensible that the effect of the bombardment can be observed after 30 seconds.

In conclusion, the writer wishes to express his sincere thanks to Professor Dr. K. Arakatsu and Professor Dr. K. Kimura for their kind guidance and invaluable suggestions during the course of his research. His hearty thanks are also due to Professor Dr. M. Sonoda, Assistant Professor Dr. S. Shimizu, Lecturer Dr. Y. Uemura, Mr. T. Yanabu and Mr. J. Muto for their kind advice and encouragement.

Appendix

The feature of this derivation is that Fermi level, ε', is obtained and therefore is easy to get the emission formula. Calculating by the usual δ-function method (9) we obtained the following results:

$$Ce^{\frac{\varepsilon'}{kT}}(kT)^{\frac{3}{2}}\sqrt{\pi}/2 = Ne^{-\frac{\Delta\varepsilon+\varepsilon'}{kT}} - (N_0 - N), \qquad (1)$$

where $C \equiv 4\pi(2m^*)^{\frac{3}{2}}/h^3$ and m^* is the effective mass of electron, N_0 the number of impurity states, N the number of electrons available at 0°K, ε' the Fermi level at T°K, $\Delta\varepsilon$ the thermal activation energy. Energy zero is taken at the bottom of conduction band. The quantity on the left-hand side of Eq. (1) is the number of electrons that have been excited from the impurity level. Then, the following two limiting cases present themselves:—

(i) If $N_0 - N \ll Ce^{\frac{\varepsilon'}{kT}}(kT)^{\frac{3}{2}}\sqrt{\pi}/2$, which holds in the case of good activation, we have approximately

$$Ce^{\frac{2\varepsilon'}{kT}}(kT)^{\frac{3}{2}}\sqrt{\pi}/2 = Ne^{-\frac{\Delta\varepsilon}{kT}}.$$

Thus,

$$\varepsilon' = -\frac{\Delta\varepsilon}{2} + \frac{kT}{2}\log\frac{N\cdot 2}{C(kT)^{\frac{3}{2}}\sqrt{\pi}}. \qquad (2)$$

Therefore the thermionic current is

$$i = A_1 N^{\frac{1}{2}} T^{\frac{5}{4}} \exp\left(-\frac{\phi + \Delta\varepsilon/2}{kT}\right), \qquad (3)$$

where $A_1 \equiv (2/h^3)^{\frac{1}{2}} (2\pi m^*)^{\frac{1}{4}} k^{\frac{5}{4}} e_0$, and e_0 is the electronic charge and ϕ the width of conduction band. Hence, the work function as obtained from the slope of Richardson's line is

$$\psi_1 = \phi + \Delta\varepsilon/2 . \tag{4}$$

(ii) If $N_0 - N \gg Ce^{\frac{\varepsilon'}{kT}} (kT)^{\frac{3}{2}} \sqrt{\pi}/2$, which holds in the case of bad activation, we have approximately

$$N_0 - N = N \exp\left(-\frac{\Delta\varepsilon + \varepsilon'}{kT}\right),$$

and consequently

$$\varepsilon' = -\Delta\varepsilon + kT \log \frac{N}{N_0 - N}. \tag{5}$$

Therefore

$$i = A_2 \frac{N}{N_0 - N} T^2 \exp\left(-\frac{\phi + \Delta\varepsilon}{kT}\right) \tag{6}$$

with $A_2 \equiv 4\pi m^* k^2 e_0/h^3$, and consequently

$$\psi_2 = \phi + \Delta\varepsilon . \tag{7}$$

REFERENCES

1. H. Kawamura, Proc. Phys. Math. Soc. Japan **17** (1943), 175.
2. W. Heinze, ZS. f. Phys. **109** (1938), 459.
   P. W. Bridgman, Phys. Rev. **11** (1919), 306.
3. J. H. de Boer, and W. C. Van Geel, Physica **2** (1935), 286.
   B. R. A. Nijboer, Proc. Phys. Soc. **51** (1935), 575.
4. R. Whiddington and H. Jones, Phil. Mag. **6** (1928), 889.
   J. Franck, Trans. Faraday. Soc. **21** (1925), Part II 536.
   E. Condon, Phys. Rev. **28** (1926), 1182.
5. N. F. Mott and H. S. W. Massey, *The Theory of Atomic Collision* (1933), 209.
6. N. F. Mott and R. W. Gurney, *Electronic Processes in Ionic Crystals* (1940), 160.
7. *International Critical Tables* (1928), VI 55.
8. R. H. Fowler, *Statistical Mechanics* (1936), 364.
9. F. Seitz, *The Modern Theory of Solids* (1940), 186.

Memoirs of the College of Science, University of Kyoto, Series A,
Vol. XXVI, Nos. 1 & 2, Article 15, 1950.

Studies on the Ion Source placed in a Magnetic Field

By

M. Sakisaka, S. Miyashiro, Y. Uemura and **S. Yasumi**

(Received July 31, 1950)

ABSTRACT

A new type of ion source without hot cathode is constructed, which is little consumable in electric power but gives comparatively intense ion current. The discharge is produced in a small cylindrical space under coaxial magnetic field. Between the iron cathodes which constitute themselves a pair of magnetic pole pieces an anode of doughnut shape is settled. The ions are generated by the agitative movement of electrons in the electric and magnetic fields and then introduced into the higher vacuum side through a canal bored in one of the cathodes.

In the case of hydrogen gas, it is operated adequately by the discharging voltage of D.C. 1000～2000 volts under the magnetic field of 200～500 gauss at the vacuum pressure of 8×10^{-4}～3×10^{-3} mmHg, and the extracted ion current is 20～300 μA. The output ion current is easily controlled by the adjustment of discharging voltage, magnetic field or vacuum pressure. The mass analysis shows that more than 60 per cent of total ions are protons.

The comparison between the theoretical and experimental results for protons passing through the canal is discussed and the most effective size of canal is deduced.

A gas leak apparatus to adjust the pressure range for proper operation is also devised.

1. Introduction

For long years we have hoped some improvements to the ion source of Rutherford-Oliphant type (1) which has been used as a proton source for atomic disintegrations in our laboratory.

Recently, ion sources produced in magnetic field have been studied by many workers (2). Almost all of them are "low voltage arc type" with hot cathode. The pressure of the discharge tubes of this type lies generally between 5×10^{-3} and 5×10^{-2} mmHg. Though they have many advantages in the usages, the life of the hot filament is often the defect of the tubes of this type, because, when strong current of ions is necessary and heavy arc discharge is made, the filament is

liable to be damaged by the bombardment of ions. Therefore it is desirable to construct a low voltage ion source without hot cathode operating at a pressure as low as possible.

We know, in some of the discharge tubes (3) which have particular arrangement of electrodes combined with magnetic field, the probability of ionization is increased and the discharge can go on in high vacuum even they are made without hot filament. Philips vacuum manometer (4) is one of these types in which electrons move agitatively between a ring anode and two disc cathodes settled at its opposite sides. A study, both theoretical and experimental, of the discharging mechanism of this tube gives us a suggestion to modify it for constructing an ion source for the purpose.

After two years' investigations a tube is obtained which is promissing to be used. It is easily controllable and durable in life and moreover it can be operated with small consumption of electric power.

2. Apparatus

The construction is shown in Fig. 1. A is the brass anode of doughnut shape having a hole of 1 cm in diameter and 1 cm in length. B and C are iron cathodes which constitute themselves at once magnetic pole pieces. A canal, whose size will be later discussed, is bored in the lower pole. The ions in this small cylindrical space are introduced through the canal to higher vacuum side and collected by the Faraday cylinder F. E is a retarding plate to suppress the secondary electrons produced from F when it is bombarded by ions. G is a Philips vacuum gauge. Gas is inletted through L from a slow leak apparatus, the details of which will be described in the following section. Coil M produces magnetic field mainly at the discharging place D.

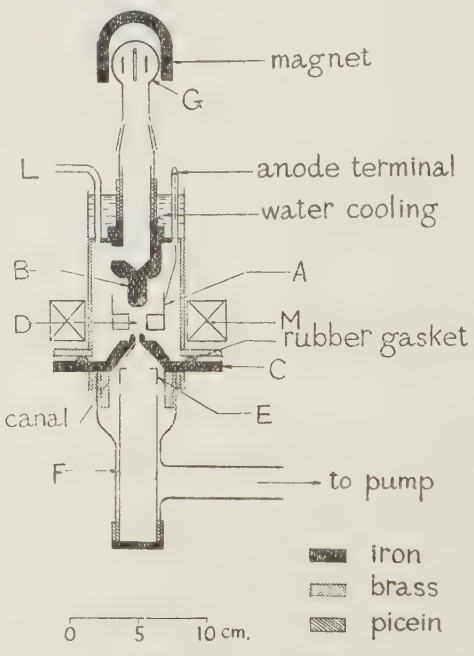

Fig. 1. Construction.

Fig. 2 shows the system of the electric power supply, which is a simple rectifying circuit. The signs in Figs. 1 and 2 are correspondently indicated. The upper part of Fig. 2 is the high voltage generator of 500～2500 volts and the lower one is that for magnetic field. R is a high wattage resistance of 3～10 KΩ for the protection of sudden break down of the discharge.

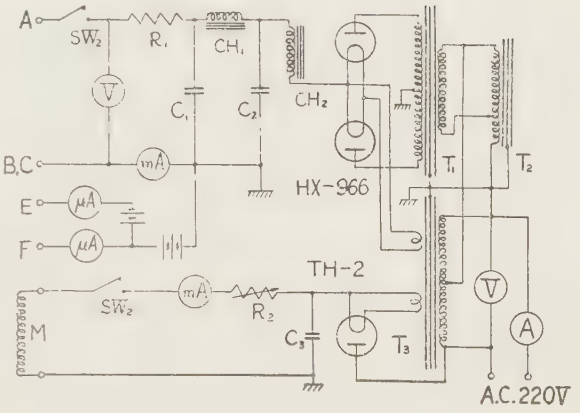

Fig. 2. Electric power supply.

3. Operation and measurements

Raising the anode potential of ion source to about 500 volts and the magnetic field to about 200 gauss, the discharge is produced when the pressure is about 1×10^{-3} mmHg. The relations between the discharging current and the anode potential is shown in Fig. 3 at various pressures. Fig. 4 gives the output ion current from the canal of 1 mm in diameter and 5 mm in length. Generally, the more the ion current is obtained, if the more the anode potential, the magnetic field and the vaccum pressure be raised. But when the pressure becomes over 3×10^{-3} mmHg, the glow discharge in the ion source transfers to an arc discharge, resulting in the drop of anode potential to about 400 volts, and the yield of output ions suddenly decreases. On the other hand, when the pressure becomes as low as about 6×10^{-4} mmHg no more ions become to be extracted. Under these

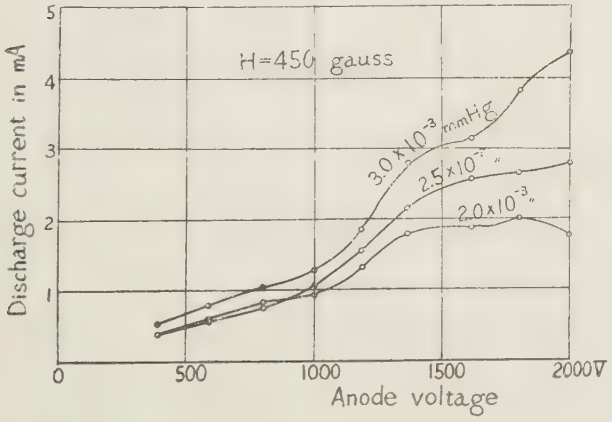

Fig. 3. Discharging current.

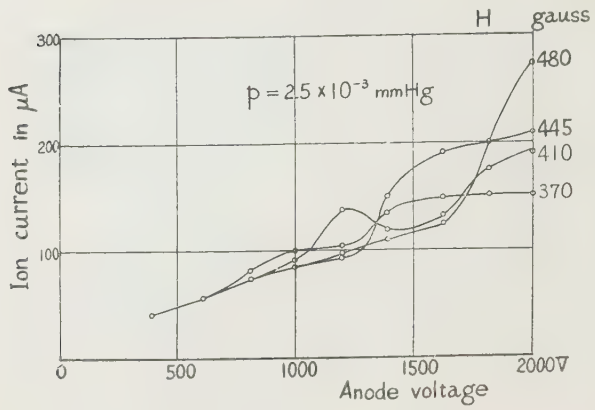

Fig. 4. Output ion current at various magnetic fields.

conditions the yield sharply gets down if the anode potential is inadequately raised. The reason is probably that, because of the inadequately strong electric field in comparison with magnetic field, the electrons emitted from cathodes by the bombardment of ions can reach the anode without necessary production of ions by collision to continue the discharge. This causes the instability of ion current by the slight variation of anode potential. But if the magnetic field be modulated by superposition of alternative current, the stability of the ion current is continued and the sharp peak in the diagram is flattened as shown in Fig. 5. The maximum electric powers consumed are about 20 watts for the discharge and 70 watts for the magnetic field respectively.

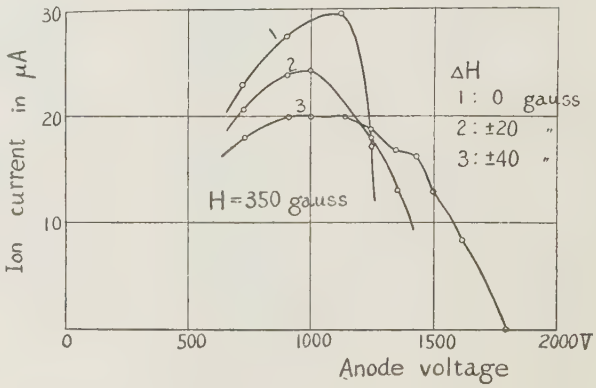

Fig. 5. Stabilization of ion current.

4. Analysis of hydrogen ions

Ions from the source were analysed by a simple mass spectrometer. In the case of hydrogen, it was found that about half of the total ions were protons at the beginning of the experiment. While, after long operation, the abundance of protons increased to 60 per cent or more. Other kinds of ions were scarcely detected in our experiment.

5. Discussion on the canal size

For atomic disintegration experiment, as much amount of ion cur-

rent as possible is requested. For this purpose it is naturally desirable to have wide canal. Since, however, the evacuation through it prevents the stable operation of the ion source at necessary vacuum pressure, there must be some restrictions to the canal conductance for proper working of vacuum system. Moreover, since a fraction of ions passing through the canal will be lost by absorption, recombination or scattering, depending upon the canal size, they make themselves the second limitations for the latter.

According to Brown (**5**), gaseous conductance of a pipe of length l and diameter a is given by

$$G = \left(\frac{\pi}{2}\right)^{\frac{3}{2}} \frac{a^3}{l + \frac{\pi}{2}\left(\frac{2}{f} - 1\right)a} \left(\frac{2}{f} - 1\right)\sqrt{\frac{RT}{\mu}}, \tag{1}$$

where f is a constant concerning pipe wall, which is experimentally determined by Brown as 0.77. R, T and μ are the universal gas constant, absolute temperature and molecular weight of the gas respectively. If we assume that the pressure p_1 of the ion source is far larger than p_2 of higher vacuum side, the quantity Q of gas passing through the pipe per second is given by

$$Q = Gp_1 . \tag{2}$$

Now, when the ions are running, they exert repulsive force to each other and produce, on the other hand, magnetic force which results in the attraction among themselves (**6**). If the cylindrical beam of ions of radius ρ_0 consists of the ions of the same mass m and charge e, a unit charge on its periphery receives these forces simultaneously from every one of ions and the beam is liable to diverge itself. The aspect is shown in Fig. 6. Calculation of these forces leads to the following formula, which shows that the ion beam of radius ρ_0 diverges to that of radius ρ after running the distance S:

$$\sqrt{\frac{ie(1-\beta^2)}{\rho_0 mv}}\, t = \sqrt{\frac{ie(1-\beta^2)}{\rho_0 mv}}\, \frac{S}{v} = \int e^{y^2} dy , \tag{3}$$

where i and v are the total ion current and the velocity of ions, and y and β are equal to $\log(\rho/\rho_0)$ and v/c, i. e. the ratio of v and the velocity of the light, respectively.

If it is assumed that protons pass through a cylindrical canal of

constant conductance and that when they collide the canal wall, they are simply absorbed without any production of secondary ions or any reflexion, the amount of protons at the outlet varies simply with the radius and length of the canal.

Furthermore, if the ion current of constant density per unit area comes to the inlet of the canal, the amount of the ions is proportional to its area, i. e. πa^2. The beam would diverge, if no canal wall were there, to the radius a' after running the distance l from the inlet, but the wall absorbs divergent ions, which are indicated by the shadowed portion in Fig. 6. Thus at the outlet only the fraction a^2/a'^2 of the total amount of the inlet ions will be obtained. In this case we can replace S, ρ_0 and ρ in Eq. (3) by l, a and a'. Combining Eqs. (1),

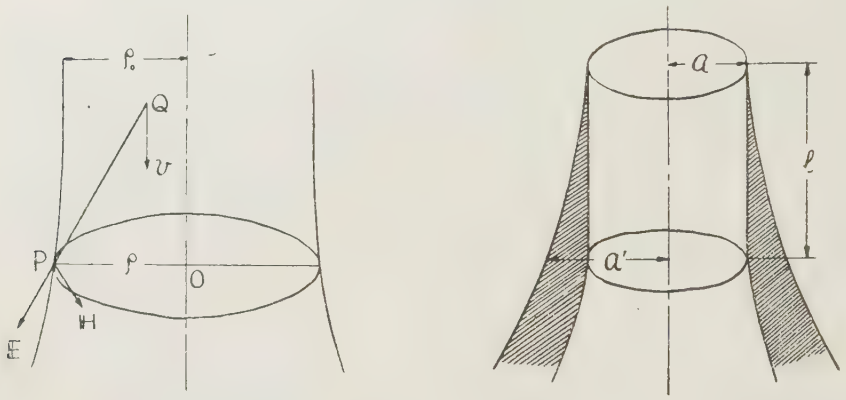

Fig. 6. Divergence and absoption of ion beam.

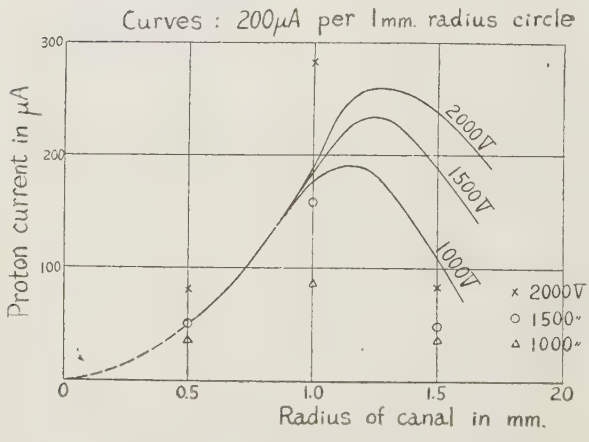

Fig. 7. Output proton current from various canals.

(2) with this fraction, the output ion current in question can be calculated. For example, the output proton currents of various energies obtained through the canal of conductance 440 cc/sec in hydrogen gas, are shown in Fig. 7. In this case the current density is taken as

200 μA per circle of 1 mm radius at the inlet of the canal.

For experimental verifications, we used the following three cylindrical canals having the same value of the above-mentioned conductance. Some of the experimental results are plotted also in Fig. 7. In this experiment there remain uncertainties concerning the uniformity of incident current density, the abundance of protons, their energy distributions and others. However, according to our simple assumptions, we find that the behaviours of experimental results and the theoretical calculations are well agreeable with each other. Moreover, the propriety of Fig. 7 is more emphasized, if we take the mean energy of ions lower than the discharging voltage of the ion source. Thus the most effective size of the canal suitable for about 1500 volts energy protons is determined to be nearly equal to 1.2 mm in radius and 10 mm in length.

TABLE 1. Size of three canals.

No.	l (length in mm.)	a (radius in mm.)
1	0	0.5
2	5.2	1.0
3	23	1.5

6. Gas leak

It is also important to know the best condition of the pressure of the ion source to be operated properly. After a series of experiments, it was found that the method of gas inlet is most influential upon it and that it is adequate to apply a simple apparatus in which gas leaks through a porcelain of small and constant conductance (g) from the gas reservoir of large volume (V). After time t the pressure p in this reservoir decreases exponentially as

$$p = p_0 \exp(-gt/V), \tag{4}$$

where p_0 is the initial pressure. The leaking quantity converted at p_0 is derived as

$$q = g \exp(-gt/V). \tag{5}$$

The experimental results are given in Fig. 8. Thus the adequate operating range of the ion source is found to lie between 8×10^{-4}

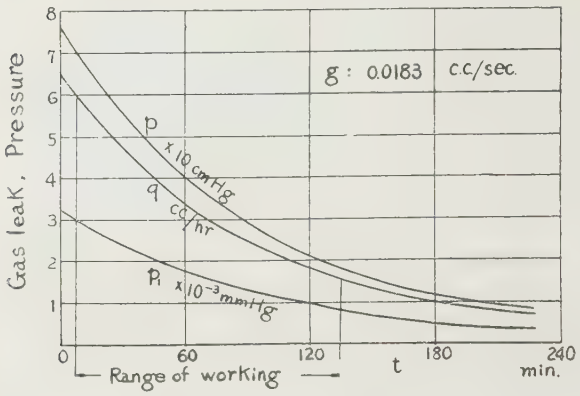

Fig. 8. Gas leak.

and 3×10^{-3} mmHg. The best condition to produce as intense ions as possible is at the neighbourhood of 3×10^{-3} mmHg. In this case the leak quantity of hydrogen gas is found to be about 6 cc/hr which is appropriate for the evacuating speed of ordinary diffusion pump.

7. Conclusion

By modifying the principle and mechanism of Philips vacuum gauge tube, it has been found that an ion source suitable for nuclear experiment may be promissingly constructed. Necessary improvements concerning magnetic field, electric and magnetic focusing and the device for intensifying current, are now being studied.

In conclusion the writers wish to express their cordial thanks to Profs. B. Arakatsu and K. Kimura for their valuable suggestions and to other members in our laboratory for their helps. The writers also acknowledge their indebtedness to the support of the Scientific Research Expenditure of the Ministry of Education.

REFERENCES

1. M. L. Oliphant and Lord Rutherford, Proc. Roy. Soc. London, **141** (1933), 259.
   A. Bouwers, F. A. Heyn and A. Kuntke, Physica, **4** (1937), 153.
2. R. B. Satlow, R. S. I., **20** (1949), 558.
   A. T. Finkelstein, R. S. I., **11** (1940), 94.
   C. Bailey, R. S. I., **20** (1949), 189.
   F. M. Penning, Physica, **4** (1937), 1190.
3. F. M. Penning, Physica, **3** (1936), 876.
4. C. Hayashi and others, R. S. I., **20** (1949), 524.
   F. M. Penning, Physica, **3** (1936), 876.
   E. C. Evans and K. E. Burmaster, Proc. I. R. E., **38** (1950), 651.
5. G. P. Brown, J. Appl. Phys., **17** (1946), 804.
6. E. E. Watson, Phil. Mag., **3** (1939), 849.
   M. Knoll, Ann. d. Phys., **12** (1932), 604.
   F. D. Fowler, Phys. Rev., **46** (1935), 1075.
   L. P. Smith, J. Appl. Phys., **11** (1940), 220.

Memoirs of the College of Science, University of Kyoto, Series A,
Vol. XXVI, Nos. 1 & 2, Article 16, 1950.

The Energy released in the Disintegration of Nitrogen by Thermal Neutrons*

By

Ryutaro Ishiwari and **Kazunori Yuasa**

(Received August 2, 1950)

ABSTRACT

The energy released in the ${}_7N^{14}(n,p){}_6C^{14}$ reaction produced by thermal neutrons has been determined by the parallel plates ionization chamber with linear amplifier filled with atmospheric air dried by $CaCl_2$. For the energy calibration, alpha-particles from ThC′ were used as standard, and the correction for the systematic error introduced by the calibration was made by the aid of the theoretical analysis of the pulse shape in the linear amplifier. By assuming the proportionality between the amount of the total ionization in air and the energy of the particle, we have obtained the Q-value of the reaction as 0.609 ± 0.005 Mev. Taking the end point energy of the beta-spectrum of ${}_6C^{14}$ as 0.156 ± 0.001 Mev, the neutron-hydrogen mass difference has been determined as 0.765 ± 0.005 Mev.

1. Introduction

The reaction of ${}_7N^{14}$ produced by thermal neutrons

$$ {}_7N^{14} + {}_0n^1 = {}_6C^{14} + {}_1H^1 + Q $$

was investigated in the earlier experiments by Chadwick and Goldhaber(1), Bonner and Brubaker (2, 3), and Burcham and Goldhaber (4). The final nucleus ${}_6C^{14}$ emits a negative electron and returns to the initial nucleus ${}_7N^{14}$ again;

$$ {}_6C^{14} = {}_7N^{14} + E_\beta . $$

Here E_β is the extrapolated end point energy of the beta-ray spectrum.**

Bonner and Brubaker (3) first pointed out that the neutron-hydrogen mass difference can be obtained from the above disintegration cycle;

$$ n - H = Q + E_\beta $$

* This paper was read at the meeting of Nuclear Physics Division, Physical Society of Japan, April 2, 1950.

** As pointed out by Kofoed-Hansen(5), the extrapolated Fermi end point involves the neutrino rest mass if any.

In 1947, Stephens (**6**) made a synthetic discussion on the experimental studies relating to the neutron-hydrogen mass difference. The most reliable result available in 1947 was the value $n - H = 0.755 \pm 0.016$ Mev obtained from the photo-disintegration of deuterium (**7**). The results obtained from various kind of disintegration cycles, though they were somewhat inaccurate, gave, on the average, $n - H = 0.757$ Mev (**6**) in agreement with the photo-disintegration data. And the consistency of the results seemed to be satisfactory to that time.

Notwithstanding, however, Bell and Elliott (8) made in 1948 an experiment determining the binding energy of deuterium by measuring the gamma-ray energy from ${}_1H^1(n, \gamma){}_1D^2$, and obtained the value $n - H = 0.804 \pm 0.009$ Mev which was about 50 Kev higher than the previously accepted value. The discrepancy was too large to be explained by the experimental errors concerned.

Under these circumstances, a keen interest has arisen for the more accurate redetermination of the binding energy of deuterium and the neutron-hydrogen mass difference. In view of the roughness of the existing data on the disintegration cycles, it has been especially desirable to investigate carefully these cycles.

As for the nitrogen cycle above mentioned, the end point energy of the beta-ray from ${}_6C^{14}$ has been accurately and consistently determined by several experiments (**9**), while the Q-values given by various investigators for the ${}_7N^{14}(n, p){}_6C^{14}$ reaction are fairly inconsistent. The results obtained by the ionization measurements are : 0.57 ± 0.04 Mev by Huber, Huber and Scherrer (**10**), 0.63 ± 0.01 Mev by Huber and Stebler (**11**), and 0.71 Mev by Barshall and Battat (**12**). Cloud chamber observations of this reaction have given, however, well consistent values of proton range, i. e., 1.00 cm (**13**). If we assume Bethe's range-energy relation (**14**) to be correct in this region, we have a Q-value of 0.60 Mev.

In the present experiment, we have attempted to determine the Q-value of the ${}_7N^{14}(n, p){}_6C^{14}$ reaction by the method of measuring the amount of total ionization as accurately as possible.

2. Experimental procedure and apparatus

The fundamental difficulties encountered in the accurate determination of the nuclear reaction energy by measuring the total ionization produced by the particles in an ionization chamber with linear amplifier are related to the following problems.

The first and more essential is the relation between the amount of the total ionization and the energy of the particle. For the purpose

of the present study, the generally accepted law of proportionality between these quantities may be considered to be somewhat daring postulation, since the law has been derived from experiments of less accuracy. Up to the present time, the exact characters of this relationship in various sorts of gases and for different natures of particles have not been studied with sufficient accuracy. Thus, we cannot but assume it for the present.

The second is concerned with the technical problems to insure the proportionality between the total ionization produced in the ionization chamber and the output pulse height of the linear amplifier. In general, the output pulse height due to a fixed total ionization produced by a particle of fixed energy (regardless of the statistical fluctuation of the ionization process) is not necessarily constant but varies corresponding to the location of the disintegrated nucleus and the direction of the emitted particle in the ionization chamber. The degree of this inhomogeneity depends upon the relative magnitudes of the time constant of the amplifier and the collecting time of ions, the latter of which is defined by the mobility of ions and the chamber voltage.

In order to guarantee the proportionality between the ionization and the pulse height, the time constant of the amplifier should be adequately large in comparison with the collecting time of ions. Since the practical limitation of the collecting time is set by the high voltage source and the chamber dimension, the amplifier should be operated with large time constant to acquire good linearity. On the other hand, this makes it difficult to reduce the low frequency noise of the amplifier such as microphonics and mechanical vibrations.

Indeed, this difficulty is overcome in principle by adopting the technique of the electron collection first introduced by Ortner(15), since the mobility of electrons in pure gases is high and the collecting time can be made sufficiently small. But, owing to the serious location effect of the tracks in the chamber, simple ionization chamber of parallel plates type cannot be used adequately. If we use, then, chambers with screen grid or chambers of cylindrical or spherical shape, it is not so easy to insure the strict proportionality between the ionization and the pulse height, though approximately it is attained. In the case of ionization chamber with screen grid, high shielding effect of the screen grid is desirable for the elimination of the above-mentioned location effect, but at the same time it promotes the capture of electrons by the grid, and it is fairly difficult to find an adequate compromise.* For the cylindrical

* The detailed discussion on this subject was reported at the meeting of Nuclear Physics Division, Physical Society of Japan, April 3, 1950.

or spherical chambers, the homogeneity attained is of essentially approximate character and the estimation of the degree of inhomogeneity by theoretical analysis is utterly troublesome unless the range of the particle is negligibly small in comparison with the chamber dimension. Thus it seems that the electron collection technique has not necessarily the decisive superiority for our present purpose.

As a consequence, we have adopted an ionization chamber of parallel plates type operated under conditions of non electron collection, and chosen the chamber voltage as high as practicable and the amplifier time constant small enough to suppress the low frequency noise. The deviation from the proportionality between the ionization and the pulse height was analysed theoretically, and the correction was made to the observed result as described later.

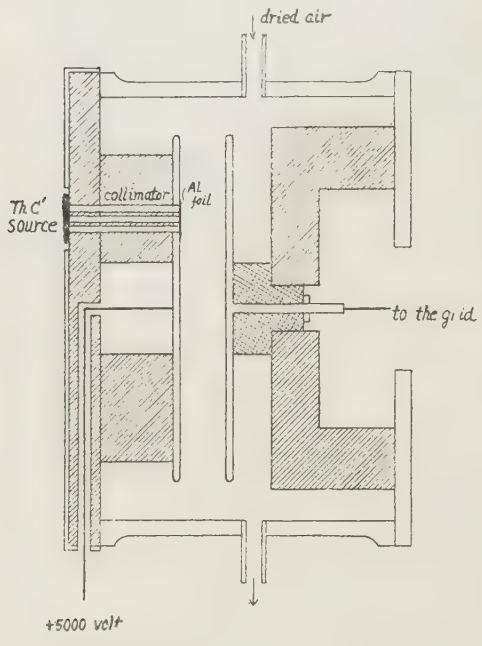

Fig. 1. The ionization chamber used.

Fig. 1 shows the ionization chamber used. It consists of a parallel plates condenser made of two copper disks of 2 mm thickness and 11.3 cm diameter (about 100 cm^2 area). The depth of the chamber was designed to be about 1.5 cm after the knowledge of the proton range 1.00 cm (**13**) of the ${}_7N^{14}(n,p){}_6C^{14}$ reaction in N. T. P. air, and the actual depth proved to be 1.473 ± 0.006 cm by the accurate measurement. It was a good compromise between the disadvantage of the so-called wall effect and the demand for short collecting time, since the voltage required for a certain collecting time is proportional to the square of the chamber depth. Actually + 5000 volt was applied to the high voltage electrode from a well-stabilized source, since this voltage was found to be the highest voltage practicable under the ordinary room humidity. The high voltage electrode has several small holes of 2 mm diameter to admit alpha-particles for the energy calibration. These holes are covered with thin aluminium foil to prevent the distortion of the field.

Now, instead of using pure nitrogen, the air of atmospheric pressure and dried by $CaCl_2$ was filled in the chamber, because the mobility of the negative ions is much greater than that of positive ions and its value is very variable when ordinary tank nitrogen is used.* The reason for the selection of air dried by $CaCl_2$ is simply that in the preliminary experiment the positive and the negative ions in such dried air have been found to have the same mobility, $k_+ = k_- = 2.2\ \mathrm{cm^2/sec/volt}$,** under the present conditions of dryness and age of ions (age $< 2.5 \times 10^{-4}$ sec), and that the theoretical calculation becomes, then, simplified by this knowledge. The existence of oxygen nuclei does not interfere the experiment, because the Q-values for the (n, p) and (n, α) reactions of oxygen are expected to be negative.

The amplifier used is a conventional resistance-capacity coupled type with four stages. This is a modification of the circuit developed by K. Kimura and Y. Uemura (**16**) in our laboratory. Great care was taken for the selection of the time constant which was small enough to suppress the noise and the gamma-ray disturbance from the Ra + Be neutron source but not so small as to distort the linearity seriously. After several trials and theoretical calculations, we have chosen the value of 1.68×10^{-3} sec for the clipping time constant (between the first and second stages) and much greater value of 1.22×10^{-2} sec for the later stages. For the determination of the values of the time constants, capacities and resistances were directly measured by the bridge method, and the plate resistances were obtained from the static characteristics of the tubes.

When usual cares for preventing the low frequency noise such as the use of rubber cushions and the fuse metal as lead wires and etc. were taken, the above combination was found to be satisfactory for the reduction of noise disturbances and yield a good resolution. The ratio of the clipping time constant to the ion collecting time (1.95×10^{-4} sec) is about 8.6. This ratio is not large enough to insure the strict proportionality between the ionization and the pulse height. The distortion, however, is not serious and the correction requested is only about 1.7 per cent as discussed later.

* Experiments are still in progress.

** The tabulated values of mobilities for air, $k_+ = 1.6$ and $k_- = 2.2$, were found in the preliminary experiment to be valid for the ions whose age is longer than 1×10^{-3} sec. These results on the ion mobility for air together with other results were reported at the meeting of Nuclear Physics Division, Physical Society of Japan, April 3, 1950, and will be soon published in this Memoirs.

The input tube used was UZ-6001* and selected carefully among many tubes of the same kind. This was operated with floating grid for the purpose of making the time constant of the input system properly greater than about one second. Under these circumstances, the distortion of the pulse shape in the input stage was negligibly small, and the possible cause of distortion was confined to the interstage coupling circuits.

For the adjustment of the gain and the linearity of the amplifier, a thyratron pulse generator similar to that used by Holloway and Livingston (**17**) was used. This pulse generator proved to have satisfactory precision if the voltage source was well stabilized.

The energy calibration of the pulse height was carried out by the comparison with the pulses of alpha-particles from ThC′. The ThC′ source deposited on a small copper disk was attached to the holes bored in the outer wall of the chamber, and alpha-particles were admitted into the chamber through collimators of 36 mm length and 2 mm diameter. The distance between the source and the inner surface of the high voltage electrode was 36.021 ± 0.055 mm, and the air equivalent of the aluminium foil was 2.82 ± 0.02 mm.

Pulses were recorded by photographing the screen of an oscilloscope of 14 cm diameter, and the pulse heights were directly measured on the films. Fig. 2 shows the linearity of the over-all system including amplifier, oscilloscope and camera measured with the above-mentioned pulse generator.

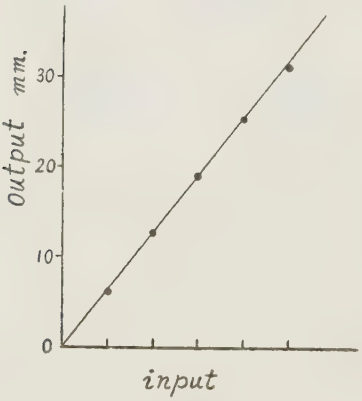

Fig. 2. The linearity of the over-all system.

The neutron source used was a 50 mg Ra + Be mixture. The geometrical arrangement of the chamber and the source is shown in Fig. 3. For the absorption of the gamma-ray from the source, a lead block of about 12 cm was used. About 10 cm of paraffin were also placed between the chamber and the source to avoid fast neutrons which would make recoil atoms in the chamber and interfere the statistics.

* Non-microphonic and low noise level pentode manufactured by Tokyo Shibaura Electric Co. Ltd., and with the same characteristics as UZ-77.

Under these geometrical conditions, apparently uniform pulses attributed to the ${}_7N^{14}(n, p){}_6C^{14}$ reaction produced by thermal neutrons were obtained at a rate of about fifteen per minutes.

In such a low counting rate, the so-called back-kick effect on the pulse height distribution is negligibly small. The time of each of the photographic exposures was from one to two minutes.

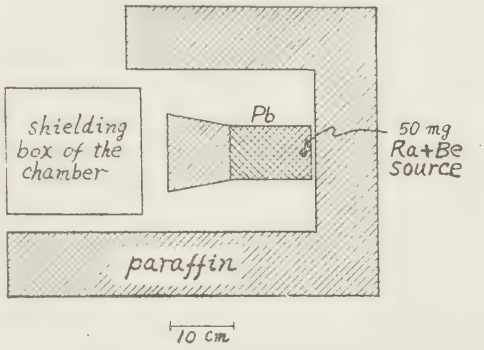

Fig. 3. The geometrical arrangement of the chamber and the neutron source.

3. Results

About one thousand pulses due to the ${}_7N^{14}(n, p){}_6C^{14}$ reaction were recorded. Fig. 4 shows the distribution in size of these pulses measured on the photographic films. The dotted curve is the distribution of the pulses of the pulse generator attached to check the gain of the amplifier. The symmetrical broadening of this curve is due to the non-systematic noise of the amplifier and to that of the gamma-ray disturbance. It is obviously approximated by Gaussian distribution. The standard deviation of this distribution, i.e., the r.m.s. value of the noise, is about 0.9 mm, and it corresponds to about 27 Kev of the input ionization energy. The width of the distribution of the ${}_7N^{14}(n, p){}_6C^{14}$ pulses is the superposition of the main noise broadening and the small amount of inhomogeneity due to the location effect of ${}_7N^{14}$ nuclei in the chamber.

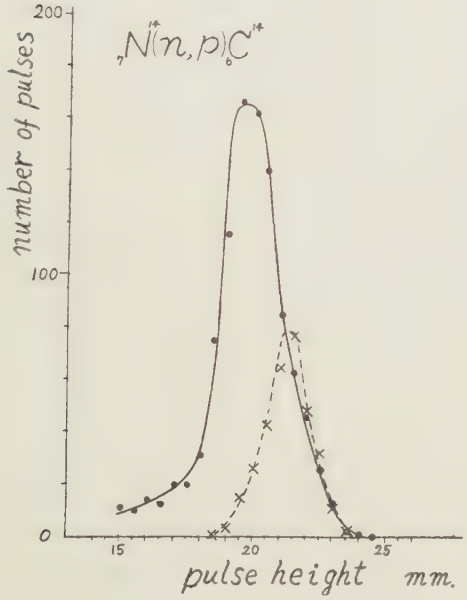

Fig. 4. The distribution of the pulses due to the ${}_7N^{14}(n, p){}_6C^{14}$ reaction. The dotted curve is the distribution of the pulses of the pulse generator showing the noise broadening.

Fig. 5 shows the distribution of the ThC′ alpha-pulses for the calibration. In this observation, the gain of the amplifier was diminished by a factor of about two in such a way that the alpha-pulses have almost the same magnitude as that of the pulses due to the ${}_7N^{14}(n, p){}_6C^{14}$ reaction. It was aimed at minimizing the error introduced by the possible distortion of the linearity of the whole recording system, though Fig. 2 showed a good linearity.

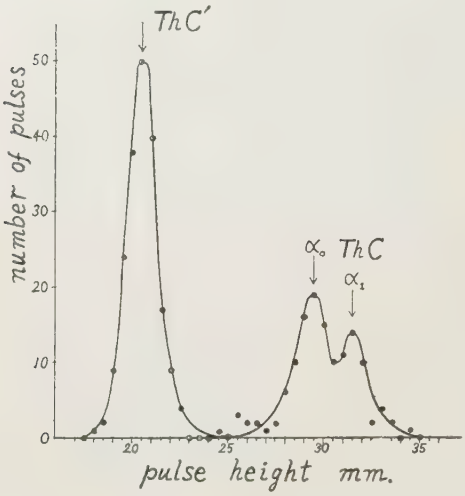

Fig. 5. The distribution of the Th(C+C′) alpha-pulses for the energy calibration.

The exact rate of the change of the gain was obtained from the measurement of the ratio of the resistances of the potential divider in the pulse generator, and the corresponding signal pulse heights in both cases. As shown in the figure, the ThC alpha-groups, α_0 and α_1, are clearly discriminated showing good resolution. For the energy calibration, the main peak of ThC′ was used.

The room temperature and the atmospheric pressure were constant throughout the observation, namely 22.3° C and 755.1 mm Hg respectively.

The energy lost by ThC′ alpha-particle in the chamber was determined by the range-energy curve of Holloway and Livingston (**17**). The situations are shown in Fig. 6 ; R_0 is the mean range of ThC′alpha-particle, b the distance between the source and the inner surface of the high voltage electrode (corrected for temperature and pressure to fit the range-energy curve in N. T. P.), a the air equivalent of the aluminium foil, and d the depth of the chamber (also corrected for temperature and pressure). The energy E_0 lost by the alpha-particle in the chamber is obtained as the difference of the energies E_1 and E_2 corresponding to the points A and B as shown in the figure. The fact that the distance b was so chosen that the alpha-particle is not stopped in the chamber but hit against the collecting electrode with adequate energy, is favourable to minimize the error introduced in the estimation of E_0.

First, if we take the value 8.570 ± 0.007 cm (17) for the mean range of ThC′ and the values already mentioned for b, a, d, and temperature and pressure, the values E_1 and E_2 are obtained as 6.124 and 4.866 Mev respectively from the range-energy curve. Thus only the most accurate region of the range-energy curve (5～9 Mev) is concerned with the estimation of E_0. Second, since we take the difference of the energies corresponding to two points on the range-energy curve, the uncertainties involved in the values R_0, a, and b take their effect on the final error through the difference of dE/dR at A and B. This also minimize the error as compared with the case when the alpha-particle is stopped in the chamber and the final error is directly connected with dE/dR at A. After all, the main sources of error accompanying estimation of E_0 are the uncertainty involved in the value of the chamber depth d and the errors introduced in the procedures of reading the graph. The error arising from the imperfection of the collimation of alpha-particles is negligibly small. After these careful considerations and procedures, the energy lost by ThC′ alpha-particle in the chamber was determined as

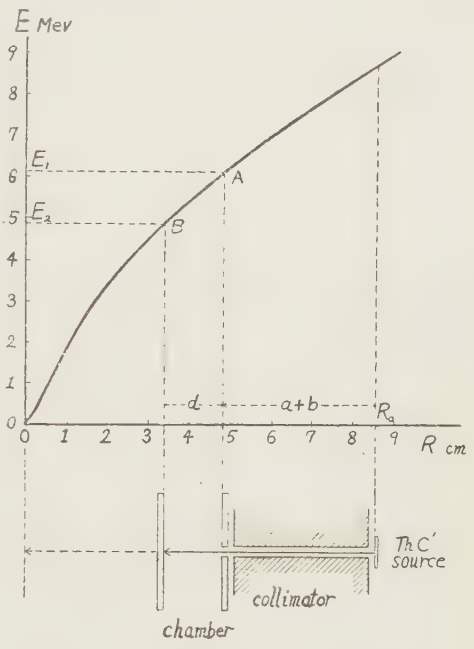

Fig. 6. The illustration of the estimation of the energy lost by ThC′ alpha-particle in the chamber.

$$E_0 = 1.258 \pm 0.006 \text{ Mev},$$

where the amount of the error attached was estimated by taking account of all sources of possible errors above mentioned.

In order to determine the Q-value of the ${}_7N^{14}(n, p){}_6C^{14}$ reaction from the distribution curves shown in Figs. 4 and 5, we must consider here about the correction for the distortion of the proportionality between the ionization and the pulse height as mentioned in the preceding section.

Now, let C be the capacity of the input system (including the chamber, lead wire, and the grid of the input tube) and q be the charge of the ions produced in the chamber, then the output pulse height h is generally expressed by

$$h = Afq/C,$$

where, A denotes the linear amplification factor* of the amplifier, and f the reduction factor of the pulse height due to the distortion of the pulse shape in the interstage coupling circuits. The value of the factor f depends upon the relative magnitudes of the ion collecting time and the time constant of the amplifier, and also the ionization density along the path of the particle. Thus, for certain values of the amplifier time constant and the applied voltage, the value of f varies with the location and the direction of the tracks of the disintegrated particle in the chamber.

Therefore, for the observation of the ${}_7N^{14}(n, p){}_6C^{14}$ reaction in which the disintegrated nuclei are distributed throughout the chamber, the variation of the f-value will exhibit a certain distribution around the average reduction factor $\bar{f}_N$. On the other hand, the alpha-particles used for the energy calibration are admitted into the chamber with a fixed geometry, so that in this case the factor f will take a definite value f_T, which is in general different from f_N. As a consequence, in the determination of the Q-value by the comparison of the pulse heights obtained from Figs. 4 and 5, the correction must be made for the discrepancy of $\bar{f}_N$ and f_T**.

We had made a theoretical analysis*** of the pulse shape and the reduction factor f in the ionization chamber of parallel plates type, and this analysis was applied to the evaluation of the numerical values of $\bar{f}_N$ and f_T for the present experiment. In this calculation, the proton range of the ${}_7N^{14}(n, p){}_6C^{14}$ reaction was taken as 1.00 cm (**13**) in N.T.P. air and the charge density along the path of the proton was approximated by a polynomial of the second degree to fit Bethe's range-energy relation. Ionizations shared between the proton and the recoil

* Under the present experimental conditions, vacuum tube itself can be regarded as a linear element of the circuit.

** It is noticeable that the correction required for the distortion of the proportionality between the ionization and the pulse height is not a definite factor characteristic to the apparatus, but the discrepancy of the reduction factors in both the real observation and the calibration.

*** The details of this analysis and its experimental verification were reported at the meeting of Nuclear Physics Division, Physical Society of Japan, April 3, 1950, and will be published in this Memoirs.

nucleus ${}_6C^{14}$ were assumed to be inversely proportional to the masses, and the range of ${}_6C^{14}$ was neglected in comparison with the chamber dimension and treated as a point charge. For ThC′ alpha-particle, the charge density along the path was also properly approximated to fit the range-energy curve of Holloway and Livingston. The effect of temperature and pressure and the distortions in the later coupling stages were also taken into account.

In Fig. 7 the calculated output pulse height under the present experimental conditions is plotted against the location of the disintegrated ${}_7N^{14}$ and the direction of the emitted proton. The abscissa represents

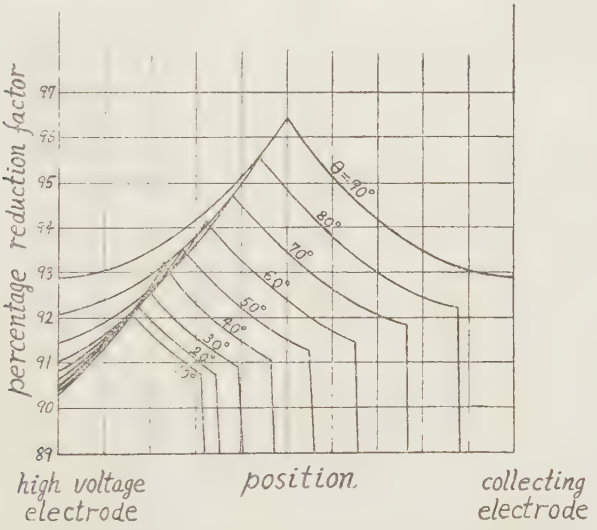

Fig. 7. The percentage reduction factor plotted against the position of the ${}_7N^{14}$ nucleus and the direction of the emitted proton in the chamber.

the position of the disintegrated nucleus in the chamber and θ denotes the angle between the direction of proton and the normal to the electrode plate. The ordinate shows the percentage reduction factor. Each curve shows the variation of f corresponding to fixed θ and various positions. In the case when $180^\circ > \theta > 90^\circ$, curves are turned over symmetrically to the vertical line drawn at the middle point of the abscissa in consequence of the fact that $k_+ = k_-$. The rapid drops in the right-hand sides of the curves represent the so-called wall-effect, i. e., the effect of the protons which are stopped by the electrode with some residual ranges.

By assuming that the occurrences of the reaction are uniformly distributed in the chamber and the directions of the emitted protons are spherically symmetrical, the distribution of the f-value in the observation of the ${}_7N^{14}(n,p){}_6C^{14}$ reaction can be obtained from the curves in Fig. 7.

Fig. 8 shows the resulting distribution of the f-value obtained by this means* (curves in Fig. 7 having been calculated for the interval of five degrees). The mean value $\bar{f}_N$ of the theoretical distribution is 92.6 per cent. In the figure, the calculated value of f_T for the calibration with ThC′ alpha-particle is also shown by a thick vertical line at 91.0 per cent.

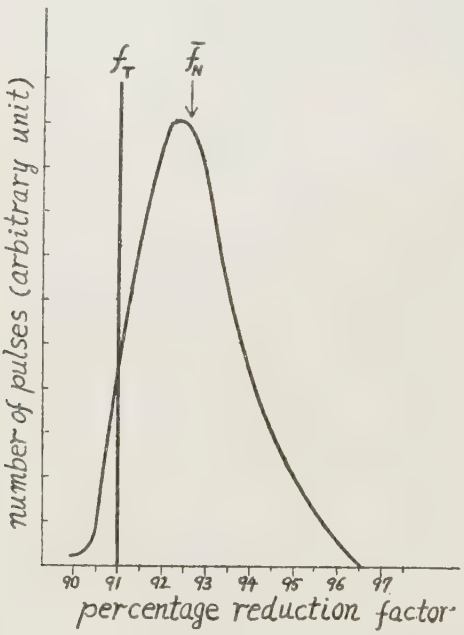

Fig. 8. The calculated distribution of f-value for the observation of the ${}_7N^{14}(n,p){}_6C^{14}$ reaction and the f-value for the calibration with ThC′ alpha-particle.

As already mentioned, the observed distribution is overlapped by the broadening due to noise and gamma-ray disturbance which composes the main part of the actual broadening**. However, if we take the mean value in the determination of the pulse height from the observed distribution, the effect of the noise broadening on the result will be eliminated automatically owing to its essentially symmetric character. Thus the above obtained factor 91.0/92.6 can be properly used for the correction***, even if the noise broadening composes the main part of the actual broadening.

* In this distribution, the edge-effect of the ionization chamber was also taken into account by assuming that the effective volume of the chamber is a clearly defined cylinder whose radius is equal to that of the electrode. Other assumptions were also made on the field distribution near the edge of the effective volume, but they yielded almost the same distributions.

** The half-maximum width for the theoretical distribution of the ${}_7N^{14}(n,p){}_6C^{14}$ pulses is only about 2.8 % of the mean value $\bar{f}_N$. In the observed distributions, this ratio amounts to 11.5 % for ${}_7N^{14}(n,p){}_6C^{14}$ and 8.8 % for ThC′.

*** There is no anxiety for the columnar recombination in the present experiment. According to Moulin's experiment (**18**) on the columnar recombination, the practical saturation is attained in atmospheric air at about 500 volt/cm. The field of 3400 volt/cm in the present experiment seems to insure the perfect saturation for the columnar recombination.

Now, if we assume the strict proportionality between the total ionization and the energy for both alpha-particle and proton, the Q-value for the ${}_7N^{14}(n, p){}_6C^{14}$ reaction is given by the following expression:

$$Q = E_0 \frac{R_2 S_T N f_T}{R_1 T S_N f_N}.$$

In this expression, E_0 is the energy lost by ThC′ alpha-particle in the chamber; R_1 and R_2 the resistances in the potential divider of the pulse generator; T and N the observed pulse heights for ThC′ and the ${}_7N^{14}(n, p){}_6C^{14}$ reaction respectively; S_T and S_N the pulse heights from the pulse generator measured to check the gain of the amplifier in both cases; and f_T and $\bar{f}_N$ are the reduction factors already discussed. The numerical values of these factors have been determined as follows:

$$E_0 = 1.258 \pm 0.006 \text{ Mev},$$
$$R_1 = 4094.4 \pm 1.0 \text{ ohm}, \quad R_2 = 2081.4 \pm 0.7 \text{ ohm},$$
$$N = 19.98 \pm 0.04 \text{ mm}, \quad S_N = 21.26 \pm 0.05 \text{ mm},$$
$$T = 20.48 \pm 0.06 \text{ mm}, \quad S_T = 21.11 \pm 0.07 \text{ mm},$$
$$f_T = 91.0\ \%, \quad \frac{f_T}{\bar{f}_N} = 0.983 \pm 0.002.$$
$$\bar{f}_N = 92.6\ \%,$$

The error accompanying the estimation of f-value is mainly due to the uncertainty of the ion collecting time, and the contribution of the uncertainty of the amplifier time constant is negligibly small in the present experiment. If we take the following values as the factors defining the collecting time; the chamber depth $d = 1.473 \pm 0.006$ cm, the ion mobility $k_+ = k_- = 2.2 \pm 0.1$, and the applied voltage $V = 5000 \pm 100$ volt, the uncertainty existing in the estimation of f-value becomes about 0.4 per cent. However, the effects of above uncertainties of the values d, k, and V on each value of f_T and $\bar{f}_N$ are not independent, but there is a direct correlation between them. Therefore, the final error for the ratio $f_T/\bar{f}_N$ is considered to be much smaller than 0.4 per cent. The above indicated error for this ratio is the upper limit that may be conceivable.

Putting these values in the above expression, we obtain the Q-value for the ${}_7N^{14}(n, p){}_6C^{14}$ reaction:

$$Q = 0.609 \pm 0.005 \text{ Mev}.$$

The probable error attached here does not include any possible error involved in the assumption on the proportionality between the ionization and the energy.

4. Discussion

By taking the extrapolated end point of ${}_6C^{14}$ beta-ray as 0.156 ± 0.001 Mev (19), the neutron-hydrogen mass difference is estimated to be

$$n - H = 0.765 \pm 0.005 \text{ Mev}$$

from the present result. This value is in agreement with the value 0.755 ± 0.016 Mev obtained from the photo-disintegration of deuterium within the limits of experimental errors, and definitely smaller than the value 0.804 ± 0.009 Mev obtained by Bell and Elliott (8).

Recently, Stephens and his collaborators (20) made a simultaneous measurement of the Q-values for ${}_7N^{14}(n,p){}_6C^{14}$ and ${}_2He^3(n,p){}_1T^3$ reactions with ionization chamber filled with mixture of argon, nitrogen and helium, and determined the average $n - H$ value as 0.785 ± 0.006 Mev. In their experiment, Q-value obtained for ${}_7N^{14}(n,p){}_6C^{14}$ was 0.630 ± 0.006 Mev. This is about 20 Kev higher than the result of the present experiment. The threshold measurement of the inverse reaction ${}_6C^{14}(p,n){}_7N^{14}$ was also made recently by Shoupp, Jennings and Sun (21). They obtained the Q-value as 0.620 ± 0.009 Mev which gave rise to the $n - H$ value of 0.776 ± 0.009 Mev. Within the limit of experimental error, this value is consistent with the result of the present experiment as well as with that of Stephens's experiments.

For the ionization measurement including the present experiment and that of Stephens, the fundamental assumption is the proportionality between the total ionization and the energy for both alpha-particle and proton in question. Up to the present time, however, this assumption has not acquired sufficient experimental support. Jesse, Forstat and Sadauskis (22) have recently examined the ionization-energy relation in argon for alpha-particle. Their result maintains the strict proportionality in argon for alpha-particle of energy 1.5 to 9 Mev. In their report, they also discussed about the proportionality in air by converting Stetter's result (23) of the ionization-range relation for alpha-particle into the ionization-energy relation, but this latter argument does not seem so reliable as their experimental result in argon. Moreover, no reliable experiments are available for proton at all. After all, it is difficult to find a proper explanation for the above discrepancy.

Meanwhile, in recent times fairly accurate determinations of the neutron-hydrogen mass difference have been made from other aspects of this subject. Tollestrup, Jenkins, Fowler and Lauritsen (24) obtained 0.789 ± 0.006 Mev from the measurement of Q-values for D-D reactions. Taschek, Argo, Hemmendinger and Jarvis (25) obtained 0.782 ± 0.002

Mev from the threshold measurement of the ${}_1T^3(p, n){}_2He^3$ reaction. These results together with that of Stephens are about 20 Kev smaller than the value of Bell and Elliott, and also about 20 Kev higher than the present result.

Though these values are in good agreement with each other, threshold measurements involve in general uncertainties arising from the voltage calibration and the nature of the yield curve near the threshold point. Therefore, it is not reasonable to discuss here merits and demerits of these results and the value of the present result and the values (7) determined from the photo-disintegration of deuterium observed by K. Kimura, Myers and van Atta, and Wiedenbeck and Marhoefer. Further examination of the ionization-energy relation and the more accurate redetermination of the binding energy of deuterium are desirable for clearing up the confusion.

5. Acknowledgment

It is a pleasure to express our most profound thanks to Professor Dr. B. Arakatsu and Professor Dr. K. Kimura for many valuable suggestions and helpful advices throughout the work. We are also indebted to our colleagues for many stimulous discussions on this subject. Finally, this work was financially supported by the special fund for the advancement of science of the Ministry of Education.

REFERENCES

1. J. Chadwick and M. Goldhaber, Proc. Camb. Phil. Soc., **31** (1935), 612.
2. T. W. Bonner and W. M. Brubaker, Phys. Rev., **49** (1936), 223.
3. T. W. Bonner and W. M. Brubaker, Phys. Rev., **49** (1936), 778.
4. W. E. Burcham and M. Goldhaber, Proc. Camb. Phil. Soc., **32** (1936), 632.
5. O. Kofoed-Hansen, Phys. Rev., **71** (1947), 451.
6. W. E. Stephens, Rev. Mod. Phys., **19** (1947), 19.
7. G. Stetter and W. Jentschke, Zeits. f. Phys., **110** (1938), 214.
   K. Kimura, Mem. Coll. Sci. Kyoto Univ., **A 22** (1939), 237.
   F. E. Myers and L. C. van Atta, Phys. Rev., **61** (1942), 19.
   M. L. Wiedenbeck and C. J. Marhoefer, Phys. Rev., **67** (1945), 54.
8. R. E. Bell and L. G. Elliott, Phys. Rev., **74** (1948), 1552.
9. P. W. Levy, Phys. Rev., **72** (1947), 248.
   A. K. Solomon, R. G. Gould and C. B. Anfinsen, Phys. Rev., **72** (1947), 1097.
   C. S. Cook, L. M. Langer and H. C. Price, Phys. Rev., **74** (1948), 548.
10. O. Huber, P. Huber and P. Scherrer, Helv. Phys. Acta, **XIII** (1940) 209.
11. P. Huber and A. Stebler. Phys. Rev., **73** (1948), 85.
12. H. H. Barshall and M. E. Battat, Phys. Rev., **70** (1946), 245.
13. J. K. Bøggild, Kgl. Danske Vid. Sels. Mat.-Fys. Medd., **23** (1945), 22.
   D. J. Hughes and C. Eggler, Phys. Rev., **73** (1948), 809.
   I. C. Cornog, W. Franzen and W. E. Stephens, Phys. Rev., **74** (1948), 1.

14. M. S. Livingston and H. A. Bethe, Rev. Mod. Phys., **9** (1937), 268.
15. G. Ortner and G. Stetter, Phys. Zeits., **35** (1934), 563.
G. Ortner and G. Protiwinsky, Win. Ber., **148** (1939), 349.
16. K. Kimura and Y. Uemura, Mem. Coll. Sci. Kyoto Univ., **A 23** (1940), 1.
17. M. G. Holloway and M. S. Livingston, Phys. Rev., **54** (1938), 18.
18. L. B. Loeb, *Fundamental Processes of Electrical Discharge in Gases.* (John Wiley & Sons, 1939), 141.
19. Cook, Langer and Price, *loc. cit.*, ref. 9.
20. W. Franzen, J. Halpern and W. E. Stephens, Phys. Rev., **77** (1950), 641.
21. W. E. Shoupp, B. Jennings and K. H. Sun, Phys. Rev., **75** (1949), 1.
22. W. P. Jesse, H. Forstat and J. Sadauskis, Phys. Rev., **77** (1950), 782.
23. G. Stetter, Zeits. f. Phys., **120** (1943), 639.
24. A. V. Tollestrup, F. A. Jenkins, W. A. Fowler and C. C. Lauritsen, Phys. Rev., **75** (1949), 1947.
25. R. F. Taschek, H. V. Argo, A. Hemmendinger and G. A. Jarvis, Phys. Rev., **76** (1949), 325.

Nuclear Research Laboratory,
Institute for Chemical Research,
University of Kyoto.

Memoirs of the College of Science, University of Kyoto, Series A,
Vol. XXVI, Nos. 1 & 2, Article 17, 1950.

Observation of Cosmic-Rays with Nuclear Emulsions

By

Kiichi Kimura,* Senzo Tokunaga,**
Ryutaro Ishiwari * and **Kazunori Yuasa ***

(Received July 31, 1950)

We have been observing cosmic-ray phenomena with nuclear emulsions NTB since last summer. A part of our results has been already published this winter (**1**). In this paper we shall report the results so far obtained. Our observation is mainly about cosmic-ray stars, but we also tried to examine the existence of the varitrons (2) by means of the grain counting of many single tracks.

1. Experimental procedure (3)

We obtained the nuclear emulsion plates Eastman Kodak NTB (50 microns in thickness) at the beginning of July 1949 and exposed them to cosmic-rays for 47 days (i. e., from July 29 to September 1) placing the surface of the emulsion vertically at the Meteorological Observatory on Mt. Norikura (2840 m a. s. l.). We developed them for twenty minutes with undiluted D–19 developer (20° C). In order to scan emulsions we used microscopes with the magnification of 45C. For scanning, the plates were put on the stand reconstructed with the comparator for spectroscopy, and made to move with constant speed by a motor. The speed was comparatively slow with about 0.1 mm per second, and moreover, it can be stopped whenever in need. So we think there are few cases when we miss some of the events in the emulsion. Most of the stars were examined in detail with oil immersion lens ($\times 90 \sim 135$), and the grain counting was performed by magnifying them $1200 \sim 1500$ times.

* The Institute for Chemical Research, University of Kyoto.
** Physical Laboratory of Saikyo University.

2. Cosmic-ray stars

(a) Distribution of the number of stars about the number of prongs.

We investigated the distribution of the number of stars about the number of prongs. In Table I we show the number of stars with more than three prongs observed in detail in two and a third sheets of emulsions and the frequency of stars per cc. of emulsion per day. Some photomicrographs of them are illustrated in Plates I (a), (b), (c) and (d).

TABLE I. Number of stars observed at 2840 m a. s. l.

Number of prongs	3	4	5	6	7	8	9	10	11	12	13	14	15	Total
Number of stars in 2.3 sheets of plates	43	25	16	12	3	1	2	1	1	0	0	1	1	106
Frequency of stars per cc. of emulsion per day	4.25	2.47	1.58	1.18	0.30	0.10	0.20	0.10	0.10	0	0	0.10	0.10	10.5

As it seemed that the considerable time had elapsed since the time of production until our plates were brought to the mountain, we took much care of the background in the emulsion, of which we shall describe in (c) of this paragraph. We have omitted such background in the first table.

(b) Variation of the number of stars with altitude.

The distribution of stars about the number of prongs has been so far reported by Wambacher (**4**), Bernardini et al. (**5**), Addario et al. (**6**), Salant et al. (**7**) and other authors at various altitudes. From their results it is learned that the distribution of stars about prong numbers at high altitudes investigated by baloon is different from that at the altitude of high mountains (about 3000 m a. s. l.). Namely, the number of stars with many prongs increases rapidly at high altitudes. The phenomena seem to be reasonable from the view that in high altitude there may exist many more nucleons with high energy, and heavy primary particles play an important role in the phenomena. In Fig. 1 is given the integral frequency curve of the stars about the number of prongs and our results are compared with those of previous investigators.

As the number of stars by the traces of radioactive substances

contained in the emulsion is not negligible in the measurement at low altitudes, there seems to be not a few cases when the number of stars with less than five prongs becomes larger to a certain degree. At any rate, comparing our results with others the difference between the distribution at high mountains and that at high altitudes seems to be conclusive.

From the data of ours, of Bernardini et al. at Laboratorio Testa Grigia (3500 m a. s. l.), and of Bernardini et al. by baloon (29000 m a. s. l.), we could obtain the altitude variation of the frequency of stars as shown in Fig. 2.

As shown in the figure the three data concerning the total number of stars with more than three prongs at different altitudes are expressed by exponential law, $\exp(-x/L_a)$, where x is the atmospheric depth expressed in g cm^{-2}, and L_a the absorption depth in g cm^{-2}. The value of L_a was found to be 137 g cm^{-2}. Also, the data concerning the number of stars with more than six prongs lie on a straight line as shown in the figure. In this case the value of L_a was found to be 124 g cm^{-2}. The value 137 g cm^{-2} is nearly equal to the hitherto known value 138 g cm^{-2} (8), and

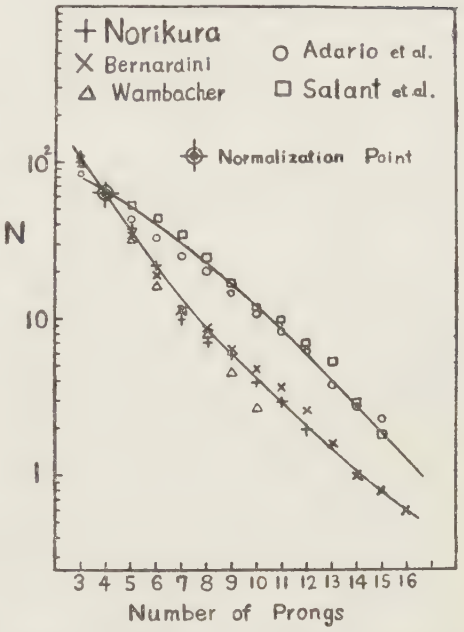

Fig. 1. Integral size frequency distribution of stars. (N in arbitrary unit.)

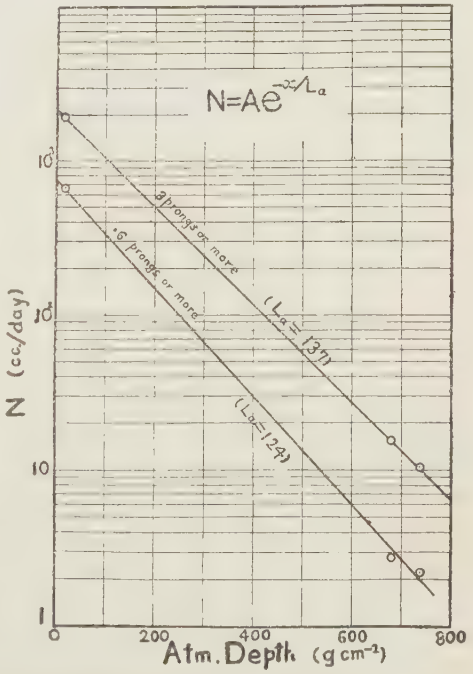

Fig. 2. Altitude variation of the frequency of stars.

that of L_a, 124 g cm^{-2}, is nearly of the same value for high energy events, i. e. 125 g cm^{-2}. Recently, Forster (9) has reported that the absorption depth for stars with prong number equal to or greater than two is 125 ± 8 g cm^{-2} which was obtained from his experiments at 11000 m, 4160 m a. s. l. and sea level respectively, but in his results the frequency of stars is much larger than that hitherto reported, which makes us feel strange.

(c) The background in the emulsion.

If we want to know exactly the effect of the cosmic-rays on Mt. Norikura, we must have a precise knowledge about the background produced after the emulsion was prepared. The background is originated from radioactive substances contained as contaminations in the emulsions and cosmic-rays which entered into the emulsions before they were brought to the mountain.

For this purpose, it will be desirable to compare them with two kinds of control plates in the same batch of our emulsions: one of which is developed at the time when our plates are brought to the mountain, and the other after they are carried back from there.

Since, however, it was not realized unfortunately, we compared them with a plate which was in the same packing in which the plates exposed on Mt. Norikura were contained, and had been kept in the laboratory. It was developed 100 days after the plates used on Mt. Norikura were developed (on 21 Dec.). A quarter of this plate was scanned, and the number of stars found in this area is shown in Table II.

TABLE II. Number of stars in the control plate (¼ of a plate).

Number of prongs	2	3	4	5	6
Number of stars	5	15	20	23	2

As it was impossible to correct our observation with the results, we adopted a means to eliminate all the stars which are distinguishable as due to radioactive substances judging from their prong lengths. Because all the stars found in the plate which was kept in the laboratory are distinguished to be of radioactive origin, we neglected the effect of cosmic-rays before the plate was brought to the mountain.

The radioactive substances expected to be in the emulsion are mainly those of Uranium-Radium series and Thorium series. In the emulsion

which passed more than a month or so, the majority of stars due to radioactive elements will be five pronged RdTh stars, and four pronged Ra stars, while the six pronged Th stars, and other three or two pronged stars will be of negligible quantity.

In the actual plates, however, we found many three or two pronged stars, and the ranges of their prongs agree with those of alpha-rays due to natural radioactive elements. As to such three or two pronged stars, we excluded them on the ground discussed in the Appendix.

All the stars were sketched with a camera lucida, and were examined about the range of every prong. As the stars in question had short prongs of 20～40 microns, their ranges were estimated exactly.

In this case there are some dangers to eliminate cosmic-ray stars with similar aspects to those of radioactive origin, but its proportion will be small.

In Table III, the number of stars is shown which we eliminated in the statistics of Table I from above considerations. The total of these stars is some 10 stars/cc./day. This number agrees with the result obtained by Jagoda (**10, 11**), who estimated it as 10 stars/cc./day for the radioactive stars with 2～5 prongs found in the Ilford C_2 plates.

TABLE III.

Number of prongs	Number of stars in 2.3 sheets of plates
2	70
3	149
4	124
5	72
6	3

The quantity of natural radioactive substances in the glass is expected to be larger than that in the emulsion. In fact we found many stars which had their origin in the glass, but we neglected these stars, because we could distinguish them easily.

3. Single tracks

Besides cosmic-ray stars there can be found a good number of single tracks in the emulsion. Among these there were about thirty tracks in one sheet of plate which had the ends of their ranges longer than

200 microns in the emulsion. The greater part of them seems to be protons and some to be mesons. On scores of tracks we examined the relations between their residual ranges and the total number of silver grains contained in residual ranges in order to estimate the masses of these particles (**12**). And on some of tracks we used the method of scattering (**13**) for the same purpose.

In estimating the masses of the particles, the uniformity of the development and the fading of the latent images present a serious problem: but the former is out of the question, because the emulsions used are 50 microns in thickness. The extent of the latter, however, being uncertain, though a few reports (**10, 11, 14, 15**) have been published on the fading of alpha-particles and protons, we tried the grain counting. The results are presented in Fig. 3.

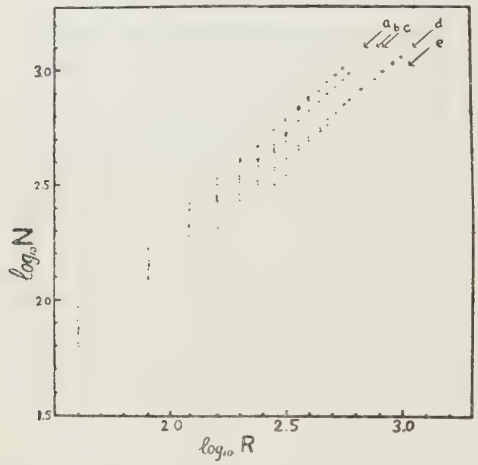

Fig. 3. Number N of grains in residual range R.

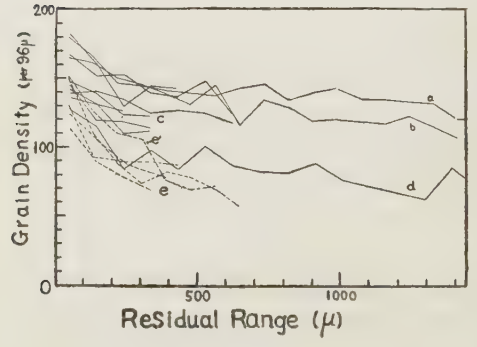

Fig. 4. Grain density *versus* residual range.

From Fig. 3 one might first be tempted to conclude that there are some different groups of particles. Assuming the group c to be proton, we estimated the mass of each groups a, b, d and e as shown in the figure by the method taken by Lattes et al. and the mass of group a particle is found to be 3～5 times that of proton, group b 2 times, group d ½～⅕ and group e 1/10～1/20. Though the results may show the existence of various particles with various masses, i. e. varitrons, we must be careful to obtain the conclusion, for the effect of the fading of the latent images plays an important role in grain density. So we rewrote the above results to the relation between grain density and residual range, which is shown in Fig. 4. If we regard all the particles illustrated by full lines in Fig. 4 to be protons

and consider that the extention of the grain density is due to the effect of fading, the ratio of the mass of particles with maximum grain density to that of those with minimum grain density will be about 0.6. The results are found nearly equal to Mather's experiment (**14**) which investigated the fading of the proton track in NTB emulsions. In his experiment the order of fading was 70 per cent after 47 days since latent images were formed. Therefore, from our results it will be adequate to consider that the extension of grain density is rather due to the effect of fading than due to the existence of various particles with various masses.

In the next place, judging from the shape of their curves, it seems clear that the particles shown by dotted lines are different particles. They also show the extension in grain density. From the relation of the mean grain density and the range of each group, we estimated the ratio of the mass of the former group to that of the latter group, and it was found to be $9\sim10$. Therefore, the latters are considered to be μ–mesons. We estimated the mass of these particles by the method of scattering taken by Latimore (**13**) and found it to be 211 $\pm$ 13. So the above consideration seems to be reasonable.

In addition, in order to testify the existence of the varitrons the effect of the fading of emulsion has the important relation as discussed above. So it would be very difficult unless much care is taken of for the effect.

In conclusion the authors express their heartfelt gratitude to Dr. Webb and Mr. Knapp of Eastman Kodak Co. for their kind offer of the nuclear emulsions, to Professor Dr. B. Arakatsu for his advice, to Mr. H. Morishita for his kind help at the Meteorological Observatory on Mt. Norikura, and Miss. K. Ishii for her aid in this work.

Appendix

Some Peculiar Aspects of Stars

By careful investigations of stars found in the photographic emulsions, we noticed that a good number of stars are followed by a few

TABLE IV.

Number of prongs	2	3	4	5
Percentage	29	57	24	0

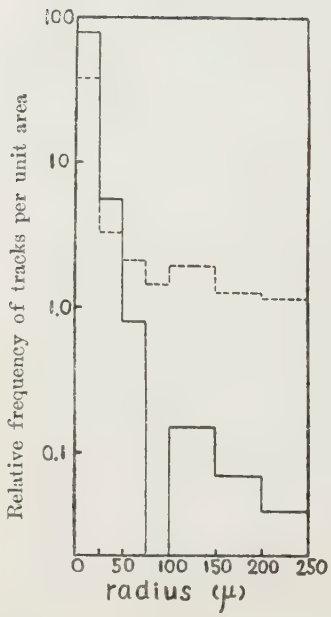

Fig. 5. Distribution of single tracks. Tracks which have both ends in the emulsions in full lines, and one end in dotted lines.

single tracks of short ranges in the neighbourhood of them. Further studies showed that these stars found together with single tracks had prongs of 20~40 microns in length, which were nearly equal to the ranges of natural alpha-rays from radioactive substances. Among the stars which have prongs of 20~40 microns length, the proportion of those which are accompanied by single tracks to the total number of stars of given prong number is shown in Table IV.

At first, we investigated whether these single tracks had relations with stars, or they fell on the star by chance. Suppose circles with their centers on the centers of stars, and with radii of 25, 50 microns and so on. Thus we counted the number of single tracks contained in each zone on 251 stars, (tracks stretching over two zones are regarded as in the zone in which the center of the track lies) and the results are shown in Table V. Also in Fig. 5 the number per unit area is shown in histogram. The counting was done respectively in the tracks having both ends in the emulsion, and only one end in the emulsion. Tracks with no end in the emulsion (these tracks are larger than 50 microns) were neglected. The tendency is very remarkable that short tracks are found near the center of stars. The range of those tracks with each end in the emulsion is shown in Fig. 6.

The mass and the charge of the particles were also investigated, but we got no conclusion because they were too short to give clear informations. Some microphotographs

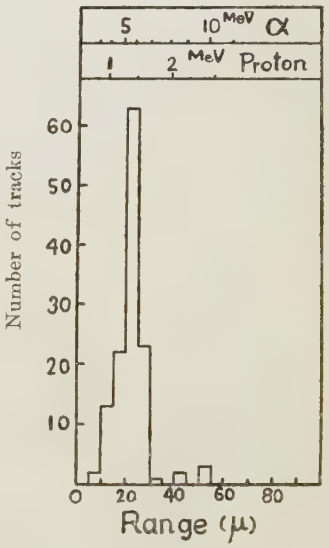

Fig. 6. Number-range histogram.

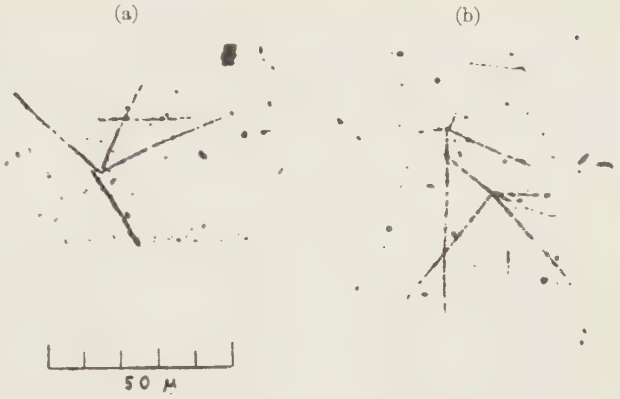

Fig. 7 (a). Microphotograph of three pronged star with two single tracks.

Fig. 7 (b). Microphotograph of Thorium star.

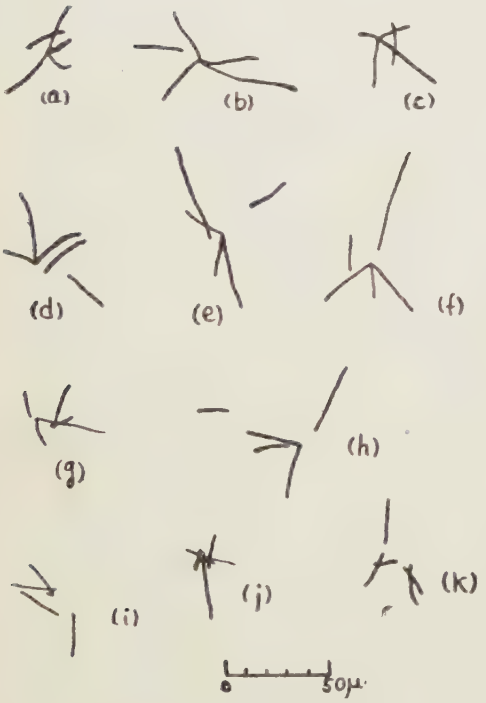

Fig. 8. Sketches of stars accompanied by single tracks.

and sketches of these stars are shown in Fig. 7 (a) and Fig. 8 (a)~(k). A microphotograph of RdTh star is also presented for comparison in Fig. 7 (b).

As easily found in the sketches, they are of various sorts. In Table VI the statistics about the prong number of the stars and the number of single tracks which were found together is shown.

In this table, "prong number 0, single track 5" for example, means an event that five single tracks are found together as shown in Fig. 8 (k). The histogram in Fig. 9 shows the distribution about the sum of number of single tracks and the number of prongs of stars found together, and we find that the majority have five or four tracks in all.

From these results, we attempted to give an explanation as follows: these stars would be RdTh or Ra stars, and though they are five or four pronged stars in nature, their origin moved during the formation of the stars by the diffusion of the atoms in the radioactive series.

TABLE V.

Radius in microns	Area (ratio)	Tracks with both ends in emulsion	The same per unit area	Tracks with one end in emulsion	The same per unit area
0～25	1	69	69	38	38
25～50	3	17	5.6	10	3.3
50～75	5	4	0.8	11	2.2
75～100	7	0	0	10	1.43
100～150	20	3	0.15	39	1.95
150～200	28	2	0.07	36	1.28
200～250	36	1	0.03	41	1.14

TABLE VI.

Number of prongs \ Single track	0	1	2	3	4	5
2	45	0	6	12	0	0
3	62	43	38	2	0	0
4	85	25	1	0	0	0
5	71	0	0	0	0	0
0	0	0	0	0	0	3

For example, a four pronged star with one single track would be considered that after RdTh emitted an alpha-particle the resulted ThX moved before it decayed (the mean life of ThX is 5.26 days) and then formed the remaining a four pronged star there. The three pronged stars with one single track would be regarded as Ra star, in which Rn moved after Ra had decayed (the mean life of Rn is 5.53 days), and then continued to decay until RaD was formed.

If we suppose that the diffusion velocity of the atoms in the radioactive series are the same, the distance of the movement would be proportional to their lives (of course it is true in the statistic meaning.) Then some of ThB would move by noticeable distance, and the existence of three pronged star with two single tracks will be

understood. But it will be a rare event for the other elements as Tn, ThA, ThC, ThC′, RaA, RaB, RaC and RaC′ to move by noticeable distance, so there are no good explanation for the abundance of other kinds of stars.

We also considered whether or not the developer is mixed with Th, Ra contaminations during the procedure, but the situation is not important because the observable number of stars will not be formed in such a short time even with appreciable large quantity of radioactive substances. Therefore, we can consider that a neutral atom moves with mean velocity of about 10^{-9}cm/sec. in the emulsion.

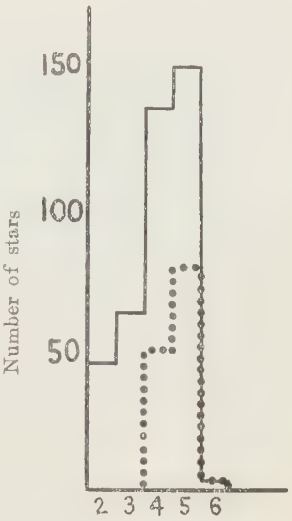

Fig. 9. Histogram of number of stars *versus* total number of prongs and single tracks.

Hence, we studied the aspects of RdTh stars. The experiments were done with some sheets of nuclear emulsion plates (Eastman Kodak NTA 25 microns in thickness) soaked in the thorium-nitrate solutions in 0.01 %～0.0005 % for several minutes. They were developed 1～3 weeks after the soakage. With the assumption that the elements are in radioactive equilibrium in the solution, the ratio of the number of stars is calculated. In our experimental results, however, the ratio was considerably different from the calculation, and the deviation had various tendencies.

The experimental result is shown in Table VII in comparison with the calculated ratio. In these results, the ratio of the five pronged star to the four pronged star is too large or too small, while the three and two pronged stars are very few and in this respect the result accords with the calculation. In the plates soaked in 0.01 % of thorium-nitrate solution, RdTh stars were found superposed one over the other, but in case of 0.0005 % they were well dispersed. We examined whether there were some stars followed by single tracks closely by them, but it seemed very few though they were covered by single tracks in the background. These results are somewhat unfavorable for the preceding assumption. We could not experiment with regard to the Ra star, but their nature will be analogous to the result with RdTh stars.

In spite of the resemblance of these stars with radioactive stars, we also assumed that they had relations to cosmic-rays. If these single tracks are recoil protons originated from neutrons emitted from the center of the star, the number of neutrons must be unreasonably large.

So there may be other unknown phenomena, but we abstain here from speculating about this problem until more sufficient ground are obtained to abandon the assumption of the radioactive origin.

TABLE VII.

Number of prongs		1	2	3	4	5	6
A	cal.	—	0	0	0.36	1	0
	obs.	—	0	0	1.29	1	0
B	cal.	7.45	0	0.12	1.35	1	0
	obs.	7.86	0	0.02	0.57	1	0

A: 0.0005 per cent 21 days. B: 0.01 per cent 7 days.

We excluded the stars with single tracks in the statistics of cosmic-ray stars in 2, considering that these stars are due to radioactive elements.

Since a definite conclusion, however, has not yet been reached, we intend to continue further studies.

REFERENCES

1. K. Kimura, R. Ishiwari, K. Yuasa and S. Tokunaga, Kagaku **20** (1950), 88.
2. A. I. Alikhanian, D. M. Samoilovich, I. I. Gurevich and Kh. P. Babayan, J. E. T. F. **19** (1949), 664.
3. K. Kimura and S. Tokunaga, Nippon Butsurigakukaishi (in press)
4. H. Wambacher, Wiener Bericht. **149** (1940), 157.
5. G. Bernardini, G. Cortini and A. Manfredini, Phys. Rev., **74** (1948), 845.
6. M. Addario, S. Tambrino, Phys. Rev., **76** (1949), 983.
7. E. O. Salant, J. Hornbostel and E. M. Dollmann, Phys. Rev., **74** (1948), 694.
8. B. Rossi, Rev. Mod. Phys., **20** (1948), 556.
9. H. H. Forster, Phys. Rev., **78** (1950), 247.
10. M. Wiener, H. Yagoda, Phys. Rev., **76** (1949), 469.
11. M. Wiener, H. Yagoda, R. S. I., **21** (1950), 39.
12. C. M. G. Lattes, G. P. C. Occhialini and C. F. Powell, Nature **160** (1947), 453; **160** (1947), 480.
13. S. Lattimore, Nature **161** (1949), 518.
14. K. B. Mather, Phys. Rev., **76** (1949), 486.
15. W. A. Lamb and E. W. Brown, Phys. Rev., **74** (1948), 104.

Plate I. Cosmic-ray star.

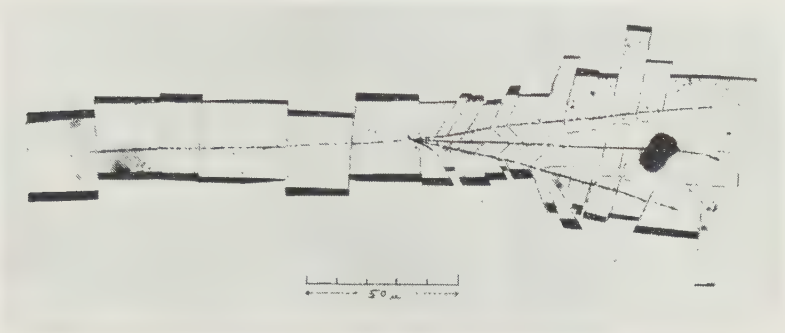

(a)

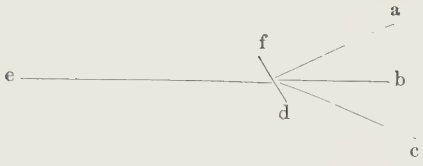

a, b, c, and d: alpha-particles f: heavier fragment e: proton

(b)

(a)

(b)

(c)

The ratio of the mass of the particle a to that of b was 2.8 from grain counting. The former seems to be triton, and the latter proton. The particle c is recoil nucleus.

a: 870 microns b: 250 microns.

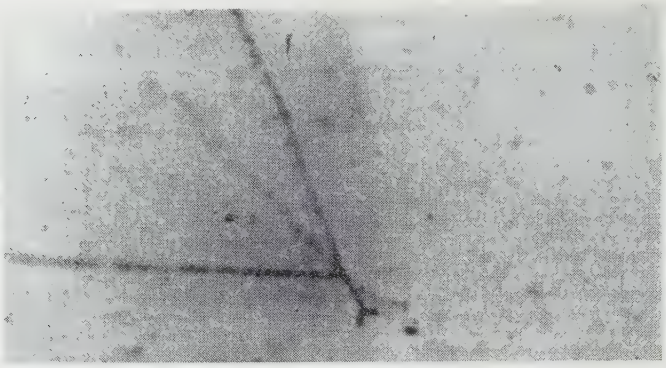

(c) The forked track shows that one of the fragments suffered scattering by the collision with a nucleus.

(d) Explosive disintegration of a nucleus (silver or bromine). The track of fourteen fragments can be seen including protons, alpha-particles and heavier nuclei.

Plate II. Track of μ-meson.

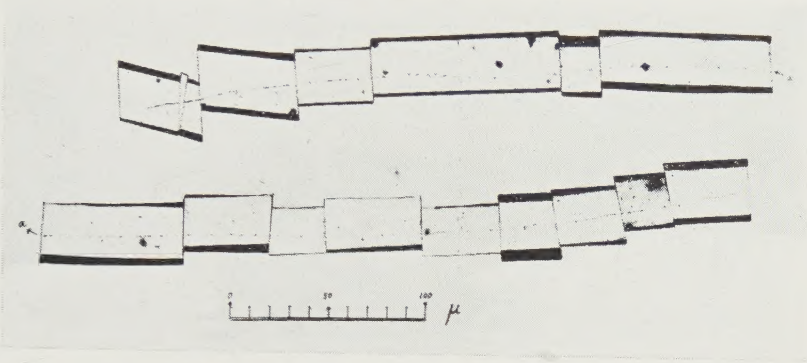

(The track continues from sign a to a.)

昭和二十五年十月二十五日　印刷
昭和二十五年十月三十一日　發行

編輯兼發行者　京都大學理學部

印刷者　河北印刷株式會社
代表者　河北喜四良
京都・二條・堺町

CONTENTS

Professor Bunsaku Arakatsu I
List of Professor B. Arakatsu's Papers on Scientific Subjects I
List of Papers by Professor Arakatsu's Pupils I
On the Bending of a Rectangular Plate with Four Clamped Edges
BY *K. Munakata* 1
The Pressure Distributions on the Surface of an Obstacle in a Running Viscous Fluid at Small Reynolds Numbers
BY *S. Tomotika* AND *T. Aoi* 9
On the Hodograph Method and Analytic Continuation of Solution in the Theory of Compressible Fluid Flow
BY *K. Tamada* 21
A Study of Ultrasonics by Magnetostriction Vibrators
BY *Y. Takesada* 31
On the Activation of Thoria Emitter by Zirconium
BY *S. Fukagawa* 45
The Faraday Effect of Colored Rocksalts
BY *Y. Uchida* AND *K. Fukuda* 63
On the K-center in KCl Crystal
BY *M. Ueta* 69
Photoconduction of Alkalihalide Crystals which adsorb Dyes
BY *H. Yagi* 75
The (γ, n) Reaction of Molybdenum produced by the Li (p, γ) γ-Rays
BY *S. Shimizu, S. Yasumi, Y. Saji* AND *J. Muto* 85
The Photo-disintegration of Beryllium by the High Energy Gamma-Rays
BY *B. Arakatsu, M. Sonoda, Y. Uemura, S. Yasumi,* AND *Y. Saji* ... 97
Measurement of the Branching Ratio of Thorium C by a Photographic Method
BY *S. Tokunaga* 109
1.5 cm Wave-length Microwave Spectroscopy
BY *I. Takahashi, A. Okaya, T. Ogawa* AND *T. Hashi* 113
On the Effect of a Conducting Screen with Concentric Aperture in the Circular Wave Guide
BY *I. Takahashi, T. Watanabe* AND *K. Tanimoto* 123
Researches on the Activation Energy of (Ba, Sr) O by Electron Bombardment
BY *K. Ohira* 131
Studies on the Ion Source placed in a Magnetic Field
BY *M. Sakisaka, S. Miyashiro, Y. Uemura* AND *S. Yasumi* 143
The Energy released in the Disintegration of Nitrogen by Thermal Neutrons
BY *R. Ishiwari* AND *K. Yuasa* 151
Observation of Cosmic Rays with Nuclear Emulsions
BY *K. Kimura, S. Tokunaga, R. Ishiwari* AND *K. Yuasa* 167